

**Engineering and evolving glyoxylate utilization in Ethylmalonyl-CoA
Pathway-deficient *M. extorquens* PA1 for the production of crotonate from
methanol**

Dissertation

zur Erlangung des Grades eines

Doktor der Naturwissenschaften

(Dr. rer. nat.)

des Fachbereichs Biologie der Philipps-Universität Marburg

Vorgelegt von

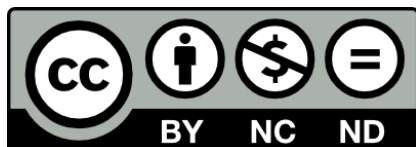
Alina Schrodt

Aus Offenbach am Main

Marburg an der Lahn, 2025

Originaldokument gespeichert auf dem Publikationsserver der Philipps-Universität Marburg

<http://archiv.ub.uni-marburg.de>



This work is licensed under Creative Commons Attribution-NonCommercial-NoDerivatives 4.0 International.

To view a copy of this license, visit

<https://creativecommons.org/licenses/by-nc-nd/4.0/>

Die Arbeit zur vorliegenden Dissertation wurde von Januar 2022 bis November 2025 unter der Betreuung von Herrn Prof. Dr. Tobias J. Erb am Max-Planck-Institut für terrestrische Mikrobiologie in der Abteilung "Biochemie und Synthetischer Metabolismus" angefertigt.

Vom Fachbereich Biologie der Philipps-Universität Marburg (Hochschulkennziffer 1180) als
Dissertation angenommen am: _____

Erstgutacher(in): Prof. Dr. Tobias J. Erb

Zweitgutacher(in): Prof. Dr. Anke Becker

Tag der Disputation: _____

Erklärung

Hiermit versichere ich, dass ich die vorliegende Dissertation selbstständig, ohne unerlaubte Hilfe Dritter angefertigt und andere als die in der Dissertation angegebenen Hilfsmittel nicht benutzt habe. Alle Stellen, die wörtlich oder sinngemäß aus veröffentlichten oder unveröffentlichten Schriften entnommen sind, habe ich als solche kenntlich gemacht. Dritte waren an der inhaltlich-materiellen Erstellung der Dissertation nicht beteiligt; insbesondere habe ich hierfür nicht die Hilfe eines Promotionsberaters in Anspruch genommen. Kein Teil dieser Arbeit ist in einem anderen Promotions- oder Habilitationsverfahren der Antragstellerin oder des Antragstellers verwendet worden. Mit dem Einsatz von Software zur Erkennung von Plagiaten bin ich einverstanden.

Marburg, den 23.11.2025 Alina Schrodtt

Statement on the contribution to publications in this dissertation

I declare that this thesis was composed by myself and without external assistance. I confirm that the work presented has not been submitted for any other degree or professional qualification. I also declare that I have not made any prior doctoral attempt. Furthermore, I confirm that no sources other than those indicated have been used and that appropriate credit has been given within this thesis where reference has been made to the work of others. I confirm that the work submitted is my own, except where explicitly stated otherwise in the text.

Marburg, 23.11.2025

Alina Schrodtt

No generative AI was used for the writing of this thesis.

Marburg, 23.11.2025

Alina Schrod

Summary

The development of methylotrophic microbial platforms for the production of value-added compounds is a crucial step towards a methanol-based bioeconomy. Methanol is a promising substrate for the synthesis of such compounds as methods for its sustainable production continue to advance. One of the most straight-forward routes to green methanol includes the use of renewable energy to power electrolysis of water, generating green hydrogen that can subsequently be used for the hydrogenation of CO₂. Moreover, methanol does not compete with the food industry and reduces the risk of contamination during fermentation. One promising organism capable of efficiently utilizing C1 substrates is the natural methylotroph *Methylobacterium extorquens*, one of the most well-studied organisms for methylotrophy. The central carbon metabolism of *M. extorquens* contains intermediates, most interestingly CoA esters in the EMCP, which could be harnessed for the production of value-added compounds using methanol as a substrate. However, rewiring of central carbon metabolism is tedious and comes with multiple drawbacks in strain performance. I therefore chose the *M. extorquens* PA1 strain, which grows faster on minimal medium and has a smaller genome, benefiting genetic engineering work. To develop an EMCP-deficient strain of *M. extorquens* PA1, I introduced the heterologous glyoxylate shunt, which would allow to exploit the EMCP for the accumulation of CoA esters and the subsequent conversion to the carboxylic acid, here crotonate. To test this, the plasmid containing the glyoxylate shunt also harbored the thioesterase encoding gene for the YciA from *E. coli*, which catalyzes the reaction of crotonyl-CoA to crotonate.

The first part of this thesis focuses on the establishment of the glyoxylate shunt in *M. extorquens* PA1 in a strain that is deficient in the EMCP at the level of the crotonyl-CoA carboxylase/ reductase. While initial introduction of the heterologous glyoxylate shunt did not yield any strain capable of growing with methanol as the sole carbon source, adaptive laboratory evolution (ALE) allowed and significantly improved growth after 45 serial transfers (P45). Here, I identified mutations in the evolved strain that redistribute carbon fluxes around the isocitrate node. Subsequent characterization of the evolved strain revealed changes in protein abundances and adaptation to the methanol-induced stress conditions during ALE. Furthermore, determination of the biomass yield on different C1 compounds during chemostat cultivation in bioreactors showed that the evolved strain is capable of accumulating wildtype-levels of biomass, while crotonate production was below wildtype levels.

In the second part of this thesis I aimed to enhance crotonate production through deletion of the competing PHB synthesis pathway. As the construction of the $\Delta ccr\Delta phaC$ double mutant strain was unsuccessful, I designed and tested different versions of a CRISPR interference (CRISPRi) system for the targeted knockdown of *phaC* and *ccr* and prototyped them in the wildtype strain during growth on methanol. Here, I tested varying expression levels by altering plasmid copy number and different promoters for the control of the CRISPRi machinery, which consists of the dCas9 and a gRNA. While constitutive expression of CRISPRi strongly affected strain viability, exchange of the constitutive promoter for an IPTG-inducible promoter enabled cell growth on methanol. I introduced this CRISPRi design in the wildtype, where the knockdown of *ccr* had a negative impact on methylotrophic growth. In contrast, downregulation of *phaC* consistently improved growth on methanol in the wildtype. This plasmid system, however, was not suitable for the knockdown of *ccr* and *phaC* in the corresponding $\Delta phaC$ and Δccr knockout strains. Therefore, to find a suitable candidate for targeted knockdowns in these strains, I designed a mismatched gRNA library to tune the binding capacity of the CRISPRi complex, which would reduce lethality of the *ccr* knockdown in $\Delta phaC$ and *vice versa*. Growth assays of the CRISPRi system containing mismatch gRNAs in the wildtype showed a correlation between sequence length, degree of mismatches and growth.

In summary, this work advanced the development of a potential production strain for EMCP-derived carboxylic acids and introduced a new approach for the downregulation of the competing PHB pathway – an alternative to the highly unstable genetic knockouts.

Zusammenfassung

Die Entwicklung methylopher mikrobieller Plattformen für die Produktion von Mehrwertprodukten ist ein essentieller Schritt in Richtung einer Methanol-basierten Bioökonomie. Methanol eignet sich hervorragend als Ausgangsstoff für die Herstellung solcher Produkte, da erneuerbare Produktionsverfahren für Methanol kontinuierlich verbessert werden. Einer der direktesten Wege zu grünem Methanol besteht darin, erneuerbare Energie zur Elektrolyse von Wasser zu nutzen, wobei Wasserstoff generiert wird, welcher zur Hydrogenierung von CO₂ genutzt werden kann. Weitere Vorteile zur Nutzung von Methanol als Substrat für die Industrie sind, dass Methanol nicht mit der Lebensmittelindustrie konkurriert und das Risiko von Kontaminationen bei laufenden Fermentationsprozessen minimiert. Ein vielversprechender Organismus, welcher C1 Substrate effizient verwerten kann, ist der natürliche Methyloph *Methylobacterium extorquens*, einer der am besten erforschten Organismen in Bezug auf Methylophie. Der zentrale Kohlenstoff-Metabolismus von *M. extorquens* beinhaltet wertvolle Intermediate, vor allem CoA Ester aus dem Ethyl-Malonyl-CoA Stoffwechsel (EMCP), welche für die Produktion von Mehrwertprodukten aus Methanol als Substrat genutzt werden kann. Das Ändern von Stoffwechselwegen des zentralen Kohlenstoff-Metabolismus ist allerdings umständlich, und führt oft zu Nachteilen im Wachstum der genetisch veränderten Stämme.

Aus diesem Grund wählte ich den *M. extorquens* PA1 Stamm, welcher schneller auf Minimalmedium wächst und ein reduziertes Genom aufweist, was genetische Manipulationen in diesem Organismus erleichtert. Mein Ziel war es durch die Einbringung des heterologen Glyoxylat-Shunts einen EMCP-unabhängigen Stamm von *M. extorquens* PA1 zu entwickeln, in welchem CoA Ester aus dem EMCP akkumulieren können, welche dann in Crotonatsäure umgewandelt werden können. Um dies zu testen enthielt das Plasmid, welches den Glyoxylat Shunt beinhaltet, zusätzlich eine Thioesterase (YciA), welche die Reaktion von Crotonyl-CoA zu Crotonatsäure katalysiert.

Der erste Teil dieser Arbeit fokussiert sich auf die Etablierung des Glyoxylat-Shunts in einem *M. extorquens* PA1 Stamm, welcher einen dysfunktionalen EMCP auf dem Level der Crotonyl-CoA Reduktase/Carboxylase (*ccr*) besitzt. Während die Einführung des Glyoxylat-Shunts das Wachstum auf Methanol zu Beginn nicht ermöglichte, verbesserte adaptive Laborevolution (ALE) das Wachstum signifikant nach 45 Übertragungen auf flüssigem Methanolmedium. Hierbei konnte ich Mutationen identifizieren, welche eine Umverteilung des

Kohlenstoffflusses im metabolischen Knotenpunkt um Isocitrat verursachen. Die anschließende Charakterisierung des evolvierten Stammes enthüllte Veränderungen der Proteinlevel und eine Anpassung an die Methanol-induzierenden Stressbedingungen der ALE. Zusätzlich konnte ich zeigen, dass Erträge der Biomasse auf verschiedenen C1 Substraten während der kontinuierlichen Kultivierung im Bioreaktor den Erträgen des Wildtyps glichen, wobei die Produktion von Crotonsäure unter dem Level des Wildtyps lag.

Das Ziel des zweiten Teils meiner Arbeit war es die Produktion von Crotonsäure durch die Deletion des konkurrierenden PHB Synthesewegs zu erhöhen. Da die Entwicklung einer $\Delta ccr\Delta phaC$ Doppelmutanten nicht möglich war, erstellte und testete ich verschiedene Versionen eines CRISPR Interferenz (CRISPRi) Systems für die gezielte Repression von *ccr* und *phaC*, und prüfte diese Konstrukte im Wildtyp während des Wachstums auf Methanol. Hierbei testete ich unterschiedliche Expressionsniveaus für die CRISPRi Maschinerie, welche aus dCas9 und gRNA besteht, indem ich die Plasmidkopienzahl sowie verschiedene Promotoren variierte. Während die konstitutive Exprimierung von CRISPRi die Lebensfähigkeit der Zellen stark beeinträchtigte, konnte Wachstum auf Methanol durch den Austausch des konstitutiven Promotors durch einen IPTG-induzierbaren Promotor erzielt werden. Im Wildtyp verursachte dieses System bei der Herunterregulierung von *ccr* ein Wachstumsdefizit auf Methanol. Im Gegensatz hierzu verbesserte die Herunterregulierung von *phaC* das Wachstum des Wildtyps auf Methanol. Dieses Plasmidsystem war jedoch nicht geeignet für die Genrepression in den Δccr und $\Delta phaC$ Deletionsstämmen. Um eine CRISPRi Variante zu finden, die für die Genregulierung in diesen Stämmen geeignet ist, entwarf ich gRNAs mit fehlerhaften Basenpaarungen, welche die Bindungskapazität des CRISPRi Komplexes verändern würde, was wiederum die Letalität der *ccr* Repression in $\Delta phaC$ (und *vice versa*) verringern würde.

Zusammenfassend trug diese Arbeit zur Weiterentwicklung eines potentiellen Produktionsstamms für Carbonsäuren aus dem EMCP bei, und stellte einen neuen Ansatz für die Herunterregulierung des konkurrierenden PHB Synthesewegs als Alternative für die höchst instabilen Deletionsstämme vor.

Table of contents

Summary	1
Zusammenfassung	3
Table of contents	5
Table of figures	7
Abbreviations	8
1. Introduction	9
1.1 Sustainable bioeconomy to reduce industrial CO ₂ emissions	9
1.2 Single carbon compounds for sustainable microbial cultivation	11
1.2.1 Gaseous feedstocks	11
1.2.2 Liquid feedstocks	12
1.2.3 Natural CO ₂ assimilation pathways for industry	14
1.3 NATURAL VERSUS SYNTHETIC METHYLOTROPHY	16
1.3.1 <i>Methylobacterium extorquens</i>	19
1.3.2 Metabolic engineering toolbox for <i>M. extorquens</i>	20
1.3.3 The Glyoxylate cycle as an alternative to the Ethyl-Malonyl-CoA Pathway	21
1.3.4 Related work	22
2. Aim of this thesis	23
3. Materials & Methods	25
3.1 Cell cultivation	25
3.2 Electroporation of <i>M. extorquens</i>	28
3.3 Adaptive laboratory evolution	28
3.4 Cultivation of <i>M. extorquens</i> in a bioreactor	28
3.5 Bioconversion growth assays	30
3.6 Whole genome sequencing	30
3.7. Sample preparation for Exometabolome Analysis	31
3.8. Sample preparation for Endometabolome Analysis	31
3.9 Sample preparation for Proteomics	32
3.10 Enzyme assays	33
3.10.1 Isocitrate dehydrogenase activity assay	33
3.10.2 Formate dehydrogenase assay	33
3.12 Oligos	36
3.13 Strains	37
4 Results	38
4.1 Optimization of the glyoxylate shunt in <i>M. extorquens</i> PA1	38
4.2 Glyoxylate shunt adaptation enables wildtype-level biomass yields	41

4.3 Crotonate production and degradation in P45.....	44
4.4 Whole genome sequencing reveals mutations in ALE	46
4.5 Mutation F156C decreases isocitrate dehydrogenase activity	47
4.6 Changes in the proteome of P45	48
4.7 Mutations in TtmR and EfgA confer enhanced formaldehyde tolerance in P45	52
4.8 Utilizing CRISPR interference for targeted knockdowns in the EMCP	53
4.8.1 Designs for CRISPRi for targeted knockdowns.....	54
4.8.2 Resting cells for crotonate production	57
4.8.3 Design of mismatch guide RNAs for targeted knockdowns	58
4.8.4 Introduction of mismatched gRNA- <i>phaC</i> in <i>P45</i>	61
5 Discussion.....	62
5.1 Adaptive Laboratory Evolution leads to improved methylotrophic growth	63
5.1.1 Mutations in <i>Icd</i> and <i>Prk</i> rewire central carbon metabolism.....	63
5.1.2 Enhanced methanol oxidation in <i>P45</i>	64
5.1.3 Altered Formaldehyde homeostasis confers higher formaldehyde tolerance.....	66
5.1.4 Improved growth on methanol growth reduces acetate utilization.....	67
5.1.5 <i>P45</i> shows wildtype-level biomass yields	68
5.2 CRISPRi for transient pathway optimization.....	71
5.2.1 Plasmid copy number strongly influences strain viability on methanol.....	71
5.2.2 Mismatch gRNAs.....	74
6 Concluding remarks	75
7 Acknowledgements.....	78
8 References	80
9 Supplementary information.....	96
Curriculum vitae	103

Table of figures

Figure 1: Industrial methanol synthesis from different substrates.....	13
Figure 2: Methanol oxidation and central carbon metabolism in <i>M. extorquens</i>	22
Figure 3: Methylotrophic growth characterization of evolved Δccr strains.....	38
Figure 4: Growth assays of evolved Δccr strains at different stages of the ALE.....	40
Figure 5: Growth characterization of <i>P45</i> on acetate.....	41
Figure 6: Bioreactor cultivation <i>P45</i> on methanol and formate.....	42
Figure 7: Crotonyl-CoA and Crotonate production of <i>P45</i> during flask cultivation.....	44
Figure 8: Crotonate production of <i>P45</i> during bioreactor chemostat cultivation.....	45
Figure 9: Crotonate degradation during flask cultivation of the Wt.....	46
Figure 10: Enzyme activity assays of mutated isocitrate dehydrogenase.....	48
Figure 11: Proteomics of <i>P45</i>	50
Figure 12: Differential abundance of proteins involved in central carbon metabolism.....	51
Figure 13: Differential abundance of proteins involved in methanol oxidation.....	52
Figure 14: Formaldehyde tolerance test.....	52
Figure 15: Two-plasmid CRISPRi system growth assay in the Wt.....	55
Figure 16: Inducible CRISPRi plasmid system in the Wt, Δccr and $\Delta phaC$	56
Figure 17: Resting cells for crotonate production with the inducible CRISPRi system.....	57
Figure 18: Mismatched gRNA screen in the Wt.....	59
Figure 19: Mismatched C5 gRNA- <i>ccr</i> in the Wt.....	60
Figure 20: Mismatched T5-G10 gRNA- <i>phaC</i> in the Wt and <i>P45</i>	61
Figure 21: Knockdown verification of the inducible CRISPRi system.....	73
Supplementary Figure 1: Growth of $\Delta ccr P0$ on succinate and methanol.....	96
Supplementary Figure 2: Growth of single colonies of <i>P45</i>	96
Supplementary Figure 3: Bioreactor chemostat cultivation of <i>P21</i> on formate.....	96
Supplementary Figure 4: Formate consumption verification tests.....	97
Supplementary Figure 5: Crotonate degradation of the Wt during flask cultivation.....	97
Supplementary Figure 6: Crotonate degradation cultivation medium controls.....	98
Supplementary Figure 7: Two-plasmid CRISPRi system test in $\Delta phaC$ and Δccr	98
Supplementary Figure 8: Inducible CRISPRi system test in Δccr and $\Delta phaC$	99
Supplementary Figure 9: Mismatched gRNA growth assays in the Wt (Final ODs).....	100

Abbreviations

<i>aceA</i>	Isocitrate lyase
<i>aceB</i>	Malate synthase
ALE	Adaptive laboratory evolution
CBB	Calvin-Benson-Bassham cycle
Ccr	Crotonyl-CoA reductase/carboxylase
CCU	Carbon capture and utilization
CDW	Cell dry weight
CoA	Coenzyme A
<i>C. glutamicum</i>	<i>Corynebacterium glutamicum</i>
<i>C. necator</i>	<i>Cupriavidus necator</i>
dCas9	Deactivated Cas9
<i>E. coli</i>	<i>Escherichia coli</i>
EMCP	Ethylmalonyl-CoA pathway
ERC	Electrochemical reduction
GHG	Greenhouse gas
gRNA	Guide RNA
h	Hours
Kan	Kanamycin
<i>M. extorquens</i>	<i>Methylobacterium extorquens</i>
MeOH	Methanol
PEP	Phosphoenolpyruvate
PHB	Polyhydroxybutyrate
Ppm	Parts per million
rTCA	Reverse TCA cycle
Ru5P	Ribulose-5-phosphate
RuMP	Ribulose-Monophosphate pathway
<i>S. cerevisiae</i>	<i>Saccharomyces cerevisiae</i>
TCA	Tricarboxylic acid cycle
Tet	Tetracycline
WLP	Wood-Ljungdahl pathway
Wt	Wildtype
XuMP	Xylulose-Monophosphate pathway

1. Introduction

1.1 Sustainable bioeconomy to reduce industrial CO₂ emissions

The continued rise of greenhouse gases (GHG) in our atmosphere is an ever-growing threat to our ecosystems and our health as they contribute to global warming, causing extreme weather conditions like heatwaves, floods and droughts. As a result, we experience the frequent occurrence and rising severity of wildfires and marine heatwaves, which causes a widespread loss of terrestrial and marine biodiversity¹.

Throughout the past decades, GHG emissions have increased steadily correlating with a rise in global surface temperature, which has increased by approximately 1.2 °C since pre-industrial levels of the mid-19th century, and each year breaking the previous record high temperatures. To stay in line with the Paris Agreement, recent assessments reported that the rise in global temperature above 1.5°C can be avoided if GHG emissions are reduced substantially, while the magnitude of further warming is determined by the rates at which anthropogenic GHG emissions are decreased². GHGs consist of a mixture of different gasses. In 2019, total CO₂ (including fossil fuel industry, land-use and forestry) made up for approximately 75% of total GHG emissions, followed by the more potent methane (~18%), nitrous oxide (~5%) and fluorinated gases (~2%)³. Although methane and the other GHGs have a higher global warming potential per unit mass, the immense increase of CO₂ from human activity has caused the majority of global warming⁴. Recent assessments estimated that CO₂ from fossil fuels alone accounted for 74.5% of total GHG emissions in 2024⁵.

The majority of emitted CO₂ is captured by natural CO₂ sinks, which are capable of absorbing and releasing CO₂, such as grasslands, forests and oceanic ecosystems. Tropical rainforests account for the majority of carbon storage, while absorption in grasslands is highly dependent on precipitation⁶. However, these natural sinks are decreasing over time due to continued deforestation and agricultural land use for livestock and crops, while increased surface temperature lower the rate of precipitation due to frequently occurring droughts⁷⁻⁹. In 2024, atmospheric CO₂ concentrations reached a record-high of 423.9 parts per million (ppm), an increase of 52% from pre-industrial levels¹⁰. With the industrial revolution in 1850, CO₂ emissions have drastically increased through the expansion of the industrial sector and the excessive use of fossil fuels¹¹. Nowadays, industry and fossil fuels are among the main contributors to the global GHG emissions with an annual production of ~37-38 Gt of CO₂ from

fossil fuels, accounting for 24% in total^{12,13}. Proposed pathways to stay below the 1.5 °C threshold emphasize the mitigation of CO₂ emissions from the industrial sector. However, according to scientists of the Global Carbon Project, global warming is predicted to exceed this threshold at current emission rates by 2030, as efforts for economic decarbonization are far too slow¹⁴. Finding solutions for the reduction in CO₂ emitted by industrial processes would therefore help to accelerate the decarbonization process, and scientists across different fields have successfully designed strategies to achieve this goal¹⁵.

Besides energy generation, chemical and manufacturing industry are one of the main sources of industrially produced carbon, and finding alternative resources for the replacement of fossil fuels for the production of platform chemicals has received considerable attention throughout recent years^{16,17}. Conventional production routes of many industrially relevant compounds rely heavily on petrochemical processes, with 67% of emissions derived from fuel combustion. These processes do not only have a high energy demand (e.g. high temperatures) but also often produce toxic wastes and cause resource depletion¹⁸. In recent years multiple strategies have been developed to create alternative production routes for the synthesis of value-added compounds¹⁹⁻²¹. Besides enzyme catalysis and biorefinery processes, the latter of which converts biomass feedstocks into value-added biochemicals, microbial fermentation is one of the most promising strategies to find more eco-friendly alternatives for the synthesis of certain chemicals from renewable resources²²⁻²⁶.

Humanity has utilized microorganisms in the production of valuable products for millennia, such as classic fermentation by *S. cerevisiae* in beer brewing and bread making or lactic acid bacteria in the production of yoghurt and cheese. While these processes still play an important role in our daily life, the microbial product spectrum has shifted drastically in the recent years through advances in biotechnology and metabolic engineering, as we are now able to produce complex chemicals like terpenoids, alkaloids or cannabinoids²⁷⁻³⁰. By altering the native cellular metabolism through the introduction of heterologous genes, a vast variety of products such as biofuel precursors, organic acids, and biopolymers can be synthesized in diverse microbial cell factories³¹⁻³⁶. Additionally, the introduction of non-native genes or entire pathways may unlock new substrates which can be utilized for strain cultivation or enhance product titers³⁷⁻⁴⁰. While common feedstocks for large-scale economically feasible microbial processes often rely on sugar- or starch feedstocks, lignocellulosic biomass or oils, these resources often directly compete with food industry and agricultural supply chains⁴¹⁻⁴³. The

ability to culture non-model organisms which are able to metabolize unconventional carbon sources has unlocked more potential for an even more sustainable bioproduction.

1.2 Single carbon compounds for sustainable microbial cultivation

The carbon source for microbial cultivations plays a vital role when it comes to creating sustainable processes for the production of value-added compounds. According to the IEA, renewable resources are defined as energy derived from natural processes that are produced faster than they are consumed and play a critical role in reducing CO₂ emissions by 2030⁴⁴. As previously mentioned, many bioproduction routes rely on non-sustainable substrates, which often directly compete with the food industry and deplete natural resources. Single carbon (C1) compounds on the other hand are a promising alternative to these feedstocks, as they are highly available and can be produced through environmentally friendly processes.

1.2.1 Gaseous feedstocks

Throughout the last few decades many studies have developed microbial cell factories for the production of industrially relevant chemicals during fermentation powered by gaseous C1 substrates such as CO₂, natural gas (CH₄), syngas (CO and H₂), or biogas (also referred to as biomethane; CH₄ from anaerobic digestion). As the main constituent of natural gas is methane and only a small fraction of other alkanes and CO₂, it comes with high energy density and could potentially serve as a substrate for the cultivation of methanotrophs. However, as natural gas is derived from fossil fuels and depleting natural gas reservoirs, it is not suitable for a sustainable bioeconomy. Despite its lower energy content, which is approximately 30% lower than natural gas, synthesis gas (Syngas) on the other hand is a more attractive resource for future industrial applications. The main components of syngas are CO and H₂, along with smaller amounts of CO₂ and methane, and its composition varies greatly depending on its origin and processing method^{45,46}. While syngas can be derived from fossil fuels like natural gas, crude oil and coal, sustainable production from biomass gasification has gathered more attention throughout recent years⁴⁷. Many studies have demonstrated the production of platform chemicals from syngas, which will be discussed further below. Coupling of gaseous feedstocks from industrial flue gases or carbon capture from the atmosphere can directly reduce industrial CO₂ emissions and are part of CO₂ mitigation strategies. However, when it comes to utilizing gaseous C1 substrates for microbial fermentation, certain drawbacks are expected. First, the low miscibility of gases in water necessitates elevated gas concentrations and efficient sparging in large reactor volumes to maintain stable growth and compound production. Also,

fluctuations in gas composition or dispersion in the culture often leads to lower growth and production rates.

1.2.2 Liquid feedstocks

As the use of gaseous feedstocks has several disadvantages, liquid feedstocks are generally preferred for industrial applications for several reasons. Besides higher energy densities, easy storage and handling as well as higher solubility in water makes liquid C1 feedstocks attractive for industrial use. Methanol, formic acid and formaldehyde have been used as feedstock for microbial fermentation in different cultivation scales. Methanol can be synthesized through different routes and from various renewable and non-renewable sources (Figure 1). To date, the vast majority of methanol is synthesized from non-sustainable sources, with 65% of global methanol production from natural gas (CH₄), through steam methane reforming. This process includes three steps: 1. Catalytic conversion of natural gas to syngas; 2. Conversion of syngas to crude methanol using Cu/ZnO catalysts; and 3. Distillation of crude methanol to high purity methanol⁴⁸. Besides the requirement of natural gas, high temperature (200-300°C) and pressure (50-100 bar) further lower the sustainability for this synthesis route. Half of global methanol is made in China, where coal gasification is the dominant manufacturing process, which requires even higher temperatures ($\geq 900^\circ\text{C}$) and high pressures of at least 20 bar^{49,50}.

In recent years, however, multiple pathways for the sustainable synthesis of methanol have been developed. For example, methanol can be produced from syngas through the Fischer-Tropsch process, in which CO is hydrogenated with H₂, and accounts for 11% of products derived from syngas⁵¹. While syngas can be produced from non-sustainable sources, biomass gasification from sustainably grown biomass is a promising alternative for methanol synthesis as the overall energy chain has potential to be GHG neutral⁴⁸. Moreover, methods such as the photocatalytic conversion or electrochemical reduction (ERC) of CO₂ as well as microbial cultivation of anaerobic acetogens or aerobic methanotrophs are promising pathways for the synthesis of green methanol⁵². Photocatalytic conversion involves carbon capture and utilization (CCU), which captures off-gases of industrial processes that have inherent CO₂ emissions like steel, cement or paper refineries. In a photocatalytic process, H₂O is dissociated into O₂ and H₂, which is then used for the hydrogenation of the captured CO₂. ERC and methanol synthesis from microbes, however, do not meet industrial requirements yet. The

efficiency of ERC is limited by overpotential requirements, low solubility of CO₂ in aqueous solutions and the lack of stable and efficient catalysts⁴⁸.

For microbial cultivations, the aerobic methanotroph *Methylophilum fumariolicum* was shown to produce methanol from methane (0.88 mmol/gCDW/h), while production was highly dependent on growth rate⁵³. Another promising liquid C1 feedstock is formate, which has great potential for industrial application. Like methanol, it can be produced from photochemical or electrochemical reduction or hydrogenation of CO₂, oxidation of natural gas, hydration of syngas or oxidation of biomass. Also, catalytic conversion of methanol can be used for the production of formate by carbonylation with CO⁵⁴. Both methanol and formate can serve as carbon and energy sources at the same time. While formate represents an interesting alternative to methanol as it is non-volatile, stable at room temperature and comes with simple production routes, its application for industry faces some downsides such as lower biomass yields due to its lower energy content and the availability of efficient formate assimilation pathways⁵⁵.

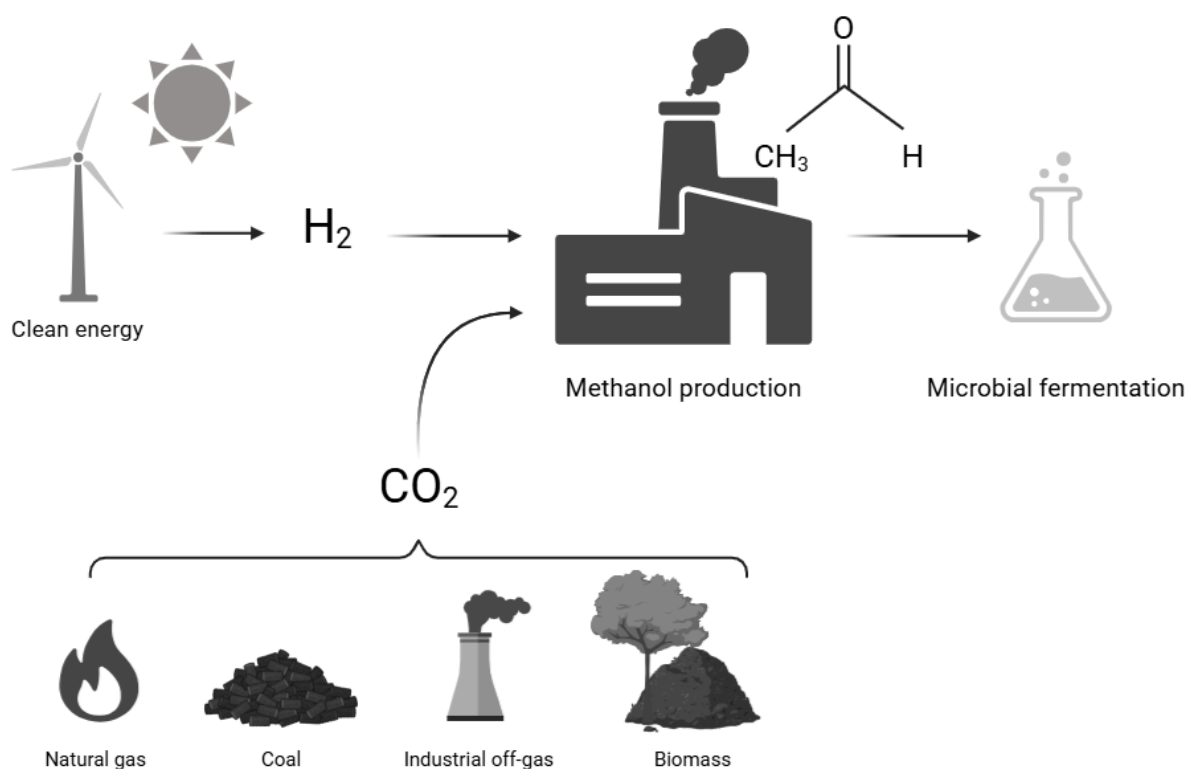


Figure 1: Industrial methanol synthesis from different substrates.

Methanol has a couple advantages over formate as substrate for microbial cultivation. With a growing number of synthesis routes and increasing annual production of the C1 compound, the price of methanol has steadily declined over the years, while green methanol production costs fluctuate depending on electricity and H₂ prices and introduction of carbon taxes⁵⁶. Moreover, methanol has a higher degree of reduction and therefore higher energy density than glucose, allowing for a more efficient production of reduced products with a lower substrate consumption for biomass formation. It is also highly miscible in water and liquid at room temperature, simplifying transport and storage, all of which are favorable properties for large-scale biotechnological productions. Another important aspect while considering methanol as a feedstock is that growth on methanol inevitably leads to the formation of formaldehyde, a highly toxic intermediate, which is a metabolic hub during methylotrophic growth and causes cellular damage due to its high reactivity with DNA and proteins. This, however, also reduces risk of contamination during cultivation and therefore highlights another advantage of methanol as a substrate.

However, the number of organisms that are able to utilize these valuable C1 carbon sources is limited. In nature there are five CO₂- and six C1-assimilation routes that are utilized by different eukaryotes, bacteria and archaea. The following section describes known naturally occurring CO₂ assimilation pathways found in bacteria and yeasts and their applicability for industrial production routes, paving the way for a GHG neutral bio-based economy. The two archaeal CO₂-fixation pathways, namely the 3-Hydroxypropionate/4-Hydroxybutyrate and the Dicarboxylate/4-Hydroxybutyrate cycle, will not be discussed as they lie outside the scope of this work.

1.2.3 Natural CO₂ assimilation pathways for industry

The most prominent aerobic pathway for C1 assimilation is the Calvin-Benson-Bassham (CBB) cycle, which is a CO₂ fixation cycle that relies on the activity of Ribulose-1,5-bisphosphate-carboxylase/oxygenase (RuBisCO), found in photoautotrophic and chemolithoautotrophic organisms. The CBB cycle is initialized by the carboxylation of ribulose-1,5-bisphosphate (RuBP) catalyzed by RuBisCO yielding 2 molecules of 3-phosphoglycerate. The C₃ compound can then be used to form biomass, or to refill the RuBP pool. For this, glyceraldehyde-3-phosphate is converted to ribose-5-phosphate, to ribulose-5-

phosphate and then to ribulose-5-phosphate, which then yields ribulose-1,5-bisphosphate catalyzed by the ATP-dependent reaction of phosphoribulokinase (Prk).

CO₂ and industrial exhaust gasses have been used frequently as C1 substrate in cultivation of genetically engineered CBB-utilizing organisms from different phyla for the production of industrially relevant compounds, for example cyanobacteria for the production of biofuels, or the production of biomass or precursor metabolites from *Chlorella* microalgae⁵⁷⁻⁶⁰. *Cupriavidus necator* is among one of the most promising organisms for C1-based biomanufacturing. Many studies have demonstrated the production of biopolymers like polyhydroxybutyrate (PHB), fatty acids and biofuel precursors CO₂⁶¹⁻⁶⁴. Langsdorf and colleagues also demonstrated the cultivation of *C. necator* in a bioreactor with continuous gassing of industrial flue gas for the production of Polyhydroxybutyrate (PHB)⁶⁵.

Another CO₂-fixation pathway is 3-Hydroxypropionate bicycle (3HP bicycle), which was first identified in *Chloroflexus aurantiacus* and occurs in green non-sulfur bacteria. It consists of two cycles, which convert two molecules of CO₂ into one molecule of glyoxylate in the first cycle, while the second cycle forms Mesoacetyl-CoA, which is cleaved into the biomass precursor pyruvate and one molecule of acetyl-CoA. In total, this pathway involved 16 enzymatic reactions that are catalyzed by 13 enzymes. While natural 3HP-utilizing organisms have not yet been used for the production of value-added compounds, part of the 3HP cycle has been implemented in *C. necator* and *E. coli* for the production of succinate. Here, however, cultivation medium was supplemented with alternative carbon sources^{66,67}.

A third CO₂ fixation pathway that is used for natural anaerobic C1 assimilation is the reductive TCA (rTCA) cycle, found in diverse anaerobic or microaerophilic bacteria, such as acetogens and methanogens, with an ATP-citrate lyase as its key enzyme. This cycle fixes two molecules of CO₂ to generate acetyl-CoA, which is subsequently reductively carboxylated to pyruvate with one additional CO₂ by the pyruvate:ferredoxin oxidoreductase (Pfor). Similarly, the Wood-Ljungdahl pathway (reductive acetyl-CoA pathway, WLP) condenses two molecules of CO₂ to one molecule of acetyl-CoA, operating through two metabolic branches: the methyl- and the carbonyl-branch. As in organisms that use the rTCA cycle, Pfor then converts acetyl-CoA to pyruvate. So far, organisms that rely on the rTCA cycle for CO₂ fixation have not yet been employed for bioproduction in industry, while organisms that employ the WLP have been utilized for the production of various industrially relevant chemicals.

A prominent example is the obligate anaerobic acetogenic bacterium *Clostridium autoethanogenum*, which was engineered at LanzaTech to produce ethanol, acetone and isopropanol from waste carbon such as industrial emission gasses from or syngas in a net carbon-negative process⁶⁸. Syngas fermentation was also demonstrated in *Clostridium ljungdahlii*, other *Clostridium* species and *Alkalibaculum bacchi* for the production of ethanol and acetate depending on culturing conditions, and high pressure fermentation of *Acetobacter woodii* resulted in the production of acetone, acetate and formate^{69–72}. While the use of CO₂ or CO₂-species has been widely applied for the production industrially relevant products, organisms that assimilate CO₂ require an external energy source such as light or hydrogen in order to grow. Methanol on the other hand can be used as both the energy and the carbon source by natural methylotrophs, which poses a major advantage over CO₂.

1.3 Natural versus Synthetic Methylotrophy

Methylotrophy is defined as the ability to utilize reduced C1 substrates such as methanol and methylamine to produce energy in form of reducing equivalents and biomass through carbon assimilation via different pathways.

To utilize methanol, natural methylotrophs possess methanol oxidation pathways, which may either fully oxidize methanol to CO₂ for energy generation, or partially oxidize it to formaldehyde or formate, which can then enter central metabolism through different routes. For the oxidation to formaldehyde, methylotrophs possess methanol dehydrogenases (MDHs), which require different cofactors and metals depending on the organism, as for example the Ca²⁺-dependent MxaF and the lanthanide-dependent XoxF MDH⁷³. For subsequent assimilation of the C1 compound into biomass there are six major naturally occurring assimilation pathways, which support growth on methanol. In aerobic organisms, pathways that use O₂ as the electron donor include the Ribulose-monophosphate pathway (RuMP), the Xylulose-monophosphate pathway (XuMP), the serine cycle and the CBB cycle, while anaerobic organisms use the WLP or the reductive glycine pathway (rGly). The RuMP is the most widespread pathway, employed by a variety of aerobic methylotrophs like *Bacillus methanolicus* and Type I methanotrophs like *Methylococcus capsulatus* and uses ribulose-5 phosphate (Ru5P) as formaldehyde acceptor for C1 assimilation, which also contributes to formaldehyde detoxification^{74,75}. The key enzymes of the RuMP are a 3-hexulose-6-phosphate synthase (Hsp) and the phosphor-3-hexuloisomerase (Phi). This pathway is generally

considered as the most efficient natural C1 assimilation route in terms of ATP consumption and biomass production by using reduced C1 compounds as the sole source of carbon and energy, generating one molecule of pyruvate from 3 molecules of formaldehyde⁷⁶. The XuMP pathway is another formaldehyde assimilation pathway, which is mostly found in methylotrophic yeasts such as *Pichia pastoris* and uses xylulose 5-phosphate (Xu5P) as its formaldehyde acceptor. For methanol oxidation, these methylotrophic yeasts rely on the alcohol oxidase (Aox), to oxidize methanol to formaldehyde. Key enzymes for subsequent assimilation are the dihydroxyacetone synthase (Das) and dihydroxyacetone kinase (Dak).

Another aerobic C1 assimilation pathway is the serine cycle, which is found less frequently than the RuMP pathway. Despite its higher energetic cost compared to the RuMP, the serine cycle can lead to higher theoretical carbon yield for acetyl-CoA-derived products, as the RuMP loses carbon through CO₂, and is especially suitable for the synthesis of reduced compounds from methanol. The serine cycle is found in many methylotrophic bacteria, predominantly in α -proteobacteria like *Methylobacterium extorquens*, and allows the assimilation of different C1 compounds. Methylene-THF (tetrahydrofolate) serves as an entry point of C1 assimilation into biomass *via* the serine cycle. While formaldehyde can react spontaneously with tetrahydrofolate (THF) to form methylene-THF, the more common route for C1 assimilation in *M. extorquens* is the oxidation of formaldehyde to formate *via* the tetrahydromethanopterin-dependent (H₄-MPT) dissimilation pathway, where it is condensed with THF by a formate-tetrahydrofolate ligase (FtfL, ATP-dependent) to formyl-THF, reduced to 5,10-methenyl-THF by the Formyl-THF cyclohydrolase (Fch), and then converted to 5,10-methylene-THF by 5,10-methenyl-THF dehydrogenase (Mtd)⁷⁷. In the serine cycle, glycine is used as the 5,10-methylene acceptor and forms serine.

These natural C1 assimilation pathways have served as a blueprint for the design of synthetic methylotrophy, and throughout recent years, multiple studies have worked on the implementation of synthetic methylotrophy in model organisms such as *E. coli*, *S. cerevisiae* and *Corynebacterium glutamicum*. One great advantage for building methylotrophy through this bottom-up approach is the availability of a vast genetic engineering toolbox, which greatly facilitates the progress of synthetic strain development. For the *in vivo* implementation of synthetic pathways, selection strains are essential tools, which facilitate the development of microbial cell factories⁷⁸. To develop metabolic dependency on the synthetic route, genetic deletions are introduced, to create an auxotrophy, which is relieved by the utilization of the synthetic route, efficiently coupling the pathway to growth. This has been used in the past to

establish the RuMP pathway in *E. coli*^{79,80}. Another common strategy to improve the establishment of synthetic routes in these selection strains is adaptive laboratory evolution (ALE). ALE allows the accumulation of mutations through specific selection conditions and continuous culture propagation, yielding an adapted strain with a beneficial phenotype. This method has also been widely applied to establish synthetic methylotrophy in *E. coli* and *S. cerevisiae* through implementation of the RuMP pathway, which in some cases enabled growth with methanol as the sole carbon source^{81–83}.

Another example for successful establishment of synthetic methylotrophy is the reductive glycine pathway (rGlyP), in which the first few reactions mirror the natural serine cycle, while the subsequent synthesis of glycine is achieved by reversal of the native glycine cleavage system. The rGlyP was shown to lead to higher biomass yields from CO₂ and formate in *C. necator*, demonstrating how synthetic pathways can outperform their natural counterparts, in this case the CBB⁸⁴. The homoserine cycle is another synthetic route, which was built as an alternative to the serine cycle and relies on the activity of two promiscuous formaldehyde-condensing aldolases, and is predicted to be more efficient than any of the naturally occurring C1 assimilation pathways in terms of synthesis of acetyl-CoA derived products⁸⁵.

Although synthetic methylotrophy has great potential for industrial applications, the introduction synthetic pathways *in vivo* encounters several challenges. The main drawback of synthetic C1 assimilation routes is the lack of established methanol oxidation and formaldehyde assimilation pathways in the target organism. This greatly limits growth rates due to insufficient MDH activities and/or regeneration of formaldehyde acceptor molecules. While several efforts to establish synthetic methylotrophy in *E. coli* have been successful, further optimization to mitigate these metabolic bottlenecks are needed^{80,86–89}. This requires codon-optimization, finding a suitable source for heterologous enzymes or the employment of ALE⁷³. Furthermore, while most model organisms already contain formaldehyde detoxification pathways, which decreases the issue of formaldehyde toxicity, these often need to be knocked out to ensure efficient formaldehyde assimilation to enable growth on methanol. This, can in turn lead to increased formaldehyde sensitivity or low methanol consumption and growth rates^{79,90}. Therefore, the greatest challenge for the implementation of synthetic methylotrophy lies within balancing and rewiring metabolic fluxes between synthetic pathways and native metabolism, which requires extensive engineering.

This poses one great advantage of natural methylotrophs, as methanol oxidation and formaldehyde assimilation pathways are already established, while formaldehyde detoxification works in favor of C1 assimilation, alleviating the need for further metabolic engineering. Despite the immense advances in the establishment of synthetic methylotrophy in model organisms, native methylotrophs still hold great potential for the development of a microbial production platform for the production of reduced compounds⁹¹. Essentially, methylotrophic strain development for bioindustry could be achieved through a top-down or bottom-up approach and to date, high-level production for target compounds does not meet industrial needs. While the development of a production strain from natural methylotrophs comes with some disadvantages, the greatest limitation being the availability of genetic tools for metabolic engineering, they harbor great potential for the production of value-added compounds from methanol for industry.

1.3.1 *Methylobacterium extorquens*

Methylobacterium extorquens AM1 has been a model organism for methylotrophy for several decades. As previously mentioned, this facultative methylotroph is able to utilize methanol and other C1 substrates such as formate and methylamine as the sole source of carbon and energy through the serine cycle. The central carbon metabolism of *M. extorquens* consists of an interconnected network of three major pathways, the serine cycle, the Tricarboxylic Acid (TCA) cycle, the Ethyl-Malonyl-CoA pathway (EMCP) as well as the Polyhydroxybutyrate (PHB) cycle. The EMCP has been the focus for genetic engineering in many studies, as it harbors valuable CoA esters, which have been used for the production of biofuel precursors such as 1-butanol⁹² and isobutanol⁹³, platform chemicals for polymer and resin industry like itaconic acid⁹⁴ and polyhydroxyalkanoates^{95,96} and various other compounds like the terpenoid α -humulene⁹⁷ or mevalonate⁹⁸. While the AM1 strain more well-known and has been used in the production of several industrially relevant compounds in the past, *M. extorquens* PA1 may prove as a more suitable strain for industrial applications. The AM1 strain contains the 5.5 Mb chromosome, a 1.3 Mb megaplasmid and three smaller plasmids and grows faster on rich medium than the PA1 strain. In contrast, *M. extorquens* PA1 does not contain any additional plasmids, and grows faster on minimal medium. Hence, the PA1 strain has gradually become more interesting for genetic engineering studies. However, one of the greatest limitations in the development of *M. extorquens* as a microbial production strain is the lack of genetic engineering tools.

1.3.2 Metabolic engineering toolbox for *M. extorquens*

In the last two decades, multiple studies worked on expanding the toolkit for non-model organisms, which led to the improvement of genetic engineering strategies. While methods such as the cre-lox system⁹⁹ or the sucrose-counterselection sacB-based vector system¹⁰⁰ have been used frequently for genetic modifications in the past, more modern methods for genetic modification include the prominent Clustered Regulatory Interspaced Short Palindromic Repeat (CRISPR) system, which allows easier and more flexible gene editing. CRISPR-Cas-based tools are under constant development and include methods for the construction of genetic knockouts, up-or downregulation of target genes, base-editing or insertions¹⁰¹ in non-model organisms.

Recently, CRISPRi has been employed in *M. extorquens* for the targeted downregulation of genes. This system regulates gene expression on an RNA level in a less disruptive fashion than genetic knockouts. Originally derived from the *Streptococcus pyogenes* CRISPR system, this knockdown system consists of an inactivated (dead) Cas9 (dCas9) and a single guide RNA (gRNA)¹⁰². The mutations that cause the loss of endonuclease activity in dCas9 are located in the RuvC-like (D10H) and the HNH (H840A) nuclease domain. The dCas9 enzyme forms a complex with a gRNA, which is able to efficiently target genes of interest resulting in a 99.9% gene repression. The gRNA contains a 20 nt base-pairing region which is complementary to the target DNA sequence and a trans-activating CRISPR RNA (tracrRNA) and a hairpin structure which forms a complex with dCas9. The complementary sequence of the gRNA can be modified to target a specific gene of interest with high accuracy and minimal off-target effects¹⁰³. Previously, CRISPRi has successfully been implemented in *M. extorquens*¹⁰⁴. This was shown through the downregulation of multiple genes such as the housekeeping gene *glyA*, an *mCherry* reporter gene and the native gene for a phytoene desaturase *META1_3670*. Besides modifications on a genomic level, the introduction of heterologous genes is an important part of engineering organisms. Vector systems that have successfully been used for heterologous gene expression in *M. extorquens* include broad-host range cloning single copy pABC vectors¹⁰⁵, the widely used pCM80-family plasmids (pCM80, pCM160)¹⁰⁶ and the very recently developed pBBR1-derivative pMis1_1B¹⁰⁷.

Despite this limited toolbox, recent studies have demonstrated the possibility of engineering a strain of *M. extorquens* that has potential for more accessible production of EMCP-derived carboxylic acids by replacing the EMCP with the glyoxylate shunt.

1.3.3 The Glyoxylate cycle as an alternative to the Ethyl-Malonyl-CoA Pathway

The serine cycle releases acetyl-CoA as product, which is efficiently assimilated in *M. extorquens* via the Ethyl-Malonyl-CoA pathway (EMCP), (Figure 2). This route was discovered nearly 20 years ago by Erb, Fuchs and colleagues¹⁰⁸ as an alternative pathway for acetyl-CoA assimilation in isocitrate lyase negative strains. This pathway allows the generation of C5 compounds from C2 starting units with the crotonyl-CoA carboxylase/reductase (Ccr) as its key enzyme. Throughout this pathway, two molecules of acetyl-CoA are converted to β -methylmalyl-CoA, which is subsequently cleaved into glyoxylate and propionyl-CoA. While glyoxylate is fed back into the serine cycle to form glycine, several steps convert propionyl-CoA to succinyl-CoA and to succinate in the TCA cycle. Hence, to assimilate C1 and C2 substrates, *M. extorquens* depends on the EMCP to regenerate glyoxylate¹⁰⁹. In nature more routes exist to assimilate acetate and acetyl-CoA. The most dominant of which is the glyoxylate cycle (also referred to as glyoxylate Shunt) which was first described in 1957 by Kornberg and Krebs¹¹⁰. It is one of the major routes for the assimilation of C2 compounds and can be found across different phyla including bacteria, plants and fungi. As in the TCA cycle, the first step of the glyoxylate cycle is the condensation of acetyl-CoA with oxaloacetate by citrate synthase, which is then isomerized to isocitrate by an aconitase. Isocitrate is then cleaved into glyoxylate and succinate by an isocitrate lyase (AceA), which is the first key enzyme of the glyoxylate cycle. The second key enzyme is a malate synthase (AceB), which condenses the resulting glyoxylate with another molecule of acetyl-CoA forming malate, which can be used to replenish the central TCA cycle intermediate oxaloacetate. While many organisms employ the glyoxylate cycle to assimilate acetyl-CoA, some organisms like *M. extorquens* and purple non-sulfur bacteria lack AceA, one of the key enzymes for the glyoxylate cycle. The next section briefly discusses previous work done for generating EMCP-deficient strains of *M. extorquens* and implementation of the glyoxylate shunt for glyoxylate regeneration.

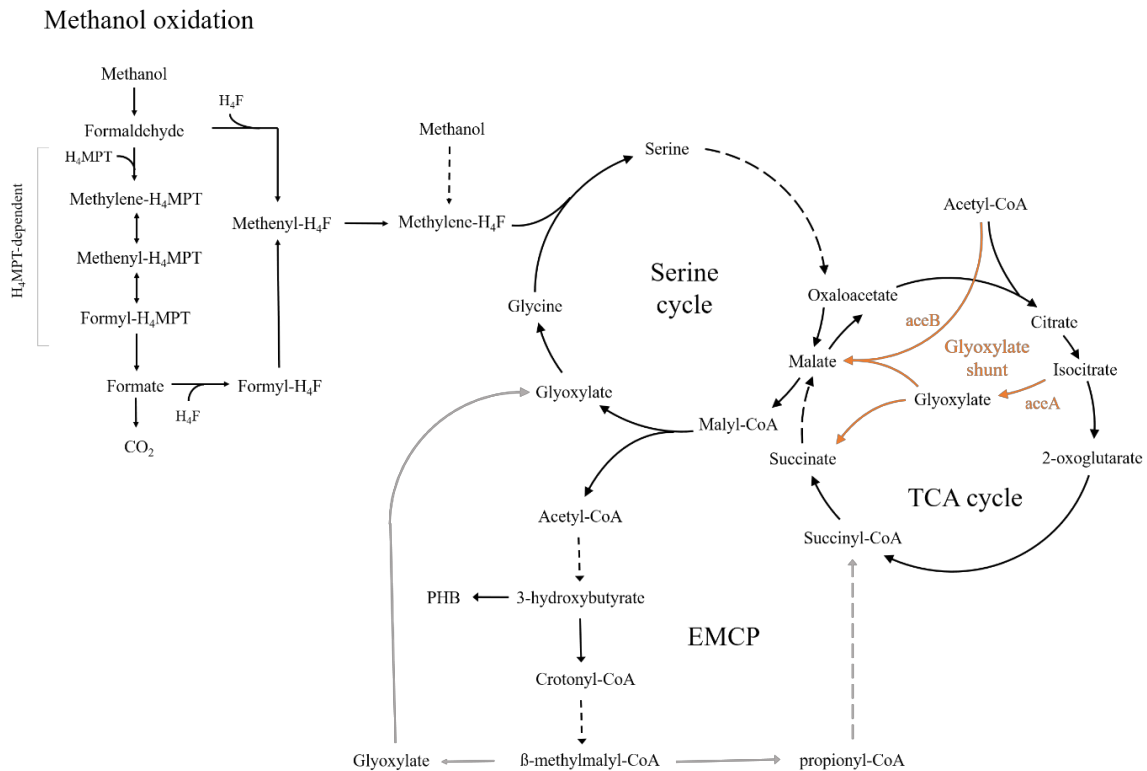


Figure 2: Methanol oxidation and central carbon metabolism in *M. extorquens*, including serine cycle, TCA cycle and EMCP. Grey lines show steps of the EMCP which are missing in the strains containing a Δccr deletion, which then depend on the glyoxylate shunt (orange) for regeneration of glyoxylate.

1.3.4 Related work

The first study that demonstrated the potential of carboxylic acid production from a downregulated EMCP was conducted by Sonntag and colleagues, who focused on the production of the EMCP-derived acids mesaconic acid and (2S)-methylsuccinic acid. Here, the production of these two acids was demonstrated by employing YciA and by cultivation on low-cobalt methanol medium, thereby reducing the activity of the cobalt-dependent mutases of the EMCP¹¹¹. This resulted in the production of mesaconic and (2S)-methylsuccinic acid with a yield of 0.17 g/g methanol.

The study that first reported the successful replacement of the EMCP with the glyoxylate shunt in *M. extorquens* AM1 was conducted by Schada von Borzyskowski and colleagues¹¹². After introducing the glyoxylate shunt on the multi-copy pCM80 plasmid in EMCP-deficient strains and confirming that enzymes were produced at sufficient levels, they tested whether the

glyoxylate shunt rescued growth on methanol, formate and methylamine. However, no growth was detected during cultivation with C1 substrates, but the glyoxylate shunt could rescue growth on acetate. They attributed this to the low activity of key enzymes of methanol oxidation, as methanol- and formate dehydrogenase had only 25% and 85% of wildtype activity, respectively. Additionally, they suspected the cause for the inability of the strain to grow on methanol by low flux through the TCA cycle during methylotrophic growth, which is enhanced during growth on acetate where growth could be restored through the glyoxylate shunt^{109,113}. In a proof-of-principle, they added the unspecific YciA thioesterase from *E. coli* on the pCM80 plasmid, which also contained the glyoxylate shunt. As the strain initially did not produce any detectable amounts of crotonate, they redirected the carbon flux from the glyoxylate shunt to the EMCP by adding 3-Nitropropionate (inhibitor of AceA) and by feeding 3 mM acetate every 24 h, which yielded 35 μ M crotonate.

In follow-up work (personal communication), the same Δccr strain with the glyoxylate shunt and YciA on the pCM80 plasmid was evolved to achieve growth on methanol. Through 52 serial transfers on liquid methanol medium growth of the Δccr strain was significantly improved and mutations in Prk and Icd were suspected to have significant impact on carbon flux redirection towards the glyoxylate shunt. This evolved strain did not produce detectable amounts of crotonate from methanol, whereas acetate feeding and 3-NP addition achieved 25 μ M crotonate. Here, the colleague suspected PHB synthesis and promiscuity of YciA to be the reason for the low crotonate concentrations. Taken together, specific production of crotonate from methanol in *M. extorquens* remains an open challenge.

2. Aim of this thesis

The goal of this work was to develop a strain of *M. extorquens* PA1 that effectively utilizes the glyoxylate shunt in place of the EMCP for C1 assimilation to grow on wildtype-like levels during growth on methanol. For this, I performed ALE in *M. extorquens* PA1, which is deficient in the EMCP at the step of the crotonyl-CoA reductase (Δccr). Initial introduction of the glyoxylate shunt on the multi-copy pCM80 plasmid did not support growth of the EMCP-deficient strain on methanol as the sole carbon source. Through 45 serial transfers of liquid methanol minimal medium, growth of Δccr significantly improved, yielding strain *P45*. I then analyzed the *P45* for mutations that led to the improved growth phenotype through whole genome sequencing and identified mutations in key enzymes, which cause a redistribution of

carbon flux in central carbon metabolism with high likelihood. I also identified changes in protein abundance in *P45* compared to the wildtype, which showed an upregulation in stress-response proteins and a downregulation of transcriptional and translational regulators involved in formaldehyde homeostasis. Through further growth characterization I demonstrated that *P45* has increased tolerance to formaldehyde, and shows wildtype-like growth during cultivation in a chemostat bioreactor on formate and methanol. Furthermore, *P45* has wildtype-level biomass yield during chemostat growth on formate, while biomass yield from methanol even surpassed the wildtype. To utilize the evolved strain for the production of crotonate from methanol, I attempted to eliminate the PHB synthesis pathway as the competing pathway for EMCP-derived acid production. I therefore developed different strategies for the introduction of a CRISPR interference system, targeting *ccr* and *phaC* in collaboration with the lab of Prof. Anke Becker (Synmikro, Marburg). I then tested the expression of the CRISPRi machinery from different plasmids and promoters in $\Delta phaC$ and Δccr knockout strains and evaluated the viability of the resulting strains for their growth on methanol. The first design was a two-plasmid system, where dCas9 was expressed from the single-copy pABCjx plasmid, while the gRNA was expressed from a multi-copy pCM80-derivative plasmid, while both modules were under the control of strong constitutive promoters. As this system strongly reduced growth of the wildtype on methanol, I switched the dCas9 promoter for an IPTG-inducible promoter, and expressed both dCas9 and gRNA from the single copy plasmid. However, introduction of this system in Δccr and $\Delta phaC$ knockout strains did not allow growth on methanol regardless of inducer presence. To reduce potential leakiness effects, I exchanged the gRNA promoter for the inducible promoter as well, and evaluated growth of the wildtype, Δccr and $\Delta phaC$. Here, I could show that the knockdown affects growth of the wildtype upon induction, while Δccr with a *phaC* knockdown was not affected, and the knockdown of *ccr* in $\Delta phaC$ resulted in cell death. To find more suitable candidates for the knockdown in Δccr and $\Delta phaC$, I designed a mismatch gRNA to alter binding capacities of the CRISPRi machinery and evaluated growth on methanol of the wildtype, Δccr and $\Delta phaC$.

3. Materials & Methods

3.1 Cell cultivation

M. extorquens PA1 was cultivated in defined minimal medium with 30 mM succinate, 123 mM methanol or in M9 medium containing 80 mM formate as carbon source in baffled flasks (Table 1-3). Cultures were incubated at 30°C and 160 rpm. Chemically competent NEB Turbo *E. coli* cells were used for construction and amplification of plasmids. Cultures of *E. coli* were grown in Lysogeny Broth (LB) medium at 37°C and 180 rpm. Antibiotic concentrations for both organisms are listed in Table 4. Due to the ability of *M. extorquens* to grow on ethanol as a carbon source, tetracycline was dissolved in water instead.

Table 1: Stock solutions for minimal media preparation.

Solutions for autoclaving:		
Mineral salts		
	Stock solution	Final media concentration [mM]
NH ₄ Cl	4.86 g	30.29
MgSO ₄ · 7 H ₂ O	0.60 g	0.81
Deionized water	600 mL	
Phosphate Buffer pH 6.7		
	Stock solution	Final media concentration [mM]
K ₂ HPO ₄	4.77 g	9.13
NaH ₂ PO ₄ · 2H ₂ O	5.40 g	11.54
Deionized water	600 mL	
Phosphate Buffer pH 7.1		
K ₂ HPO ₄	4.80 g	13.78
NaH ₂ PO ₄ · 2H ₂ O	2.16 g	6.92
Deionized water	600 mL	
Succinate stock solution		
Succinic acid disodium salt hexahydrate	41.65 g	30.83
Deionized water	500 mL	
2 x Agar	3 g/100 ml	

Table 2: Iron and trace element solutions.

Solutions for sterile filtering (0.22 µm filter):		
Iron solution (1000x)	Stock solution	Final concentration [µM]
Na ₂ EDTA · 2H ₂ O	2.16 g	6.92
FeSO ₄ · 7H ₂ O	3.00 g	10.79
MilliQ water	1000 mL	
Trace element solution I (1000x)	Stock solution	Final concentration [µM]
ZnSO ₄ · 7H ₂ O	4.50 g	15.65
CoCl ₂ · 6H ₂ O	3.00 g	12.61
MnCl ₂	0.64 g	5.09
H ₃ BO ₃	1.00 g	16.17
Na ₂ MoO ₄	0.40 g	1.65
CuSO ₄ · 5H ₂ O	0.30 g	1.20
CaCl ₂ · 2H ₂ O	3.00 g	20.41
MilliQ water	1000 mL	

Add all trace elements and adjust pH to 1-2 until all salts are dissolved.

Table 2: Iron and trace element solution (continued)

Solutions for sterile filtering (0.22 µm filter):		
Trace element solution II (100x)	Stock solution	For 1L
CuCl ₂ · 2H ₂ O	1.70 g/100 mL	765 µl
CoCl ₂ · 6H ₂ O	4.76 g/100 mL	210 µl
H ₃ BO ₃	0.62 g/100 mL	1.6 mL
MnCl ₂ · 6H ₂ O	19.8 g/100 mL	8.1 µl
ZnCl ₂		84 mg
FeCl ₃ (anhydrous)	498 mg	

Dissolve 5 g EDTA in 800 mL water and adjust the pH to 7.5 with NaOH. Then add the components mentioned above and add deionized water to the final volume of 1L.

Table 3: Media recipes for *M. extorquens* on different carbon sources.

Media preparation for growth on methanol	For 1L
Buffer pH 7.1	300 mL
Mineral salts	200 mL
Sterile water or 2 x Agar	493 mL
Sterile MeOH	5 mL
Iron solution	1 mL
Trace element solution I	1 mL

Media preparation for growth on succinate	For 1L
Buffer pH 6.7	200 mL
Mineral salts	200 mL
Sterile water or 2 x Agar	498 mL
Succinate stock solution	100 mL
Iron solution	1 mL
Trace element solution I	1 mL

Media preparation for growth on formate/ formic acid	For 1L
5 x M9 salt solution	200 mL
Trace element solution II	10 mL
1M MgSO ₄	2 mL
1M CaCl ₂	0.1 mL
Sodium formate/ formic acid	5.44 g/ 3.08 mL
Deionized water	790 mL

First add MgSO₄ and then add CaCl₂ slowly while stirring constantly to avoid precipitation.

Table 4: Antibiotics and their corresponding concentrations used in this study.

Antibiotic	Stock concentration [mg/ml]	Final concentration [µg/ml]
Kanamycin	50	50
Tetracycline	10	10
Spectinomycin	50	50

3.2 Electroporation of *M. extorquens*

For electrocompetent cells, a preculture was grown overnight in succinate minimal medium with the appropriate antibiotic selection marker, and inoculated to $OD_{600} = 0.01$. Cells were harvested at mid-log phase (OD_{600} of 0.8 – 1.5), spun down (4000 rpm, 4°C), washed twice with one volume of cold, sterile water and once with ½ volume of cold, sterile 10% glycerol solution. Cells were resuspended in 1/100 volume of the same glycerol solution and aliquots of 50 µl were shock-frozen with liquid nitrogen and stored at -70°C. Electroporation was done with ~ 500 ng of DNA in cold electroporation cuvettes (1 mm gap) with a pre-set bacterial program (1.8 kV, 5 ms time constant). Cold nutrient broth was added immediately after the pulse and cells were transferred into a 2 mL Eppendorf tube. Cells were incubated at 30°C and 160 rpm for at least 2.5 h for regeneration. Cells were plated in appropriate dilutions on minimal medium agar plates containing the corresponding carbon source and antibiotic for selection. Plates were incubated at 30°C for 2 - 4 days until colonies appeared.

3.3 Adaptive laboratory evolution

To evolve *M. extorquens* PA1 strains for improved growth on methanol, the initial strain (P0) from a succinate liquid culture was plated on a solid agar plate containing methanol and incubated at 30°C. Once colonies appeared, they were inoculated in liquid methanol medium and grown to mid-exponential phase. The culture was split and diluted in three flasks containing the same medium and incubated at 30°C and 160 rpm to stationary phase (first round of evolution). The culture which first reached an OD_{600} of 2-3 was used to inoculate the next round of evolution. Each passage was saved as a cryo stock and stored at -70°C for follow up experiments.

3.4 Cultivation of *M. extorquens* in a bioreactor

Strains of *M. extorquens* PA1 were grown in precultures of minimal medium or minimal M9 medium with either 123 mM methanol or 80 mM formate added. Cells were grown to late exponential/ stationary phase (OD_{600} of 2 – 3 for methanol, 0.4 – 0.6 for formate) and inoculated in 1L bioreactor volume. The bioreactor vessel was a DASGIP GPI-100 vessel OD110 x H255mm, flat bottom with an advanced stirrer (suitable for 500 – 1500 ml reactor volume) and equipped with an L-Sparger for aeration. The pH was set to 7 and controlled with acid (2M HCl) and base (2M NaOH) pumps, which operated with a shot volume of 1 ml, flow rate of 40 ml/h and at a set deadband of 0.2. The system was aerated with synthetic air (79%

nitrogen, 21% oxygen) and an air flow of 60 sL/h for 1L of reactor volume. Dissolved oxygen concentration was controlled by agitation and monitored with a polarographic electrochemical sensor. The temperature measured through an internal thermometer and was kept at 30°C through integrated heating pads in the DASGIP® vessel block. Growth was monitored through optical density measurement with an NIR turbidity sensor. For every bioreactor cultivation, the system was cleaned properly and filled with the cultivation medium. The pH probe was calibrated in a two point calibration with calibration solutions of pH = 7 (first point) and pH = 4 (second point), after which the system was autoclaved at 120°C for 20 min. Afterwards, the DO sensor was calibrated in a two point calibration procedure. The first point at 100% DO saturation was taken by agitation and gassing under cultivation conditions (400 rpm, 60 sL/h) and the system was left to equilibrate for 20 min. For the second point of the calibration, the DO probe was disconnected from the system until DO reached 0%. Lastly, the pumps for acid, base and medium pumping were calibrated. For this, the pump tubes were attached to needles and filled with 70% ethanol. The needles were then attached to 50 ml falcon tubes with punctured lids, which were previously weighed. The weight of the falcon tubes was entered into the DASGIP® software. For calibration, the pump speed was set to max. relevant procedure conditions (e.g. 40 ml/h) and volume was pumped for 1h. Afterwards, the filled falcon tubes were weighed and the new value served for pump calibration in the DASGIP® software. Finally, cultivation was started by inoculation of the preculture.

3.4.1 Chemostat cultivation

For a chemostat cultivation, *M. extorquens* was grown in precultures with M9 minimal medium and Methanol or formate. Cells were inoculated in 1 L of the same medium and all parameters were set as mentioned previously. After sufficient growth had occurred (OD₆₀₀ of 0.8 – 1.5 for methanol, OD₆₀₀ of 0.4 – 0.6 for formate), cells kept in mid-log phase by pumping fresh medium at different dilution rates. A flow rate of 40 ml/h in 1L bioreactor volume corresponds to a dilution rate of 0.04h⁻¹. Bioreactor volume was kept at a consistent level by adjusting a metal tube inside the reactor to the initial volume level and attaching a pump to it, which constantly removed excess volume at maximum speed. For cultivations on formate, the pH was controlled by titration of fresh formic acid medium (pH = 3.5 – 3.7) into the reactor at a given flow rate. For methanol cultivations, pH was regulated by pumping acid or base as mentioned previously.

3.4.2 Biomass yield measurements

For the determination of biomass yields, aluminum trays were dried for two days in an oven at 90°C. The weight of the trays was determined after trays were cooled down to RT in a dessicator. For cell dry weight (CDW) measurement, 50 ml sample volume was harvested from fresh waste of a chemostat bioreactor cultivation in three replicates. Samples were centrifuged at 4000 x g and cell pellets were washed twice with deionized water. The washed cell pellet was resuspended in 1 ml deionized water and loaded onto the dried aluminum trays. Samples were dried for two days at 90°C, cooled down to RT in a dessicator and weighed to determine cell dry weight (CDW). The measured CDW was divided by the collected sample volume to calculate harvested gCDW/L culture volume. The yield was calculated by dividing gCDW/L by the moles of carbon source, under the assumption that all carbon is consumed.

3.5 Bioconversion growth assays

Strains for the bioconversion assays were grown in precultures containing succinate as carbon source and the appropriate antibiotics for selection. After cells reached an OD₆₀₀ of 3-4, the culture was harvested by centrifugation at 4000 x g for 15 min. The resulting cell pellets were washed twice with sterile deionized water and resuspended in flasks containing minimal medium with methanol as carbon source and 1 mM IPTG. Growth was monitored over 96 h by measuring OD₆₀₀, and samples for exometabolomic analysis were taken after 2, 6, 24 and 96 h.

3.6 Whole genome sequencing

Strains for sequencing were streaked out on agar plates with succinate as carbon source (+ selection marker) and subsequently inoculated in 20 ml liquid medium containing succinate (+ selection marker) in baffled flasks. Cultures were grown at 30°C 160 rpm for two days until stationary phase was reached (OD₆₀₀ 2-3). Cell pellets from 5 ml of culture were harvested by centrifugation at 4000 x g at RT. Genomic DNA was then prepped using the NucleoSpin® Microbial DNA Kit from Macherey Nagel. The cell pellets were resuspended with 100 µl Elution Buffer BE. Then, 40 µl of Buffer BE and 10 µl Protein Kinase were added to the cell suspension, which was then transferred into a bead tube (MN Tube B) and cells were lysed by agitation for 10-12 minutes. Subsequent washing steps were conducted according to the user

manual of the preparation kit. The quality and quantity of prepped gDNA was assessed by NanoDrop measurements. Approximately 100 ng of gDNA were sent to Novogene for microbial whole genome sequencing.

3.7. Sample preparation for Exometabolome Analysis

For the analysis of the exometabolome, 1 ml of sample volume was taken from growing cultures and centrifuged at 4000 x g for 10 min. The supernatant was filtered with a PTFE filter and samples were snap frozen with liquid nitrogen and stored at -20°C until measurement.

3.8. Sample preparation for Endometabolome Analysis

For endometabolomic analysis, a quenching solution (70% MeOH, 30% deionized water (v/v)) was prepared. 1 ml of quenching solution was added to a 2 ml Eppendorf tube and frozen at -70°C for two days before sampling. On the day of sampling, 1 ml of culture volume was added to the tubes containing the quenching solution in a pre-cooled aluminum rack, inverted once and centrifuged at 13.000 x g for 10 min at -9°C. In the meantime, samples for CDW determination or OD₆₀₀ measurement were taken. The supernatant of the samples was removed carefully with a syringe and cell pellets were snap frozen with liquid nitrogen and stored at -70°C until further processing. For endometabolome extraction, the extraction fluid was made by combining 5 ml MeOH (LC-MS grade) with 5 ml TE buffer pH = 7 (10 mM TRIZMA, 1 mM EDTA), which, along with Chloroform, was stored at -20°C at least 12h before extraction. The necessary volume for extraction fluid was calculated based on the CDW or OD₆₀₀ measurement taken on the day of sampling (extraction volume = 200 x biovolume (CDW), or 200 µl extraction fluid for 1 ml culture volume of OD₆₀₀ = 1). The calculated amount of extraction fluid and the same volume of chloroform was added to the cell pellet on a pre-cooled (-20°C) aluminum rack and samples were vortexed in short intervals. Samples were incubated in a shaker at 4°C for 2h. Phase separation was achieved through centrifugation, and the upper phase was extracted carefully with a syringe. The syringe needle was exchanged with a PTFE filter and the sample was filtered into a new Eppendorf tube, snap frozen with liquid nitrogen and stored at -70°C until measurement.

3.9 Sample preparation for Proteomics

Cells were cultivated in 20 ml liquid minimal medium containing succinate and methanol to stationary phase. To avoid quantitative variation, a total OD₆₀₀ 3 was harvested for every sample. These culture samples were centrifuged and the resulting cell pellet was washed twice with ice cold PBS. Buffer was removed and cells were freeze dried with liquid nitrogen and stored at -70°C until further processing. For protein extraction, 200 µl Lysis Buffer (2% SDS in 100 mM Ammoniumbicarbonate) were added to the cell pellets and cells were lysed at 90°C for 15 min. The cell suspensions were then lysed via sonication for 30 s to shear DNA, and centrifuged for 5 min at 14.000 rpm. The clear lysates (supernatant) were then used for acetate precipitation by addition of six sample volumes of ice cold acetate and one sample volume of ice cold methanol. The mixtures were then vortexed and incubated for two hours at -20°C. After centrifugation (max. speed), and careful removal of supernatant, the pellets were washed thoroughly with 200 µl ice cold methanol and vortexed. The washing step was repeated once and the pellets were air dried, after which they were reconstituted by addition of 0.5 % SDS and heat incubation for 10 min until the pellets dissolved. Protein concentration was then determined by BSA assay. Afterwards, 5 µl TCEP (Tris (2-carboxyethyl)phosphine hydrochloride; 40 x dilution in volume lysis buffer) were added, samples were vortexed, incubated for 15 min at 90°C and cooled down to RT. The samples were spun down to remove the liquid from the lid and 5 µl of freshly prepared iodoacetamide (40 x dilution, 74 mg/ml) were added, after which the sample was vortexed and incubated at 25°C for 20 min in the dark due to light sensitivity of iodoacetamide. After incubation, 50 µg of total protein were added to a new tube. Protein digestion was started by addition of trypsin to a final enzyme/protein ratio of 1:50 and incubation at 30°C overnight. The next morning, samples was spun down and TFA (5% trifluoroacetic acid in HPLC grade water) was added to a final concentration of 1.5% (pH must be < 2). Samples were centrifuged at 14.000 rpm for 10 min at 4°C until the supernatants were clear. Supernatants were then used for solid phase extraction. For this, C18 columns were placed in an Eppendorf tube, conditioned with 400 µl Buffer 1 (100% Acetonitrile) at 200 rpm for 30 s and then equilibrated with 400 µl Buffer 2 (50% Acetonitrile / 50% water (v/v)) at 300 rpm for 30 s. Samples were loaded onto the equilibrated columns at 300 rpm for 2 min and washed once with 400 µl Buffer 3 (5% Acetonitrile/ 95% water (v/v) and 0.1% TFA). Columns were then loaded onto a new tube and bound peptides were eluted by addition of 400 µl Buffer 1 and quickly spun down at 200 rpm for 30 s to dry the column completely. The eluted peptide mixtures was then concentrated through vacuum drying, after

which they were reconstituted in 100 μ l Buffer 5 (0.1% TFA) and vortexed for 10 s. Finally, samples were filled into LC vials and stored at -20°C until measurement.

To compare the results of the Wt and the evolved P45 Δccr , I calculated the log₂-fold ratio of protein abundance and summarized all strongly differentially expressed proteins. I initially identified 2112 proteins that were differentially expressed, which ranged from 0.01 – 10 log₂-fold change. To filter for relevant candidates, I set the cutoff to a ≥ 2 -fold change. Significance cutoff was set to < 0.01 .

3.10 Enzyme assays

3.10.1 Isocitrate dehydrogenase activity assay

Activity assays for Icd were carried out on 37°C in 200 μ l reaction volume containing 50 mM HEPES buffer pH 7.5, 10 mM MgCl_2 , 1.5 mM NADP^+ , 4 μ M purified icd and 0.01 – 10 mM DL-isocitrate. The production of NADP(H) was monitored at 340 nm with a thermostated Cary 300 UV-Vis spectrophotometer. Enzymatic activity was calculated with a molar extinction coefficient of 6.22 $\text{mM}^{-1}\text{cm}^{-1}$. Enzyme kinetics at given substrate concentrations were measured in three replicates. The assays were started by addition of substrate after establishing a baseline reading at 340 nm.

3.10.2 Formate dehydrogenase assay

The formate dehydrogenase enzyme assay was employed to detect residual formate in supernatants of our bioreactor cultivation during biomass yield determination. Here, the formation of NADH from NAD^+ and HCOO^- catalyzed by the FDH is monitored over the measurement cycles by the NADH specific absorption at 340 nm.

3.11 Plasmids

The CRISPRi knockdown plasmids in this study were constructed and provided by Doreen Meier (RG Becker, Synmikro).

Table 5: Plasmids used in this study.

Name	Genetic content	Selection marker	Insert description	Source
pCM80-Glyox.	pCM80_pcoxB-aceAB_pmxAF-yciA	Tet	Glyoxylate shunt under the control of pcoxB, thioesterase <i>ycaA</i> under control of pmxAF	RG Erb
pABCjx	repABC-rrnB T2 terminator	Kan	Single copy plasmid for expression of dCas9 and/or gRNA	RG Becker
pEQT-H-Li	pEQT-H-Li-PJ ₃₂₁₁₉ -gRNA	Tet	Derivative of pCM80 for gRNA expression in two-plasmid CRISPRi system (Figure 15)	RG Becker
pABC-J30	pABCjx_LP2F_PA1/o4/o3-dCas9_pmxAF-gRNA30	Kan	Knockdown plasmid with inducible dCas9 and constitutive gRNA targeted against <i>ccr</i> (Supplementary Figure 7)	RG Becker
gRNA- <i>ccr</i> (J30)	pABCjx_LP2F_PA1/o4/o3-dCas9_PA1/o4/o3-gRNA30	Kan	Knockdown plasmid with inducible dCas9 and gRNA targeted against <i>ccr</i> (Figure 16; Figure 17)	RG Becker
gRNA- <i>ccr</i> (J31)	pABCjx_LP2F_PA1/o4/o3-dCas9_PA1/o4/o3-gRNA30	Kan	Knockdown plasmid with inducible dCas9 and gRNA targeted against <i>ccr</i>	RG Becker
gRNA- <i>ccr</i> (J32)	pABCjx_LP2F_PA1/o4/o3-dCas9_PA1/o4/o3-gRNA30	Kan	Knockdown plasmid with inducible dCas9 and gRNA targeted against <i>ccr</i>	RG Becker
gRNA- <i>phaC</i> (J39)	pABCjx_LP2F_PA1/o4/o3-dCas9_PA1/o4/o3-gRNA39	Kan	Knockdown plasmid with inducible dCas9 and gRNA targeted against <i>phaC</i>	RG Becker
gRNA- <i>phaC</i> (J40)	pABCjx_LP2F_PA1/o4/o3-dCas9_PA1/o4/o3-gRNA39	Kan	Knockdown plasmid with inducible dCas9 and gRNA targeted against <i>phaC</i> (Figure 16; Figure 17)	RG Becker

gRNA- phaC (J41)	pABCjx_LP2F_PA1/o4/o 3-dCas9_PA1/o4/o3- gRNA39	Kan	Knockdown plasmid with inducible dCas9 and gRNA targeted against <i>phaC</i>	RG Becker
gRNA-nt (J48)	pABCjx_LP2F_PA1/o4/o 3-dCas9_PA1/o4/o3- gRNA39	Kan	Knockdown plasmid with inducible dCas9 and non-targeting gRNA	RG Becker
-	pTwist Amp icd _{F156C}	Amp	Multi copy plasmid containing mutated icd _{F156C}	Twist Bioscience

3.12 Oligos

All oligos used in this study are listed in Table 6. Sequences for the mismatched gRNA library can be found in the supplementary information (Supplementary Table 1, Supplementary Table 2).

Table 6: Oligos used in this study.

Name	Sequence (5' – 3')	Description
021_pCM80 seq-fw	TTATGCTTCCGGCTCGTATG	Amplification of pCM80-P _{coxB} -aceAB-P _{mx} aF-y <i>ci</i> A
022_pCM80 seq-rv	TCGCAATCGGAGGTGATCAGATCC	Amplification of pCM80-P _{coxB} -aceAB-P _{mx} aF-y <i>ci</i> A
421_ccr-rv	CCAACAGGGAGTGCCACG	Control for <i>ccr</i> knockout.
422_ccr-fw	GCCGAGGCCTGCTTGAGG	Control for <i>ccr</i> knockout.
426_phaC-fw	GAGCTTCTCGATGACGTG	Another primer to check the <i>phaC</i> deletion.
427_phaC-rv	CTTGTCGGAGTCGAGAAG	Another primer to check the <i>phaC</i> deletion.
428_pCM80-seq-fw	CCGCAAGGCCCGCGATAC	Sequencing primer to confirm presence of pCM80.
429_pCM80-seq-rv	GGCTGCCGGGGATTGCCTC	Sequencing primer to confirm presence of pCM80.
434_icd_F156C - fw	GCCTCACCATCAAGTaCGAGGGTGACGAC	Remove mutation in <i>icd</i> through overlap PCR.
435_icd_F156C - rv	GTCGTACCCTCGtACTTGATGGTGAGGC	Remove mutation in <i>icd</i> through overlap PCR.
gRNA 30	GCCGTCTGCCCCGGTCCAGGC	Guide RNA for <i>ccr</i> in plasmid J30.
gRNA 31	TCGCCCTTGTGCACGTCGAA	Guide RNA for <i>ccr</i> in plasmid J31.
gRNA 32	GAACAGCATGCGGTAGGCCG	Guide RNA for <i>ccr</i> in plasmid J32.
gRNA 39	TCCGCCCGCATCCCCGCCCG	Guide RNA for <i>phaC</i> in plasmid J39.
gRNA 40	TGTCTCCGCGACCCGCGTGA	Guide RNA for <i>phaC</i> in plasmid J40.
gRNA 41	TTCGTCATCACGAAGTTCGA	Guide RNA for <i>phaC</i> in plasmid J41.

3.13 Strains

Deletion strains used in this study were constructed previously through *sacB*- mediated allelic exchange with sucrose counterselection as described in Marx et al. 2008¹⁰⁰. *M. extorquens* Δccr strains for ALE were constructed and provided by Doreen Meier (RG Becker, Synmikro), (Table 7).

Table 7: Strains used in this study.

Name	Relevant Genotype	Description	Creator
Wildtype	Δcel	Deletion in cellulose synthase	RG Becker
Δccr	$\Delta cel\Delta ccr$	Δcel + deletion in crotonyl-CoA reductase	RG Becker
$\Delta phaC$	$\Delta cel\Delta phaC$	Δcel + deletion in polyhydroxybutyrate synthase	RG Becker
<i>P0</i>	$\Delta cel\Delta ccr$ pCM80-aceAB-yciA	Deletion in <i>cel</i> and <i>ccr</i> . Contains glyoxylate shunt plasmid.	RG Becker
<i>P11</i>	$\Delta cel\Delta ccr$ <i>attB C31 LP1</i> pCM80-aceAB-yciA	Based on <i>P0</i> . Product of ALE after 11 serial transfers. Mutations are described in Table 11. Contains landing pads for serine integrases (<i>attB C31 LP11</i>)	RG Becker
<i>P21</i>	$\Delta cel\Delta ccr$ <i>attB C31 LP1</i> pCM80-aceAB-yciA	Based on <i>P0</i> . Product of ALE after 21 serial transfers. Mutations are described in Table 11. Contains landing pads for serine integrases (<i>attB C31 LP11</i>)	RG Becker
<i>P38</i>	$\Delta cel\Delta ccr$ <i>attB C31 LP1</i> pCM80-aceAB-yciA	Based on <i>P0</i> . Product of ALE after 38 serial transfers. Mutations are described in Table 11. Contains landing pads for serine integrases (<i>attB C31 LP11</i>)	This study
<i>P45</i>	$\Delta cel\Delta ccr$ <i>attB C31 LP1</i> pCM80-aceAB-yciA	Based on <i>P0</i> . Product of ALE after 45 serial transfers. Mutations are described in Table 11. Contains landing pads for serine integrases (<i>attB C31 LP11</i>)	This study

4 Results

4.1 Optimization of the glyoxylate shunt in *M. extorquens* PA1

To develop a strain which exclusively relies on the glyoxylate shunt for C1 and acetate assimilation, the Becker lab previously introduced a plasmid encoding isocitrate lysase (*aceA*) and malate synthase (*aceB*), which together form the glyoxylate shunt (pCM80-Glyox.), into an EMCP-deficient *M. extorquens* PA1 strain (Δccr). To improve growth on methanol ALE was performed which is where I joined the project. Additionally, one lineage of Δccr was constructed, which contained landing pads for serine integrases that allow the genomic integration of genetic cargo.

The aim of my PhD was the optimization of methylotrophic growth via the glyoxylate shunt to create a promising chassis for production of the EMCP intermediate crotonate. Hence, I first assessed how far the ALE had progressed by determining the growth phenotypes on methanol and succinate (as a positive control media). To compare the improvements in methylotrophic growth at different stages of the ALE experiment of Δccr pCM80-Glyox. (+/- landing pads), I saved an aliquot of each culture before transfer for the next round of evolution. For simplification, I will henceforth refer to each strain with the number of passages that were conducted up to this point (e.g. *P11* for eleven transfers on liquid medium). The initial strain *P0*, where pCM80-Glyox. was newly introduced, did not show any growth on methanol (Supplementary Figure 1). I characterized methylotrophic growth of the intermediate strain *P11* and *P21*, without landing pads (LP) (Figure 3, Table 8).

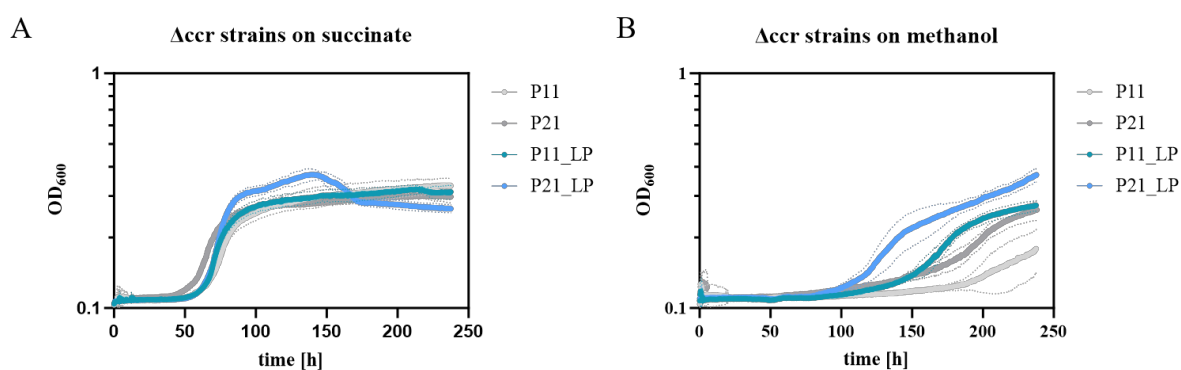


Figure 3: Methylotrophic growth characterization of evolved Δccr strains after 11 (*P11*) and 21 (*P21*) transfers with and without landing pads (+/- LP). Strains were grown in medium containing (A) 30 mM succinate or (B) 123 mM methanol. Each line represents five biological replicates.

Table 8: Growth rates of evolved Δccr strains on succinate and methanol. Growth rates were calculated in Matlab.

Strain	Succinate $\mu[h^{-1}]$	Methanol $\mu[h^{-1}]$
<i>P11</i>	0.138 ± 0.002	0.051 ± 0.004
<i>P21</i>	0.138 ± 0.005	0.080 ± 0.007
<i>P11_LP</i>	0.121 ± 0.017	0.040 ± 0.013
<i>P21_LP</i>	0.117 ± 0.006	0.084 ± 0.020

While the parent strain was unable to grow on methanol, methylotrophic growth of intermediate strains of the ALE was significantly improved after ten transfers, regardless of the presence of integrated landing pads, while growth on succinate was not changed and remained similar among all characterized strains. In strains without landing pads, the growth rate on methanol was improved from $0.051 \pm 0.004 \text{ h}^{-1}$ (*P11*) to $0.080 \pm 0.007 \text{ h}^{-1}$ (*P21*), while the strains containing landing pads showed a similar trend from $0.040 \pm 0.013 \text{ h}^{-1}$ (*P11_LP*) to $0.084 \pm 0.020 \text{ h}^{-1}$ (*P21_LP*). While the methylotrophic growth of the strains had already increased it still did not approach the performance of the wild-type at growth rates of 0.14 h^{-1} (5 h doubling time) and still showed a long lag phase. To improve the strains performance further I decided to continue the ALE experiment.

Based on the characterization results I chose strain *P21_LP*, as the landing pads may prove useful for future applications and since they did not seem to have a significant impact on growth. This strain will be referred to as *P21* in the following chapters. The ALE of this strain yielded even further improved growth on methanol in flask cultivations after 45 total transfers (24 passages since passage 21) (Figure 4, Table 9). While the growth rate of *P45* of 0.138 h^{-1} was not yet at wildtype-level I decided to stop the ALE experiment as smaller increases in growth rate were expected to take much longer when approaching the maximal growth rate¹¹⁴ and since the growth rate was comparable to growth of other organisms on C1 substrates^{115,116}. In order to assess potential heterogeneity within the population, single colonies of selected passages were tested for their methylotrophic growth on single colony level. From this I determined that the single colonies did in fact represent the phenotype of the evolved population (Supplementary Figure 2).

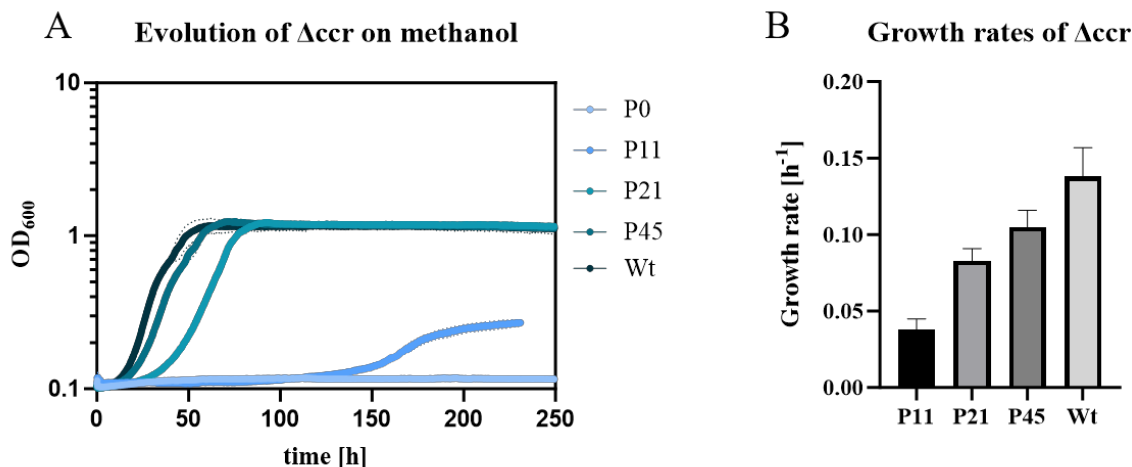


Figure 4: Growth assays on methanol of evolved Δccr strains at different stages of the ALE (*P11*, *P21*, *P45*), the parent strain *P0* (Δccr pCM80-Glyox.) and the wildtype (Wt). (A) Growth assays were conducted in medium containing 123 mM methanol. (B) Growth rates on methanol were calculated for each passage of our ALE and the Wt via Matlab. Each growth assay was conducted in three biological replicates.

Table 9: Growth of evolved Δccr strains from the ALE on methanol compared to the parent strain *P0* and the wildtype (Wt).

Strain	Doubling time [h]	Growth rate [h^{-1}]	Timepoint of fastest Doubling time [h]
<i>P0</i>	n.g.	-	-
<i>P11</i>	18.2 ± 3.6	0.038 ± 0.007	158.7 ± 4.2
<i>P21</i>	8.3 ± 0.8	0.083 ± 0.008	54.2 ± 4.8
<i>P45</i>	6.6 ± 0.7	0.105 ± 0.011	29.0 ± 0.7
Wt	5.0 ± 0.7	0.138 ± 0.019	20.9 ± 0.9

In *P45*, I was able to further improve the growth rate on methanol ($0.105 \pm 0.011 h^{-1}$) although there still was a significant difference to the Wt ($0.138 \pm 0.019 h^{-1}$, $p = 0.042$). Notably, the timepoint of the fastest doubling time, which was calculated via Matlab and serves as an indicator for the end of lag phase had decreased, therefore indicating further adaptation to the methylotrophic growth conditions. While *P11* has a long lag phase ($158.7 \pm 4.2 h$), this point is reached significantly earlier in *P21* (54.2 ± 4.8 , $p < 0.0001$), and much earlier in *P45* ($29.0 \pm 0.7 h$) approaching that of the Wt ($20.9 \pm 0.9 h$).

In previous work on *M. extorquens* AM1 $\Delta ccr + pCM80-Glyox.$, an improvement of methylotrophic growth resulted in an inability to grow on acetate due a lower flux through the TCA cycle, caused through mutations during ALE. Therefore, I also conducted a growth assay

comparing growth of *P45* to the wildtype on acetate, succinate and methanol (Figure 5). During characterization of the evolved *P45* strain on different carbon sources I observed the previously described lower growth rate of *P45* ($0.116 \pm 0.036 \text{ h}^{-1}$) compared to the Wt ($0.135 \pm 0.073 \text{ h}^{-1}$) on methanol, as well as succinate *P45* ($0.200 \pm 0.075 \text{ h}^{-1}$), Wt ($0.274 \pm 0.099 \text{ h}^{-1}$). Interestingly, growth on acetate was reduced in *P45* ($0.114 \pm 0.015 \text{ h}^{-1}$) compared to the Wt ($0.165 \pm 0.086 \text{ h}^{-1}$), indicating metabolic changes that occurred throughout ALE.

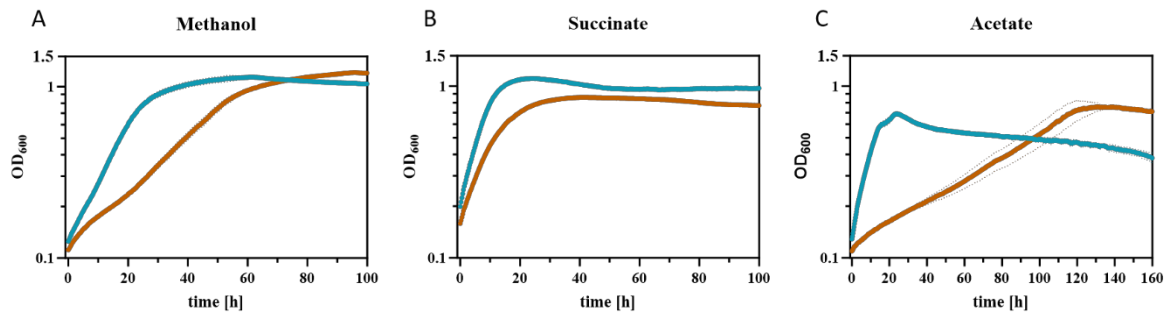


Figure 5: Growth of Wt (teal) and *P45* (orange) in medium containing (A) 123 mM methanol, (B) 30 mM succinate or (C) 30 mM acetate. Each assay was conducted in five biological replicates.

4.2 Glyoxylate shunt adaptation enables wildtype-level biomass yields

Since methylotrophic growth of the evolved strain *P45* had increased significantly compared to the parent strain, I next intended to determine and compare the biomass yield of the improved strain *P45* to the Wt on methanol using chemostat bioreactor cultivations. Chemostat cultivations are ideal for biomass determination as cells are maintained at exponential phase and the growth yield per dilution rate can be obtained, allowing accurate yield determination without influence of wasteful lag and stationary phases. This experiment also marks the first chemostat comparison of the methylotrophic growth of a serine cycle using microbe with the EMCP option for glyoxylate regeneration compared to a serine cycle + glyoxylate shunt option. To calculate the maintenance demands and theoretical maximum yield I determined the biomass yields at several dilution rates (Figure 6). I also determined the biomass yield of the *P45* and Wt strain during growth on formate as reliable literature values for this were lacking. As this might also allow improved crotonate production, I took samples for exometabolome analysis, which will be discussed in the next section. During the cultivations in the bioreactor I observed strong differences between the strains.

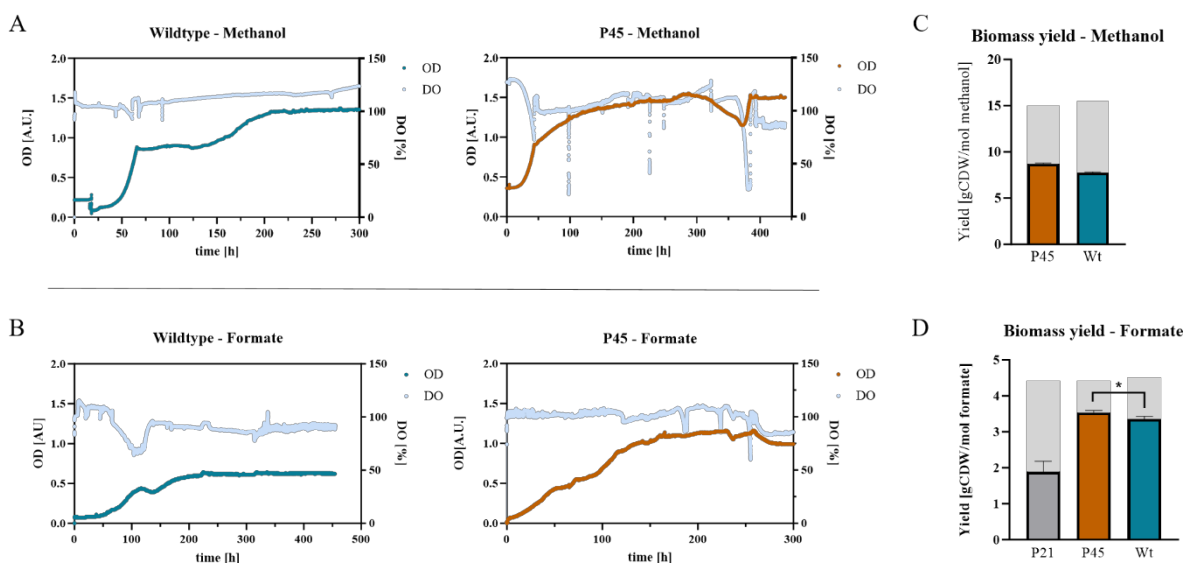


Figure 6: Bioreactor cultivation of Wt (teal) and the evolved *P45* (orange) in 1L culture volume chemostat mode. (A) Cultivation with methanol as sole carbon source. The pH was controlled by titration of HCl and NaOH throughout cultivation. (B) Growth on formate as sole carbon source. The pH was controlled by titration of formic acid. (C) Biomass yield on methanol with a dilution rate of 0.024 h^{-1} for *P45* and Wt. (D) Biomass yield of *P45* and Wt during growth on formate at a dilution rate of 0.024 h^{-1} , and 0.040 h^{-1} for *P21*. The theoretical optima were deduced from Cotton et al. 2020 and are indicated with faint grey bars. The bars for both biomass yield experiments each represent three biological replicates. Complete formate consumption was confirmed via an FDH assay (Supplementary Figure 4).

Biomass yield from methanol was significantly enhanced for *P45* ($8.70 \pm 0.05 \text{ gCDW/mol}$ methanol) compared to the Wt ($7.73 \pm 0.08 \text{ gCDW/mol}$ methanol). Here, however, yields were far below the theoretical optimum, which are $\sim 15 \text{ gCDW/mol}$ methanol for the glyoxylate shunt, and $\sim 15.5 \text{ gCDW/mol}$ methanol for the EMCP according to a report from Cotton et al.¹¹⁷. These low yields may be the result of a relatively low dilution rate during the cultivation (0.02 h^{-1}), as higher dilution rates should result in a higher biomass yield as the growth rate increases, lowering the effects of cellular maintenance (non-growth associated maintenance, NGAM). The report from Cotton et al. also stated theoretical optima of biomass yields during growth on formate using the serine cycle and either the EMCP or the glyoxylate shunt. As experimentally assessed yields during growth on formate mentioned in this report surpassed the theoretical optimum, I next determined biomass yield on formate. With this, I simultaneously investigated whether the evolved strain may have an advantage over the Wt regarding methanol assimilation. Here, I expected the overall biomass yield in both the Wt and *P45* to be lower on the less reduced formate than on methanol since fewer reducing equivalents can be deduced from this compound.

During bioreactor cultivation on formate, the Wt showed no pronounced lag-phase during initial batch cultivation, reached a high culture density (OD [A.U.] = 1.5) and remained stable at the dilution rates from 0.012h⁻¹ to 0.040 h⁻¹. At the lowest dilution rate of 0.012 h⁻¹ the Wt reached a biomass yield of 3.24 ± 0.02 gCDW/mol formate, which increased steadily to 3.64 gCDW/mol formate at a dilution rate of 0.040 h⁻¹. In contrast, the bioreactor batch cultivation of *P21* resulted in a pronounced lag-phase during batch cultivation and an overall lower optical density in chemostat mode (OD [A.U.] = 1.0; Supplementary Figure 3), which consequently resulted in a much lower biomass yield of 1.9 gCDW/mol formate at the maximum tested dilution rate of 0.040 h⁻¹. The cultivation of *P45* was similar to the Wt, with steady growth and an overall high optical density (OD [A.U.] = 1.1). Here, however, I did not observe an increase in biomass yield with an increase of the dilution rate. At the lowest dilution rate, the evolved strain reached a biomass yield of 3.75 ± 0.23 gCDW/mol formate, which appeared to be the maximum yield, as *P45* reached 3.42 ± 0.40 gCDW/mol formate at 0.014 h⁻¹ and 3.53 ± 0.04 gCDW/mol formate at 0.024 h⁻¹. While these yields show that both the Wt and *P45* are lower than the theoretical optimum, which lies at approx. 4.5 gCDW/mol formate for the Wt (HP/MC/EM) and at approx. 4.4 gCDW/mol formate for *P45* (HP/MC/GX)⁸⁷, they match expected experimental values, which usually are below the proposed optimum. As biomass yields of *P45* on both methanol and formate matched Wt yields, these results reflect a well-functioning glyoxylate shunt.

Table 10: Biomass yields in methanol and formic acid medium at different dilution rates. Each value is the result of three replicates.

Dilution rate [h ⁻¹]	Biomass Yield [gCDW/mol methanol]		
	Wt		<i>P45</i>
0.020	7.73 ± 0.08		8.70 ± 0.05

Dilution rate [h ⁻¹]	Biomass Yield [gCDW/mol formate]		
	Wt	<i>P21</i>	<i>P45</i>
0.012	3.24 ± 0.02	-	3.75 ± 0.23
0.014	3.10 ± 0.21	-	3.42 ± 0.40
0.024	3.35 ± 0.05	-	3.53 ± 0.04
0.040	3.64 ± 0.19	1.9 ± 0.3	-

4.3 Crotonate production and degradation in *P45*

With the much more optimized strain in hand I next set out to test preliminary production of crotonate. Since the plasmid containing the glyoxylate shunt also harbored the thioesterase encoding gene *yciA* and with the EMCP disrupted *via* deletion of *ccr* I expected to produce crotonate when growing on methanol. To test this I performed an experiment in shake flasks and took samples for LC/MS during early exponential phase (OD_{600} of 0.8 – 1.0), late exponential phase (OD_{600} of 1.2 – 1.6), and stationary phase (OD_{600} of 2 – 2.5). To assess intracellular crotonyl-CoA levels, I prepared samples for endometabolomics, while I analyzed crotonate production through exometabolomics, assuming crotonate would be excreted by the cells. Unfortunately, the evolved strain did not produce any crotonate, and crotonyl-CoA levels did not differ from the wildtype (Figure 7). In fact, the engineered strain show almost no detectable crotonate production whereas I detected up to 5 μ M crotonate in the wildtype strain.

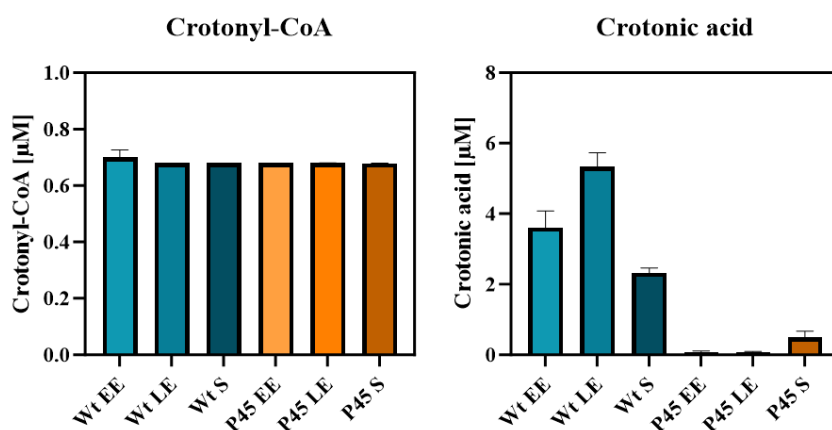


Figure 7: Crotonyl-CoA and Crotonate production in the final evolved strain *P45* compared to the wildtype (Wt). Samples to evaluate crotonyl-CoA and crotonate production were taken during early exponential (EE), late exponential (LE) and stationary phase (S). Each bar represents three biological replicates.

As cultivation conditions in flasks, however, do not provide ideal growth and production conditions, which in may in turn result in the observed low crotonate levels. I therefore expected cultivation in a bioreactor during chemostat mode to lead to higher production of crotonate, as cells are kept at a consistent growth rate in a chemostat cultivation and are therefore at their metabolic optimum, which supports maximum productivity. Hence, I analyzed exometabolomic samples from the chemostat bioreactor cultivation during growth on formate. These samples were taken every 24 h after cells reached steady-state (Figure 8).

Unfortunately, as previously observed in flask cultivations, crotonate levels remained in low micromolar range in *P45* ($0.209 \pm 0.02 \mu\text{M}$) and did not differ greatly from the wildtype ($0.205 \pm 0.02 \mu\text{M}$). Here, crotonate concentrations in the wildtype were even lower than during flask growth.

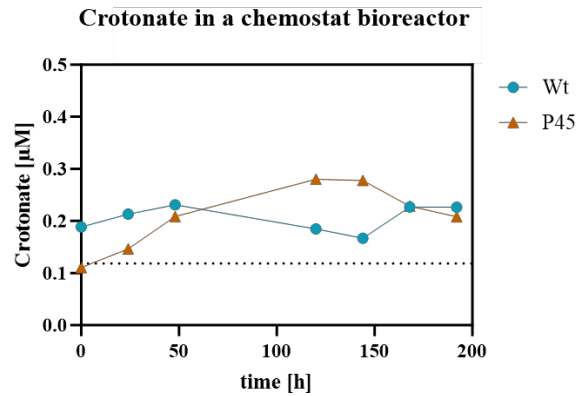


Figure 8: Crotonate production of wildtype (Wt) and *P45* during chemostat cultivation with formate as the sole carbon source.

Due to the low concentrations of crotonate in the bioreactor and flask cultivation, I suspected a reuptake of crotonate by *M. extorquens*, e.g. via the combined action of a transporter and subsequent activation to crotonyl-CoA by an acyl-CoA synthetase or transferase. In the Wt strain, crotonyl-CoA could simply be fed back into the EMCP, which does not apply for the evolved *P45*. In both strains, however, crotonyl-CoA could be re-assimilated through the β -oxidation pathway, where crotonyl-CoA is converted to 3-hydroxybutyryl-CoA by an enoyl-CoA hydratase, which could either be polymerized to PHB by PhaC or oxidized to acetoacetyl-CoA and cleaved to acetyl-CoA. I first tested whether the Wt strain would be able to grow on crotonate as the sole carbon source, which not the case (data not shown). To test whether *M. extorquens* consumes crotonate during methylotrophic growth, I added 5 mM of crotonate to our methanol growth medium and analyzed the concentration changes by taking exometabolomic samples at the beginning and the end of the experiment (Figure 9). In the beginning of the growth assay I detected $6.04 \pm 0.25 \text{ mM}$ crotonate, which decreases to $2.79 \pm 0.47 \text{ mM}$ after 216 h of cultivation, while the culture grew to a high final OD_{600} of 3.43 ± 0.69 . To confirm that this effect did not occur due to instability of crotonate at 30°C cultivation, a flask without cells was cultivated as well. Here, I did not observe any decline in crotonate concentrations (Supplementary Figure 6). This growth assay shows that *M. extorquens* indeed has the capability to activate and perhaps consume crotonate.

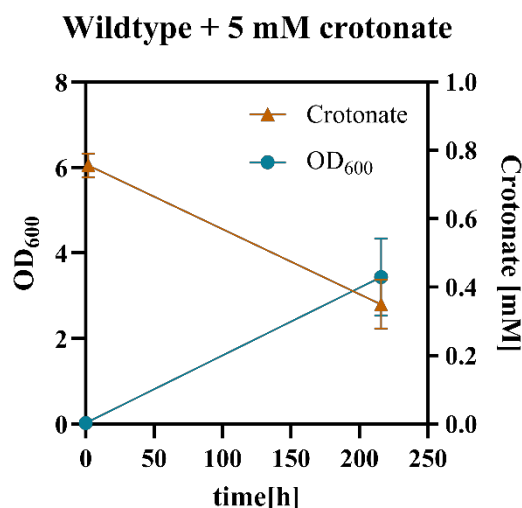


Figure 9: Growth assay of the wildtype (Wt) during flask cultivation with 123 mM methanol and 5 mM crotonate. OD₆₀₀ (teal) and crotonate content (orange) was determined at the beginning and the end of cultivation after 216 h. The growth assay was conducted in three biological replicates.

4.4 Whole genome sequencing reveals mutations in ALE

Since growth characterization revealed that the evolved *P45* strain had indeed improved methylotrophic growth considerably, I wanted to elucidate the underlying reasons for this improvement. As a first step, I analyzed several isolated clones of the evolved passages on a genomic level by whole genome sequencing using the Illumina pipeline (Novogene, Cambridge UK). In total, eight mutations had arisen during 45 transfers on methanol (Table 11). Despite the generally high frequency of non-annotated genes in the genome of *M. extorquens*, almost all mutated genes were assigned to their corresponding product with the exception of *Mext1540*, whose product is a hypothetical protein. Considering genes related to C1 or central carbon metabolism, the mutations in *prk* (T176I) and *icd* (F156C) are especially interesting. *Prk*, the product of which is phosphoribulokinase, is essential for growth on C1 substrates for its production of ribulose-1,5-bisphosphate, which is involved in transcriptional regulation and formaldehyde assimilation¹¹⁸. Both of these mutations are found in *P11*, and may therefore be found at some step between *P0* and *P11*. In *P21* a mutation was located in *Mext_0179* encoding for the β -subunit of the integration host factor (P64L). Interestingly, this is the only mutation distinguishing *P11* and *P21*, where I previously observed a pronounced growth improvement on methanol. In *P45*, additional mutations were found at the intergenic region of *Mext_1681* (glyoxylase resistance protein) and *Mext_1682* (bleomycin resistance protein), in *Mext_0925*, whose product is a MarR-family transcriptional regulator and in

Mext_2640, encoding for a FAD-dependent oxidoreductase. While sequencing results of three single colonies of each passage usually coincided, I found an additional mutation in *ppc* (Phosphoenolpyruvate (PEP) carboxylase) in one single colony of *P45* (Colony 1). PEP carboxylase plays an important role in the central carbon metabolism of *M. extorquens* by shuffling carbons between oxaloacetate (OA) and PEP. However, when comparing methylotrophic growth of the single colonies of *P45*, no benefit is seen for colony 1 (Supplementary Figure 2). To analyze the mutation in the MarR family protein, I investigated the position of the affected gene in the *M. extorquens* genome. I determined the sequence of this gene to align with *ttmR*, a transcriptional regulator involved in a stress response caused by the presence of formaldehyde. TtmR is also known to affect EfgA, another stress response regulator involved in formaldehyde sensing.

Table 11: Whole genome sequencing of *evolved* Δ *ccr* strains, the parent strain *P0* and the wildtype (Wt). Genomic DNA of three single colonies of each strain grown on solid medium containing methanol as sole carbon source was extracted and sent to Novogene for Illumina sequencing.

Gene	Product	Mutation	Wt	<i>P0</i>	<i>P11</i>	<i>P21</i>	<i>P38</i>	<i>P45</i>
[<i>Mext_0288</i>]	Ccr	Δ 1006 bp	-	+	+	+	+	+
<i>Mext_0980</i> →	Prk	T176I	-	-	+	+	+	+
<i>Mext_3141</i> ←	Icd (NADP-dependent)	F156C	-	-	+	+	+	+
<i>Mext_0179</i> ←	integration host factor, beta subunit	P64L	-	-	-	+	+	+
<i>Mext_1681</i> ← / → <i>Mext_1682</i>	Glyoxylase/ bleomycin resistance	intergenic (-657/-51) G→C	-	-	-	+	+	+
<i>Mext_0925</i> ←	MarR	coding (453/588 nt) Δ 1 bp	-	-	-	-	+	+
<i>Mext_1540</i> →	hypothetical protein	coding (410/663 nt) Δ 1 bp	-	-	-	-	+	+
<i>Mext_2640</i> →	FAD-dependent oxidoreductase	R116C	-	-	-	-	+	+

4.5 Mutation F156C decreases isocitrate dehydrogenase activity

As part of the TCA cycle, Icd shares its substrate (isocitrate) with the isocitrate lyase of the glyoxylate shunt. In a previous study, it was hypothesized that the successful implementation of the glyoxylate shunt as an alternative to the EMCP would require increased flux towards the heterologous pathway in order to support growth on methanol¹¹². Since I observed significant improvement in methylotrophic growth in *P11*, I suspected that the mutation in Icd lowered its enzymatic activity, hence resulting in decreased flux of the TCA cycle and increased flux through the glyoxylate shunt. Indeed, testing the enzymatic activity of the mutated Icd_{F156C}

showed that activity towards isocitrate was reduced 4-fold compared to the Wt enzyme, with a k_{cat} of $0.336 \mu\text{mol}/\text{min}$ (Wt: $1.620 \mu\text{mol}/\text{min}$) and a K_m of 0.159 mM (Wt: 0.065 mM) (Figure 10). I therefore concluded that the mutation in Icd is one of the main contributors to flux redistribution towards the glyoxylate shunt.

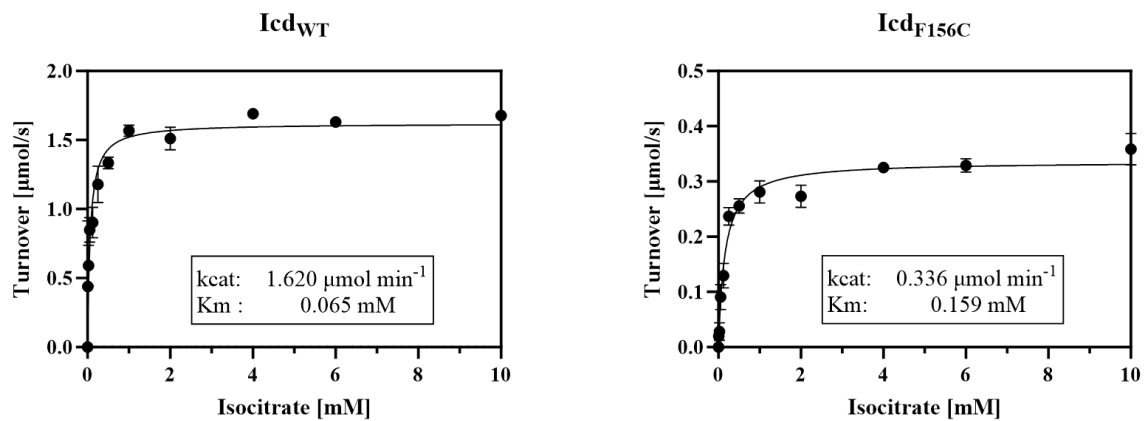


Figure 10: Enzyme activity assays of wildtype (Wt) Icd and mutated Icd (F156C). Sequences synthesized by Twist Bioscience were introduced on pTE5323 for protein expression in *E. coli* BL21-A1 cells and purified with the His-Tag. Assays were conducted with varying concentrations of DL--isocitrate.

4.6 Changes in the proteome of P45

To investigate the cellular changes of the evolved strains on the proteome level, I performed label-free proteomics analysis for relative abundance estimation of the wildtype and *P45* strains during growth on methanol. To compare the results of the two strains I summarized all strongly differentially expressed proteins as a ratio of the evolved strain over the Wt (Figure 11) and enzymes for all pathways of central carbon metabolism of *M. extorquens* (Figure 12). I initially identified 2112 proteins that were differentially expressed, which ranged from 0.01 – 10 -fold change. To filter for relevant candidates, I set the cutoff to a ≥ 2 -fold change, leaving us with 110 proteins, 73 of which were upregulated while 37 were downregulated. Here, I found proteins involved in stress response among the most upregulated proteins.

Among these were Hsp20 (molecular chaperone of the Hsp family), which was the most upregulated protein in our evolved strain (+ 8.51-fold), Gst (glutathione S-transferase, + 7.16-fold), EshA (late growth phase protein, + 5.49-fold) and MexAM1_META1p3731 (Crp/Fnr-family protein, + 5.62-fold). Other strongly upregulated proteins with diverse functions in *M. extorquens* were MexAM1_META1p0466 (PepSY-domain containing protein, + 7,01-fold) and of MexAM1_META1p0970 (oleate hydratase, + 6.86-fold). In central carbon metabolism

of *M. extorquens*, I found an upregulation of proteins of the serine cycle, among which were Sgat (serine-glyoxylate aminotransferase, + 1.64-fold), Hpr (hydroxypyruvate reductase, + 1.30-fold), Ppc (PEP carboxylase, + 2.14-fold), MtkA/B (malate thiokinase, + 1.87-fold / 2.07-fold) and Mcl (malyl-CoA lyase, + 1.87-fold). Proteins involved in the TCA or the EMCP, on the other hand, were not found to be differentially expressed, with the exception of Ccr due to the genetic deletion (- 4.76-fold). The reason for this relatively low downregulation is explained by the genetic deletion having left a small truncated rest of the gene (293 bp), which can still produce a small number of peptides (19 in total) that are detectable in proteomic analysis. While Icd and Prk were not upregulated, the potentially altered Prk activity could have activated the LysR-family protein QscR (Quayle Serine Cycle Regulation), indirectly explaining the upregulation of essential serine cycle genes in the evolved strain. While multiple LysR-family proteins were found in the proteomics analysis, only one of them was upregulated by 1.18-fold which could be QscR.

Additionally, proteins involved in methanol oxidation, which are also regulated by QscR, are MtdA/B (Methylene tetrahydromethanopterin dehydrogenase; + 1.54-fold) and Fch (Methenyl-THF cyclohydrolase; + 1.14-fold), which were also found to be upregulated¹¹⁹. In terms of methanol oxidation, I also found XoxF (lanthanide-dependent methanoldehydrogenase; + 1.60-fold) to be upregulated, while MxaB (-1.41-fold), MxcQE (-1.30-fold) and MxbDM were downregulated (Figure 13). The latter three proteins are transcriptional regulators involved in an intricate regulatory network and will be discussed in detail later. Another group of upregulated proteins were involved in urea degradation (UreA (+ 4.31-fold), UreC (+ 4.31-fold), UreD (+ 5.75-fold), UreE (+ 4.02-fold), UreG (+ 4.41-fold)). The reason for this, remains enigmatic, as neither does *M. extorquens* produce urea, nor is any urea added to the growth medium. I also found MetY (O-acetyl-L-homoserine sulfhydrylase) to be upregulated (2.34-fold), potentially contributing to an increased formaldehyde tolerance. For downregulated proteins I detected decreased abundance for TtmR (MarR transcriptional regulator, - 5.27-fold), which likely also caused the downregulation of EfgA (- 2.54-fold). This is in line with the findings of whole genome sequencing, where I found that the mutation introduced an early stop codon.

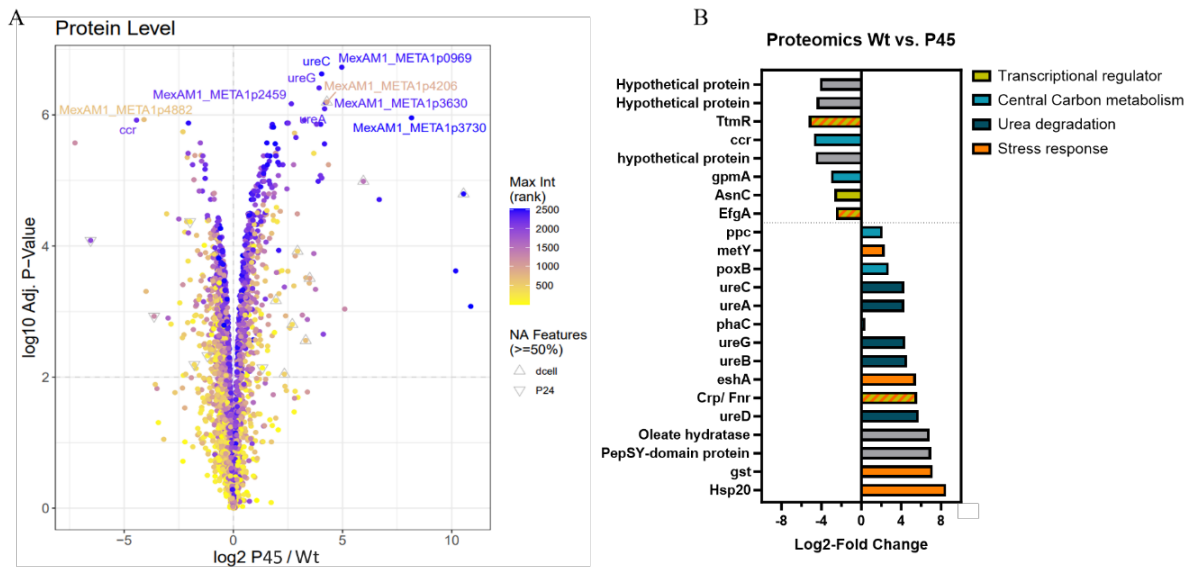


Figure 11: Differentially expressed proteins in *evolved P45* vs. wildtype (Wt) during growth on methanol. (A) Summary of most significantly up- and downregulated proteins in *P45* and their metabolic role. (B) Volcano plot of proteomics results.

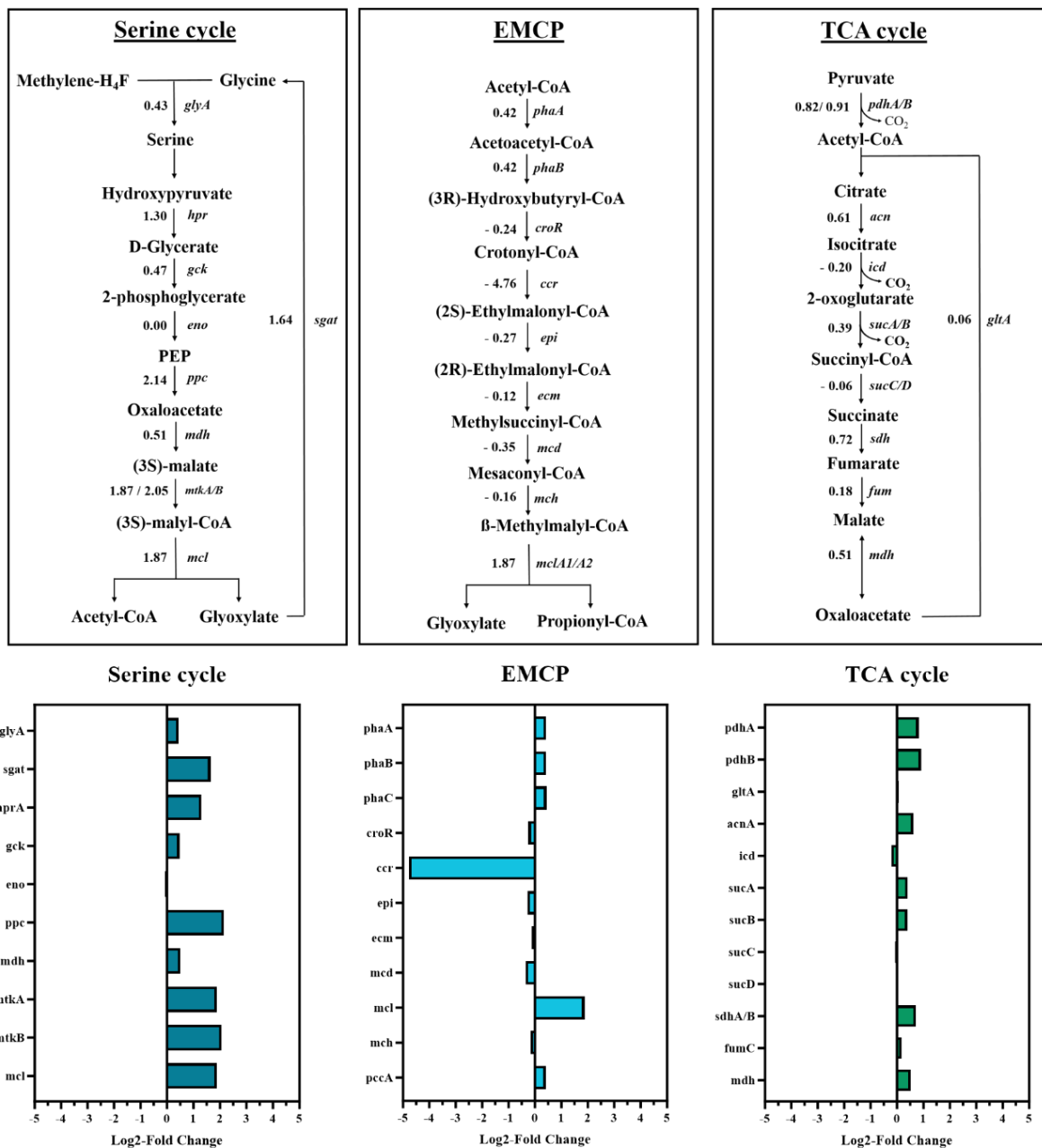


Figure 12: All enzymes of the central carbon metabolism pathways (Serine cycle, TCA cycle, EMCP) and their log₂-fold abundance change in *P45* vs. *Wt*.

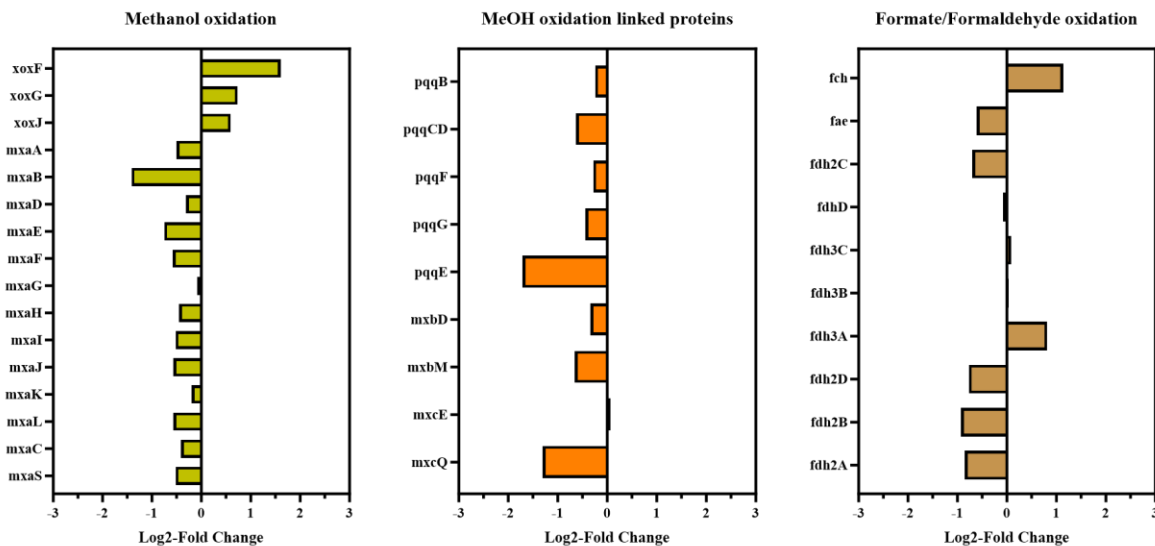


Figure 13: Differential log₂-fold abundance of proteins in evolved *P45* vs. wildtype (Wt) involved in methanol oxidation during growth on methanol.

4.7 Mutations in TtmR and EfgA confer enhanced formaldehyde tolerance

Based on the genomic and proteomic analysis, I suspected *P45* to have an increased tolerance to formaldehyde due to the strong downregulation of TtmR, likely caused by the single point mutation in the MarR transcriptional regulator discovered during whole genome sequencing, which also results in a downregulation of EfgA. Mutants in *ttmR* and *efgA* are known to have a disturbed formaldehyde homeostasis, which confers higher resistance to elevated formaldehyde levels¹²⁰. To investigate this, the wildtype and *P45* were cultured in methanol minimal medium with varying concentrations of formaldehyde (Figure 14).

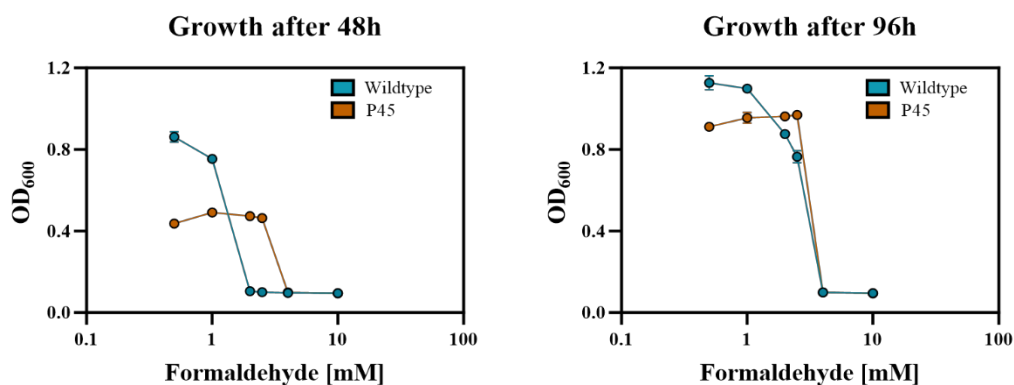


Figure 14: Formaldehyde tolerance test comparing growth of the wildtype (Wt) and *P45* after 48 h and 96 h with rising concentrations of formaldehyde. Cultures were grown in methanol minimal medium with 0, 0.5, 1, 2, 2.5, 4 and 10 mM formaldehyde. Each curve represents three biological replicates.

While the wildtype grew to a higher OD₆₀₀ than *P45* in medium with 0.5 mM formaldehyde, early growth was strongly impaired at 1 mM formaldehyde and above. In contrast, *P45* did not show any growth defects on formaldehyde levels of up to 2.5 mM, while neither of the strains grew in the presence of 4 or 10 mM formaldehyde. Overall, the growth assay shows that the evolved *P45* strain has a higher formaldehyde tolerance than the wildtype, confirming the previous assumption that the decreased abundance of TtmR and EfgA confers a tolerance to the toxic intermediate.

4.8 Utilizing CRISPR interference for targeted knockdowns in the EMCP

Through pathway engineering and optimization I developed a strain that can effectively utilize the glyoxylate shunt in a Δccr background through ALE, which resulted in improved growth on methanol and formate. As crotonate production remained low, I suspected that a great portion of the carbon flux was directed towards the synthesis of polyhydroxybutyrate (Poly-(R)-3-hydroxybutyrate, PHB), a common storage compound in α -proteobacteria that was shown to accumulate in *M. extorquens* during growth on acetate and methanol. Previous studies have demonstrated that deleting the PHB synthesis pathway or decreasing the stability of PHB granules can increase product titers^{94,121}. I therefore attempted to delete PHB synthase *phaC* to generate a $\Delta ccr\Delta phaC$ strain, which should result in strongly decreased PHB accumulation. Despite numerous attempts to introduce a *phaC* deletion in a Δccr strain, I was not able to construct the double knockout. Altering PHB metabolism has been discussed thoroughly in literature, where multiple attempts to knock out or downregulate PHB metabolism often resulted in phenotypes deficient in methylotrophic growth or lead to the emergence of suppressor mutations when *phaC* was deleted^{94,97,122,123}. A genetic knockout may therefore not be suitable for the construction of a $\Delta ccr\Delta phaC$ strain due to lethality effects.

While the cause for the observed cell death remains enigmatic, I hypothesized that cells may experience strong effects of redox imbalances due to insufficient levels of NADP(H), as both *ccr* activity and PHB synthesis involve NADP(H) consuming reactions (NADP⁺ regenerating). To circumvent this potential lethality and still achieve a similar phenotype expected for the double knockout, I explored the use of CRISPR interference (CRISPRi) for the targeted knockdown of *ccr* in collaboration with RG Becker (Synmikro, Marburg). Through the use of CRISPRi I tried to balance the downregulation of *phaC* to push carbon flux towards crotonyl-CoA while allowing a level of activity that does not result in cell death. Simultaneously, we

designed gRNAs for the knockdown of *ccr* to test the knockdown in a $\Delta phaC$ background to determine which combination of knockout and knockdown leads to the desired result of increased crotonyl-CoA and decreased PHB formation more reliably. First tests of the knockdown systems included growth assays on methanol to determine which design enables cellular growth and result in a viable strain.

4.8.1 Designs for CRISPRi for targeted knockdowns

Our first designs for the expression of the CRISPRi machinery included a two-plasmid system and a single-plasmid system, in which dCas9 (from *S. pyogenes*) and gRNA were expressed on separate plasmids or on the same plasmid. To test the knockdown variants I conducted initial growth assays in the wildtype strain during growth on methanol. Here, a strong growth deficit is expected upon induction of the CRISPRi machinery targeting *ccr* as the wildtype strain relies on a functional EMCP for C1 assimilation.

For the two-plasmid system, both modules (dCas9 and gRNA) were constitutively expressed, while dCas9 was placed on a single-copy plasmid, and gRNAs were expressed from a multi-copy plasmid. Growth assays in the wildtype showed that the knockdown through the two-plasmid system strongly inhibits cellular growth on methanol (Figure 15). Although this confirms the functionality of the knockdown, I determined that this severe impact on growth is not suitable to achieve a viable $\Delta ccr\Delta phaC$ phenotype and that decreased CRISPRi expression levels would be needed.

Therefore, we designed a single-plasmid system on a single-copy plasmid, which contained both dCas9 and a gRNA. Additionally, we switched the constitutive promoter of dCas9 to an IPTG-inducible promoter, while gRNAs remained under the control of a constitutive promoter. This way, the expression of dCas9 can be activated by addition of the inducer IPTG. Initial tests of this system in the wildtype were conducted by our collaborators and showed growth deficiencies during growth on methanol when *ccr* was knocked down, confirming the functionality of the knockdown. I then introduced the new single-plasmid system targeting *ccr* or *phaC* in the corresponding $\Delta phaC$ and Δccr knockout strains and tested methylotrophic growth behavior of the resulting strains. However, cells were once again unable to grow on methanol (Supplementary Figure 7). Here, I observed that the presence of the CRISPRi genetic constructs still result in a lethal phenotype regardless of inducer presence, suggesting leakiness of the inducible promoter.

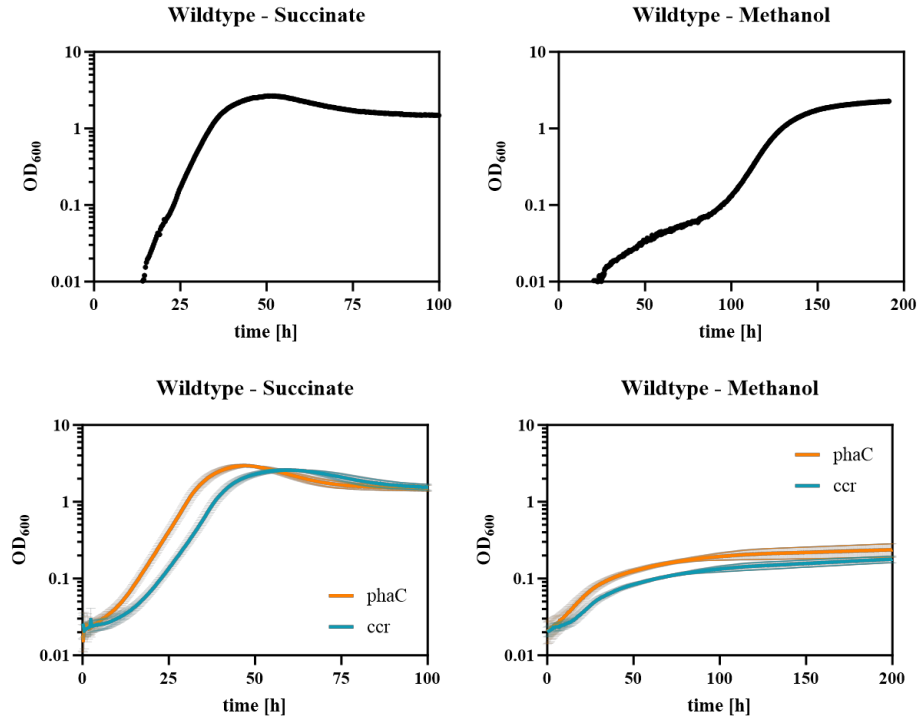


Figure 15: Two-plasmid system test in wildtype during growth on methanol and succinate. dCas9 was introduced on the single-copy plasmid controlled under the control a constitutive promoter. The gRNAs were constitutively expressed from a multi-copy plasmid. Cells were grown on medium containing methanol as sole carbon source. Each line represents five biological replicates.

While the wildtype strain may not be susceptible to leakiness of the IPTG-inducible promoter, the Δccr and $\Delta phaC$ knockout strains may suffer from low levels of transcript especially during early stages of growth. To reduce potential leakiness effects, we therefore replaced the constitutive promoter for gRNA expression with the same inducible promoter that we used for dCas9 expression, and evaluated growth on methanol with full induction (Figure 16) and with different inducer concentrations (Supplementary Figure 8). By including a non-targeting gRNA control and comparing it to cells without the CRISPRi plasmid system, I could determine that neither expression of dCas9 alone nor the addition of IPTG affects cellular growth negatively.

When targeting gRNAs for *ccr* and *phaC* were expressed in the wildtype, I observed growth deficiencies in induced cultures of the *ccr* knockdown, while targeting *phaC* lead to improved growth upon induction. After 100 h of incubation cells recovered from the growth defects of the *ccr* knockdown.

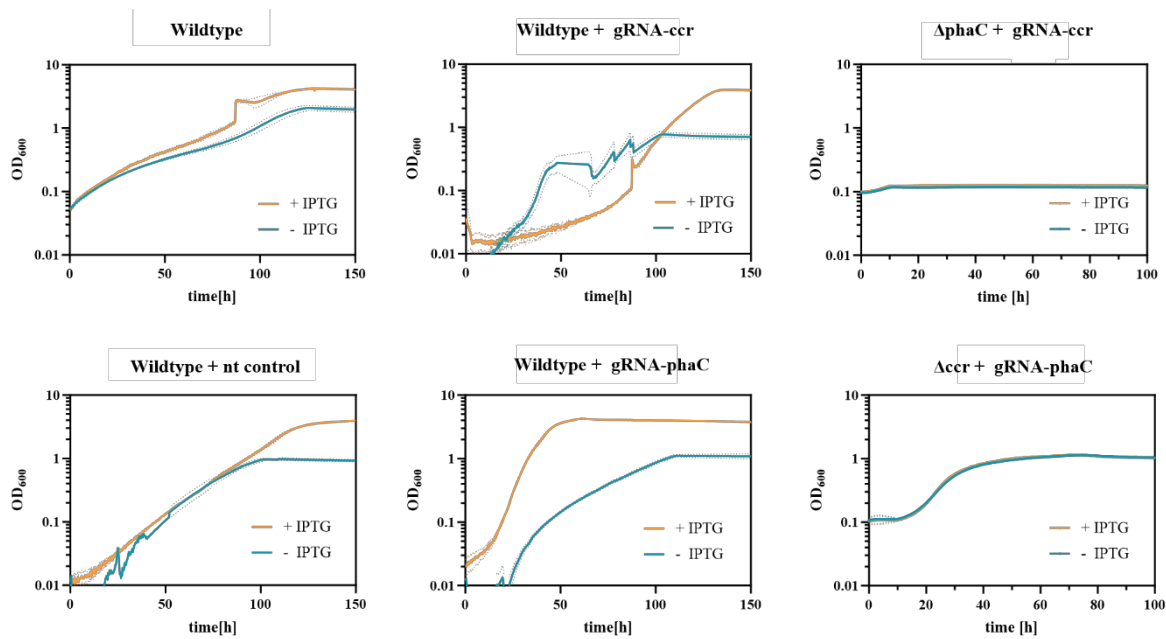


Figure 16: Growth assays of wildtype, Δccr and $\Delta phaC$ containing the double inducible CRISPRi plasmid system on methanol (+/- IPTG). Both dCas9 and gRNA were expressed from a single-copy under the control of an IPTG-inducible promoter. nt: non-targeting gRNA control. Expression of CRISPRi was induced by addition of 1 mM IPTG.

Switching from the multi-copy to a single-copy plasmid appeared to reduce the strength of knockdown effects on growth we previously observed with our two-plasmid system. However, the expression of gRNA-*ccr* in a $\Delta phaC$ background completely abolished growth and repeated attempts to cultivate this strain on methanol were unsuccessful. In contrast, growth of Δccr with gRNA-*phaC* was not affected, and the system did not respond to inducer addition.

I could however not reproduce growth assays for Δccr gRNA-*phaC*, as the results were inconsistent among biological replicates. In some instances, growth was not impeded regardless of inducer concentrations, while in other growth assays, improved growth seemed to correlate with higher concentrations of IPTG or growth was completely inhibited. As I chose growth assays for initial readouts a definite cause cannot be attributed to these results and there are several possibilities for the observed growth behavior of our knockdown strains, which will be discussed in detail.

4.8.2 Resting cells for crotonate production

As I suspected that our inducible knockdown system may prevent growth of $\Delta phaC$ gRNA-*ccr* on methanol due to leakiness of the inducible promoter and thereby formation of low levels of dCas9 and gRNA transcript, I attempted to circumvent the potential lethality of our CRISPRi system during early growth stages with a 2-stage growth assay, in which I aimed to decouple growth from production by using resting cells.

I hypothesized that allowing the cells to accumulate biomass would alleviate potential knockdown toxicity effects in early growth stages. Subsequently the accumulated biomass would be used for the production of crotonate from methanol by inducing the CRISPRi machinery. In theory, cells would switch from growth to production as part of the carbon flux may be directed towards the deficient EMCP. For this, I inoculated Δccr gRNA-*phaC* and $\Delta phaC$ gRNA-*ccr* in succinate precultures and harvested the cell pellet upon reaching stationary growth to maximize biomass formation. After washing the cells, I inoculated them into methanol medium containing the inducer (1 mM IPTG) and monitored growth and crotonate production over time (Figure 17). Prolonged cultivation of both strains did not result in growth after 96 h and no formation of crotonate was observed for $\Delta phaC$ gRNA-*ccr*. In Δccr gRNA-*phaC*, low amounts of crotonate were detected, however, they remain in the high nanomolar range.

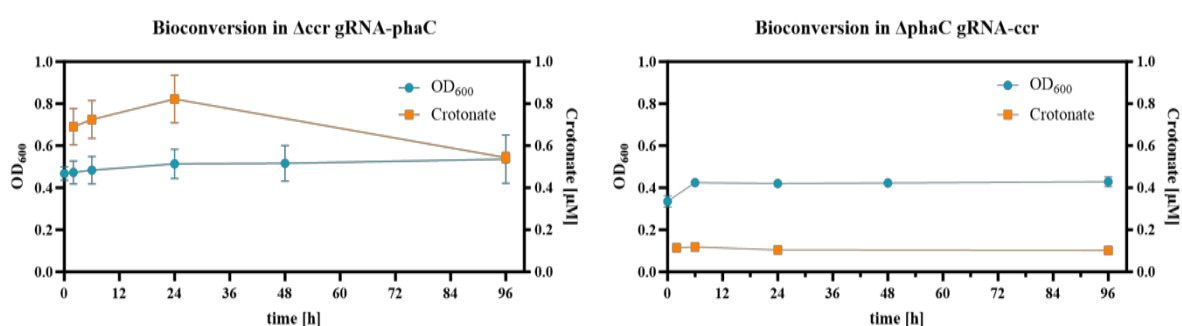


Figure 17: Growth assays of Δccr gRNA-*phaC* and $\Delta phaC$ gRNA-*ccr* during a bioconversion experiment. Precultures were grown in medium containing succinate to stationary growth and inoculated in methanol medium + 1 mM IPTG upon reaching stationary phase. Crotonate samples were taken at the same timepoints of OD₆₀₀ measurements, with one exception after 48 h.

While knockdown toxicity is still a reasonable explanation for the lack of growth on methanol, it is also possible that the switch of carbon sources from succinate to methanol and immediate induction of the knockdown system could pose a substantial metabolic burden. Accumulating biomass prior to induction did not result in continued growth on methanol, and only low amounts of crotonate were produced in the cultivation of Δccr gRNA-*phaC*. Despite switching to the double inducible single-copy plasmid knockdown system, lethality appears to hamper cell growth on methanol. Whereas growth of Δccr gRNA-*phaC* was not reproducible, $\Delta phaC$ gRNA-*ccr* was unable to grow on methanol across all versions of expression for the CRISPRi system. While our previous designs focused on the modulation of expression levels, we designed yet another knockdown system directed at altering the binding capacity of the gRNAs.

4.8.3 Design of mismatch guide RNAs for targeted knockdowns

As previous growth assays with the double-inducible knockdown system still prevented growth of $\Delta phaC$ gRNA-*ccr* and did not yield reproducible results for Δccr gRNA-*phaC*, and since even the basal leaky expression of the CRISPRi system abolished growth, we next tested mismatching guide RNAs. Here the expectation was that the effect of downregulation through binding of the CRISPRi gRNA could be titrated by lowering binding affinity through procedurally mismatching gRNAs and would decrease the risk of previously observed lethality effects during early stages of growth.

Based on the designs of Daniel Stukenberg and colleagues¹²⁴, we generated a mismatched gRNA library, with truncated sequences of 14, 16, or 20 basepairs (bp) and alternating nucleotides at positions 5 and 10. Covering all possible combinations, we ended up with a gRNA library of 48 different sequences for each *ccr* and *phaC*, including one fully binding version. For the expression of this new CRISPRi variant we chose the same plasmid as in our previous experiments, where the expression of dCas9 and the mismatch gRNAs is controlled by the IPTG-inducible promoter.

We conducted our first screens of this new CRISPRi system in a wildtype background targeting *ccr* and *phaC* during growth on methanol, as stronger binding capacities of the gRNA targeting *ccr* should result in severely reduced growth. These initial growth assays were conducted by our collaboration partners in tube cultures (RG Becker, Synmikro). We expected reduced binding efficiency for truncated gRNAs of 16 and 14 bp and thus also less impaired growth. As I previously observed the strongest effects of our gRNAs after incubation for more than

50 h, I chose the final OD₆₀₀ of our growth assays as our readout and calculated the ratio of the final OD₆₀₀ between non-induced and induced cultures to determine which gRNA variant responds to addition of the inducer (Figure 18).

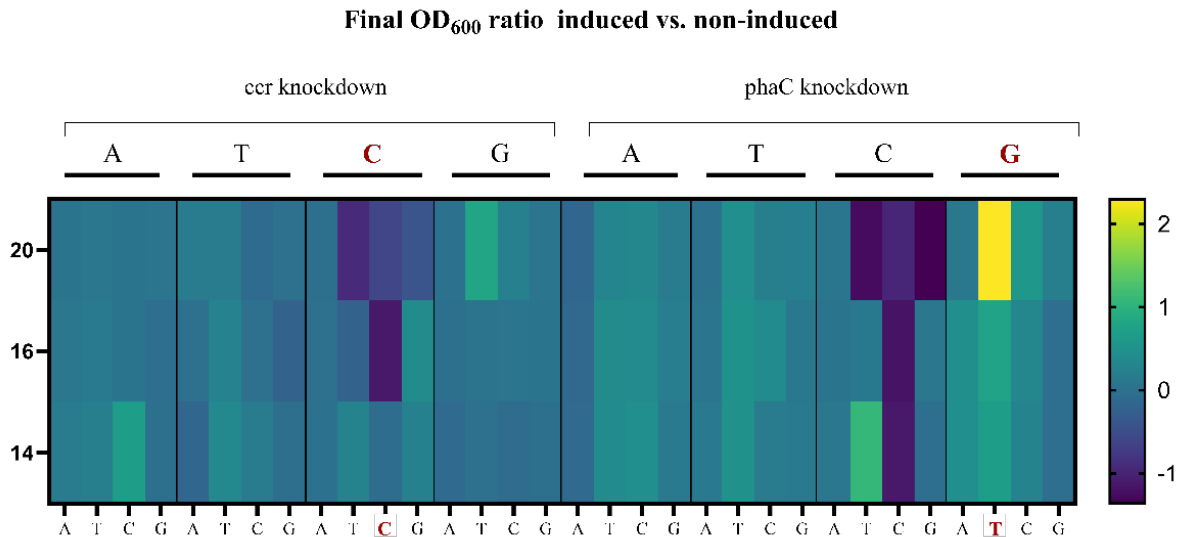


Figure 18: Final OD₆₀₀ ratio between induced and non-induced wildtype cultures after 56 hours during growth on methanol, containing the mismatch gRNA library. We determined the final OD₆₀₀ in non-induced and induced cultures. Mismatches at position 5 are indicated above (A5, T5, C5, G5), mismatches at position 10 are indicated below (A, T, C, G). Perfectly binding gRNA versions are indicated in red letters (*ccr*: C5C10; *phaC*: G5T10).

When we tested the knockdowns of *ccr* in the wildtype background we observed the expected strong growth deficiency in the fully binding non-truncated C5-C10 gRNA upon induction. While we still observed decreased growth in the 16 bp C5-C10 gRNA, none of the other 16 bp versions, nor any of the 14 bp gRNAs exhibited a strong negative effect on growth. Interestingly, only cells harboring a gRNA which is complementary to the target sequence at position 5 (C5) suffered growth deficiencies depending on the addition of IPTG, with the exception of C5-A10, which lead to cell death regardless of inducer presence. When solely position 10 was complementary to the target sequence, I did not observe any growth defects in our initial growth assay. However, since overall cell viability was reduced during cultivation in tubes, as the non-targeting and empty vector control only reached an OD₆₀₀ of 0.5 (Supplementary Figure 9), I repeated the growth assay for *ccr*-gRNAs in flask cultivations with truncated versions of C5-C10. Here, I simultaneously evaluated the relevance of position 10 for target binding by introducing the gRNA complementary to the target sequence at position 5 and alternating nucleotides at position 10 (C5-X10)(Figure 19). In our second growth assay, I could see a similar trend as in our previous experiment. Cells carrying the non-truncated C5

gRNAs had strong growth deficiencies regardless of the substitution in position 10. For the 16 bp truncated gRNAs, however, I saw that the fully binding C5-C10 gRNA as well as C5T10 resulted in cell death when induced, while C5-A10 and C5-G10 grew to the same level of the non-induced cultures. For induced cultures with the 14 bp truncated gRNAs, only C5-C10 had negative impact on growth. I therefore suspected that shorter gRNA sequences rely on complete sequence complementarity for DNA binding, while position 5 is overall more relevant for binding the target sequence, which is in line with reports from literature^{124,125}.

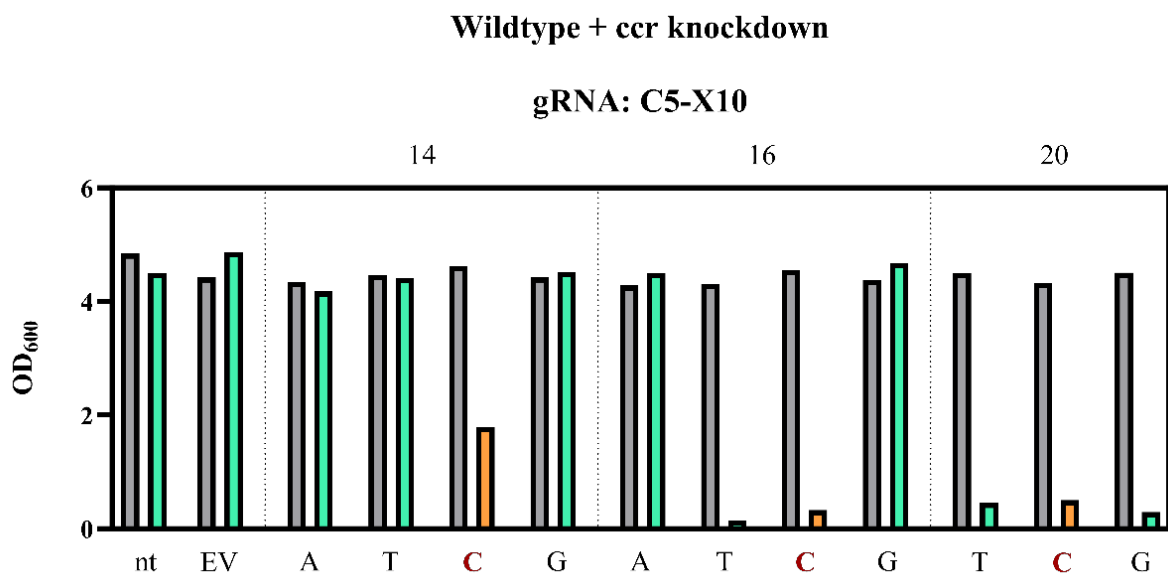


Figure 19: Final OD₆₀₀ after 72h of cultivation of the wildtype during growth on methanol containing a C5 guide RNA for *ccr* with altered nucleotides for position 10. (B) Grey bars: Non-induced cultures, green bars: Induced cultures (+ 1 mM IPTG). Orange bars and red letters indicate the fully binding gRNA (C5-C10). Nt: non-targeting control. EV: Empty vector control.

I next tested the mismatched gRNA knockdown of *phaC* in the wildtype background to find suitable gRNA candidates, which could eventually be implemented in Δccr . Interestingly, when *phaC* was targeted, the fully binding gRNA lead to improved growth in the wildtype when induced, which matches observations of previous tests of CRISPRi designs in the wildtype background. While growth for other gRNA versions was mostly unaffected, growth of cells containing C5-C10 gRNAs was affected negatively. I therefore investigated whether this gRNA versions is predicted to bind to different regions in the genome of *M. extorquens* PA1, but no other targets could be identified. Hence, I chose C5-C10 to conduct further growth assays.

4.8.4 Introduction of mismatched gRNA-*phaC* in *P45*

To combine the use of this mismatched CRISPRi system with the optimized glyoxylate shunt utilizing Δccr strain, I introduced the CRISPRi system with the C5-C10 gRNA targeting *phaC* in *P45*. Unfortunately, growth assays of *P45* containing this gRNA were not reproducible (data not shown). Here, I suspected that growth may still be inhibited to a strong degree, and hence tested the T5-G10 gRNA in the wildtype and *P45* Δccr to alleviate potential lethality effects (Figure 20). While overall growth was significantly reduced compared to the Wt, I also observed lower growth of the non-targeting and empty vector controls, indicating that *P45* may suffer from plasmid burden effects. For the T5-G10 gRNA targeting *phaC*, induction of the CRISPRi system did not affect growth of *P45*, regardless of the level of truncation for the mismatched T5-G10 gRNA.

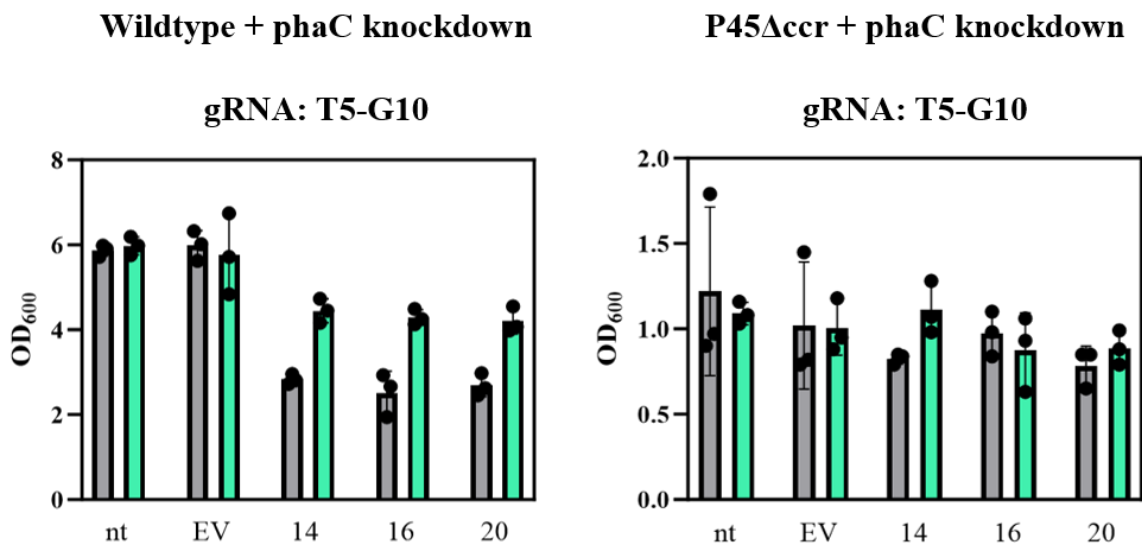


Figure 20: Final OD_{600} after 72 h of cultivation of wildtype and *P45* containing the knockdown of *phaC* in the wildtype and *P45* with the T5-G10 gRNA on methanol. Grey bars: non-induced cultures, green bars: induced cultures (+ 1 mM IPTG). Nt: non-targeting control. EV: Empty vector control.

I therefore concluded that further tests of our gRNA library will be necessary to find a suitable candidate for the knockdown of *phaC* in Δccr . For the knockdown of *ccr* in $\Delta phaC$, the truncated 14 bp C5-C10 gRNA seems promising as it caused slight growth deficiencies without abolishing growth entirely and may lead to the generation of a viable $\Delta ccr\Delta phaC$. Due to time constraints as I was approaching the end of my PhD, I was not able to test crotonate production in *P45* containing the mismatched T5-G10 gRNA, which would be an interesting experiment for the future.

5 Discussion

The aim of this thesis was to develop a highly advanced strain of *M. extorquens* to produce crotonate while growing on methanol. To achieve this the EMCP was disrupted by deletion of *ccr* and an orthogonal glyoxylate regeneration pathway was introduced; the glyoxylate shunt. I optimized this glyoxylate shunt-utilizing strain using adaptive laboratory evolution and characterized it.

My evolved serine cycle-dependent and glyoxylate shunt employing *M. extorquens* strain has similar growth rates compared to the wildtype strain and an equal biomass yield on methanol and formate indicating a high degree of metabolic optimality. Chemostat experiments, NGS and proteomic analysis, growth- and enzyme kinetic assays were used to elucidate the cellular changes of the final evolved strain. Here I found key mutations in Icd and Prk, which alter the carbon flux through the glyoxylate shunt. While the enzymatic activity of Icd was 4-fold reduced compared to the Wt enzyme, the mutation in Prk likely plays a more regulatory role regarding methylotrophic growth. Furthermore, I found that a mutation in a MarR transcriptional regulator results in increased formaldehyde homeostasis in the evolved *P45*. Initial tests to produce crotonate from methanol using this strain showed only limited production. Crotonate degradation was identified as one factor limiting production, while additional carbon sinks to PHB production were proposed as another potential sink.

Since deletion of the PHB polymerase encoding gene did not succeed, I explored the use of knockdowns via the CRISPRi machinery testing different expression levels for the targeted downregulation of *phaC* and *ccr*. While strong expression of dCas9 and gRNA from constitutive promoters in the wildtype strongly decreased growth on methanol when *ccr* was targeted, the switch to inducible promoters reduced the negative impact on growth in the wildtype. Introduction of this inducible system in Δccr did not alter growth behavior on methanol, while the knockdown of *ccr* in $\Delta phaC$ resulted in cell death regardless of inducer addition. I then employed a combined strategy of mismatched and truncated guide RNAs to lower the effect of CRISPRi on $\Delta phaC$ and aimed to find a suitable candidate for the knockdown of *phaC* in Δccr . Here, I found promising gRNAs for the knockdown of *ccr*, but not for the knockdown of *phaC*, for which further experiments would be necessary.

5.1 Adaptive Laboratory Evolution leads to improved methylotrophic growth

Adaptive laboratory evolution is a powerful tool frequently used in strain engineering and optimization, as it allows for the accumulation of mutations which benefit growth under the given selection conditions. During ALE it is generally assumed that the change of certain traits is connected to increased fitness. Hence, the population will acquire mutations that confer a selective advantage over the ancestral strain, whose abundance gradually decreases until it is replaced entirely⁵⁵. I started my work in this project in collaboration with Doreen Meier from RG Becker (Synmikro, Marburg), who had introduced the glyoxylate shunt on the pCM80 plasmid in *M. extorquens* PA1 Δccr , added serine integrase landing pads and started the ALE with serial transfers on liquid methanol medium. I then evaluated the methylotrophic growth of passage *P11* and *P21*, and continued the evolution on liquid methanol medium, which yielded the final evolved strain *P45*. This strain showed significantly improved methylotrophic growth compared to the parent strain. Analysis of the underlying changes on a genomic and proteomic level revealed several mutations and changes in protein levels of enzymes directly and indirectly involved in central carbon metabolism of *M. extorquens*. Here, I provide evidence of carbon flux rerouting and changes in regulatory networks involved in C1 assimilation.

5.1.1 Mutations in Icd and Prk rewire central carbon metabolism

Analysis of the passages from ALE through WGS revealed multiple mutations involved in central carbon metabolism of *M. extorquens*. Among these was a mutation in Icd (F156C), which strongly decreased enzymatic activity towards isocitrate (Figure 10). As Icd shares its substrate with isocitrate lyase (AceA), it is likely that the reduced activity of Icd (F156C) redirects flux towards the glyoxylate shunt. In a similar study by my former colleague Francesca Severi (unpublished results), *M. extorquens* AM1 Δccr was evolved for glyoxylate shunt utilization on methanol, which also led to mutations in Icd and Prk, but with the substitutions Icd (Y139C) and Prk (I214S), while I observed Icd (F156C) and Prk (T176I).

While enzyme assays of the mutated Icd did not show any activity in cell-free lysates, it seems very likely that this mutation also reduces enzyme activity, as was the case in *M. extorquens* PA1 Δccr . Interestingly, in both evolved strains, an aromatic residue was exchanged for a cysteine. Cysteins are very potent in changing protein conformation through the formation of

cysteine-cysteine bonds, and are often deliberately introduced to alter enzymatic activities¹²⁶⁻¹²⁸. These results suggest a high relevancy for a mutation in *Icd* to increase flux towards the glyoxylate shunt, which was also hypothesized by Schada von Borzyskowski and colleagues¹¹². Here, the reason why the substitution of the EMCP by the glyoxylate shunt did not support growth on methanol was thought to be an insufficient flux through the TCA cycle, and therefore also the glyoxylate shunt. This is supported by metabolic flux analysis, which showed that flux through the TCA during methylotrophic growth is reduced¹¹³. In accordance, I did not observe an upregulation of TCA cycle proteins. I therefore suggest that the mutation in *Icd* alone is sufficient to increase flux towards the glyoxylate shunt to support methylotrophic growth of the EMCP deficient strain. Downregulation of flux through the TCA cycle was also observed in the establishment of synthetic methylotrophy in *E. coli*, where laboratory evolution improved formaldehyde assimilation through the RuMP pathway through mutations that reduced the activity of the cycle⁸⁷.

Reverse engineering of the *Icd* mutation in the original *M. extorquens* PA1 Δccr containing the pCM80-Glyox. plasmid could be done to test this hypothesis. I further suspect that the mutated *Prk* also has an influence on carbon flux distribution. A study by Ochsner and colleagues demonstrated that *Prk* is essential in *M. extorquens* for methylotrophic growth¹¹⁸. The reason for this is that *Prk* produces ribulose-1,5-bisphosphate, an inducer for QscR, which regulates serine cycle enzymes such as GlyA. While QscR itself was not annotated in the proteomic dataset, the majority of LysR-family transcriptional regulators was not upregulated, with the exception of one, which was upregulated by 1.18-fold. Despite this, my proteomic analysis revealed an upregulation of many enzymes of the serine cycle, including GlyA, MtkA/B, Sgat and Hpr, which may be caused by increased activity of the mutated *Prk* (T176I). Therefore, I hypothesize that *Icd* (F156C) increases glyoxylate regeneration, while an altered activity of *Prk* (T176I) enhances serine cycle activity, leading to improved methanol assimilation.

5.1.2 Enhanced methanol oxidation in P45

For the assimilation of methanol, *M. extorquens* contains two pyrroloquinolinequinone (PQQ)-dependent methanol dehydrogenases (MHD): The Ca²⁺-dependent MxaF, and the lanthanide-dependent XoxF. Expression of methanol dehydrogenases (MHD) is highly regulated in *M. extorquens* and involves a sophisticated response cascade, which involves the two-component systems MxcQE, MxbDM and the response regulator MxaB¹²⁹. MxcQE is required

expression of MxbDM, which in turn negatively regulates *xoxF* expression while activating *mxoF* expression. XoxF, on the other hand, has been shown to be essential for normal expression of both two-component systems *mxoDM* and *mxoQE* and for the expression of *mxoF*¹³⁰. The fourth component of this regulatory cascade is MxaB, whose regulatory role in methanol oxidation is not well understood to date. Evidence points towards a regulatory role of MxaB in the expression of MxaF and PqqD¹²⁹. *M. extorquens* mainly relies on the Ca²⁺-dependent methanol dehydrogenase (MDH) MxaF, while it also contains the lanthanide-dependent XoxF MDH. Previous studies have demonstrated that XoxF is capable of methanol oxidation to formaldehyde, and its expression is upregulated and even becomes the dominant enzyme for methanol oxidation in the presence of lanthanides^{131,132}. In nature, the availability of two functionally redundant MDHs that depend on different cofactors may prove advantageous in an ever changing environment.

During proteome analysis, I found that XoxF is upregulated, along with a downregulation of MxoQE and MxbDM and a slight downregulation of MxaF (Figure 13). Although XoxF represses MxaF, a study of Good et al. demonstrated that similar expression levels of both MDHs are observed if the lanthanide concentration is not greater than 100 nM, suggesting that *M. extorquens* is able to utilize MxaF and XoxF simultaneously. The same study also investigated the activity of XoxF in different lanthanide concentrations, which showed that 2.5 nM of La already support XoxF activity. Although we did not add lanthanides to our growth medium, it is possible that trace amounts of lanthanides enable XoxF activity. This has been demonstrated in a study by Hoogendorn et al., in which the highly catalytically efficient XoxF from *M. fumariolicum* SolV still showed activity in medium devoid of lanthanides⁵³. While many studies suggested that XoxF is able to oxidize methanol to formate, another more recent study from Good and colleagues have shown that formaldehyde activating enzyme Fae and the H₄MPT pathway are required for lanthanide-dependent growth on methanol¹³³. As XoxF as well as MtdA are upregulated in *P45*, increased methanol oxidation to formaldehyde and subsequent loading on H₄MPT by MtdAB could enhance methanol assimilation.

The importance of sufficient methanol oxidation was seen in the previously mentioned study by Schada von Borzyskowsky et al., where the EMCP was replaced by the glyoxylate shunt in *M. extorquens* for glyoxylate regeneration. While the introduction of the glyoxylate shunt rescued EMCP-deficient strains on acetate, growth on methanol could not be rescued. When they tested the activity of the MDH, they observed a strong downregulation of MxaF activity (25% of wildtype activity) and attributed this to the absence of growth with methanol as the

sole carbon source¹¹². Hence, activity of MDH may be an additional factor that enables adaptation to the glyoxylate shunt, and therefore determines viability of the EMCP-deficient strain during growth on methanol.

5.1.3 Altered Formaldehyde homeostasis confers higher formaldehyde tolerance

In methylotrophy, the oxidation of methanol inevitably leads to the formation of the toxic intermediate formaldehyde, and is hence a crucial step in C1 assimilation into biomass. Formaldehyde can easily pass the cell membrane into the cytosol, where it interacts with aromatic residues of proteins, causing cross-linking in proteins and nucleic acids, which ultimately leads to cell damage¹³⁴.

As formaldehyde naturally occurs in the environment, all organisms have developed formaldehyde detoxification mechanisms to effectively balance the accumulation of the toxic intermediate. One of these mechanisms found in natural methylotrophs includes the formaldehyde activating enzyme Fae, which connects formaldehyde with H₄F to form methylene-H₄MPT as the second step in methanol oxidation. Besides this, formaldehyde can also spontaneously form methylene-H₄MPT, a side mechanism that has likely evolved to decrease formaldehyde accumulation when activity of Fae is too low. Apart from direct conversion of formaldehyde to a less reactive intermediate, formaldehyde sensors can prevent transcription and translation at elevated concentrations of the toxic compound in order to reduce DNA damage. In my ALE, I found a mutation which introduces an early stop-codon in a MarR-family transcriptional regulator. Upon further investigation, I discovered that this transcriptional regulator is the formaldehyde-sensing TtmR, which was described by Bazurto et al. to be involved in formaldehyde homeostasis by regulation of EfgA. EfgA is a translational regulator, which prevents translation at elevated intracellular formaldehyde concentrations¹²⁰. The same study shows that *ttmR* and *efgA* null mutants show an increased tolerance to enhanced formaldehyde concentrations, and had elevated intracellular levels of the toxic compound. My proteomics analysis showed that the introduced early stop codon drastically decreases protein levels, confirming an effective knockout (Figure 11). I therefore tested formaldehyde tolerance of *P45* and compared it to the wildtype strain, which revealed that the evolved strain had indeed developed increased tolerance to the formaldehyde (Figure 14).

Although tolerance of *P45* and the wildtype was not as high as the wildtype and $\Delta ttmR$ strain from Bazurto et al., I could observe that growth of *P45* was not impeded in the presence of up to 2.5 mM formaldehyde, while the wildtype struggled with concentrations above 0.5 mM after 48 h of growth. The differences in formaldehyde tolerance may be explained by different techniques for cultivation, as they conditioned their strains in two separate precultures before inoculating the main culture. Interestingly, *hsp20* and genes for a Crp/Fnr family protein and UspA domain containing protein were upregulated in the $\Delta ttmR$ mutant, which I could also observe in *P45*. All of these proteins are involved in stress response, whereby proteins of the Hsp20 family are well a well-known chaperones that prevent protein aggregation and misfolding. The increased abundance may therefore prevent excessive protein damage in presence of elevated intracellular formaldehyde concentrations. Also, besides downregulation of *TtmR* and *EfgA*, the increased activity of *MtdA/B* in *P45* could facilitate formaldehyde detoxification through elevated methylene-THF pools. Increased formaldehyde tolerance, however, did not confer a growth advantage on methanol compared to other strains of the ALE. Formaldehyde resistance may simply be an adaptation mechanism to prolonged exposure to stressful conditions (i.e. methanol), an effect which has also been observed during ALE in yeast, where exposure to environmental stressors like butanol or n-hexanol led to increased tolerance to the stressor¹³⁵. While increased tolerance of the toxic compound may prove useful in the conditions of ALE, it has been demonstrated that disturbed formaldehyde homeostasis caused by *ttmR* and *efgA* deletions decrease adaptability to switches from multi- to single carbon sources, as both formaldehyde sensors are critical for transition to methylotrophy¹²⁰. In a lab setting, this trade-off likely does not negatively affect the cells. However, the evolved strain would likely have a hard time to survive in nature where the environment and available carbon sources change frequently and a fast response to a changing environment determines strain survival.

5.1.4 Improved growth on methanol growth reduces acetate utilization

While the goal of ALE is the improvement of strain performance to the given conditions, it is often observed that this leads to a trade-off, in which the capability of adapting to a changing environment decreases. In *P45* growth significantly improved on methanol, while the underlying metabolic changes worsened growth performance on acetate. Since the EMCP in *P45* is dysfunctional, the only way to assimilate acetyl-CoA is the TCA cycle, and with reduced

Icd activity the TCA cycle is possibly running at lower rates. Interestingly, while *P45* was still viable on acetate, the evolved AM1 strain was not able to grow on acetate at all (Francesca Severi; unpublished)¹³⁶. While the reason for this could be an even lower activity of Icd, another explanation could be the point mutation I found in *ppc*, which may lead to the increased protein abundance that was determined during proteomics analysis. Ppc plays an important role in the central carbon metabolism of *M. extorquens* by shuffling carbons between oxaloacetate (OA) and PEP, meaning that the mutation found in *ppc* could alter fluxes in the TCA and serine cycle. While this mutation did not seem to have any effect on methylotrophic growth, it may very well have influence during growth on acetate, as Ppc could compensate for the reduced Icd (F156C) activity. Furthermore, the observed upregulation of PoxB and AckA could work to increase flux towards the TCA cycle, as PoxB may break down pyruvate to acetate, which is then converted by AckA to acetyl-CoA. A metabolomics analysis may grant further insight into the cellular mechanisms of the potentially increased serine cycle activity and the decreased TCA flux. To determine whether the mutated Ppc is responsible for the difference in growth phenotypes between the two evolved *M. extorquens* strains, previous passages which do not contain this mutation could be tested for growth on acetate.

5.1.5 P45 shows wildtype-level biomass yields

It was previously shown that replacing the EMCP with the glyoxylate shunt in Δccr and Δepi mutant strains led to wildtype level growth rates on acetate, indicating that conversion of acetyl-CoA into biomass is as efficient as in the EMCP¹³⁷. Indeed, biomass determination with formate and methanol as the carbon source showed that Δccr is able to reach at least wildtype-levels, while biomass yield in *P45* from methanol even surpassed the wildtype. Since the EMCP is more energy efficient than the glyoxylate shunt, increased biomass yield cannot be a result of more efficient substrate utilization¹¹⁷. A possible explanation could be increased PHB accumulation, as the storage compound can make up to 40% of CDW¹²³. PHB has also been mentioned as a major bottleneck for crotonate production in the work of my former colleague (Francesca Severi), where she demonstrated that fed carbon was stored in PHB, which made up for 13.7% of CDW¹³⁶, and multiple studies could show that a great portion of the carbon flux is directed towards PHB. The suspicion that *P45* accumulates PHB is supported by observations of growth profile of *P45*, as the growth rate of the evolved strain never surpassed the wildtype. An increased PHB accumulation could be facilitated further in response to the

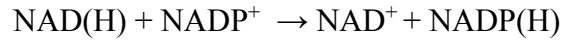
deletion in *ccr*, which may cause a redox imbalance through accumulation of NADP(H). Unfortunately, while I attempted to assess intracellular NADP⁺/NADP(H) levels, I was not able to obtain reproducible results as samples were susceptible to rapid oxidation.

The synthesis of PHB has been described as a major redox sink, and is likely the main route to restore redox imbalances caused by a disbalance in reducing equivalents, which may be the reason why a deletion of *phaC* in Δccr was unsuccessful thus far. Table 12 and Table 13 show a summary of reactions that regenerate and consume reducing equivalents in the central carbon metabolism of *M. extorquens*. An increased flux towards PHB would also decrease the flux towards crotonyl-CoA, or even convert accumulated crotonate back to crotonyl-CoA by an acyl-CoA synthetase, to 3-hydroxybutyryl-CoA through an enoyl-CoA hydratase and to acetoacetyl-CoA by the reverse reaction of CroR. While an upregulation of enzymes capable of these conversions was not observed, this might not be necessary in the first place. Multiple different acyl-CoA synthetases and enoyl-CoA hydratases are expressed in *M. extorquens*, and the mere abundance of these enzymes may outcompete the YciA thioesterase.

While testing crotonyl-CoA and crotonate levels in the wildtype and *P45*, I determined that crotonyl-CoA levels did not differ from the wildtype, while the wildtype produced more crotonate than *P45* (Figure 7, Figure 8). The reason for this may be that the wildtype has a higher carbon flux through the EMCP than *P45*, in which crotonyl-CoA is the metabolic endpoint of the EMCP and potential redox imbalances may favor the formation of PHB. The notion that crotonate may be activated back to crotonyl-CoA and perhaps to PHB is supported by the growth assay, in which the wildtype was cultivated in methanol medium in presence of 5 mM crotonate, where I observed that crotonate concentration had decreased by the end of cultivation (Figure 9). Therefore, I hypothesize that strains may attempt to restore redox balance by synthesizing PHB. Further analysis of the redox state and ¹³C labelling experiments as well as PHB quantification in the evolved strain may shed some light on the metabolism of *P45*.

To control intracellular redox balance, *M. extorquens* possesses pntAB, which is a membrane protein complex that functions as a proton pump across the membrane, regulating NADP:NADP(H) redox homeostasis in the direction of NADP(H), which influences the ATP:ADP ratio¹³⁸. PntAB mutants were shown to have growth deficiencies in *Synechocystis* sp. PCC6803, emphasizing the importance of redox balance for cell viability. As the Δccr strain

is suspected to accumulate NADP(H), the activity of this transhydrogenase may be reduced, thereby altering the ATP:ADP equilibrium¹³⁹.



While organisms such as *E. coli* possess multiple transhydrogenases which can flexibly restore redox balance, pntAB is the only identified enzyme with transhydrogenase activity. Therefore, the introduction of a transhydrogenase working in the opposite direction, such as SthA from *E. coli*, could help to repair the possible redox imbalance. Another possibility would be to introduce a production pathway that synthesized reduced products to keep redox balance in order, which has been successful in recent studies^{140,141}.

Table 12: Reactions for reducing equivalent regeneration in *M. extorquens*

Enzyme	Name	Reaction	Reducing equivalent	Differential expression in (Wt/P45)
MxaF/ XoxF	Methanol dehydrogenase	Formaldehyde → Methylene-THF	Cytochrome c _{ox} Cytochrome c _{red}	-0.57/ +1.60
MtdA	Methylene-THF dehydrogenase	Methylene-THF → Methenyl-THF	NADP ⁺ → NADP(H)	+ 1.54
Fdh	Formate dehydrogenase	Formate → CO ₂	NAD ⁺ → NAD(H)	- 0.81
Sdh	Succinate dehydrogenase	Succinate → Fumarate	FAD → FADH ₂	+ 0.61

Table 13: Reducing equivalent consuming reactions in *M. extorquens*

Enzyme	Name	Reaction	Reducing equivalent	Differential expression (Wt/P45)
Hpr	Hydroxypyruvate reductase	Hydroxypyruvate → glycerate	NAD(H) → NAD ⁺	+ 1.30
Mdh	Malate dehydrogenase	Oxaloacetate → Malate	NAD(H) → NAD ⁺	+ 0.51
PhaB	Acetoacetyl-CoA reductase	Acetoacetyl-CoA → 3-Hydroxybutyryl-CoA	NADP(H) → NADP ⁺	+ 0.42
Ccr	Crotonyl-CoA reductase/carboxylase	Crotonyl-CoA → Ethyl-Malonyl-CoA	NADP(H) → NADP ⁺	- 4.76

5.2 CRISPRi for transient pathway optimization

While in the first part of this thesis I developed an EMCP-independent *M. extorquens* PA1 strain that grows efficiently on methanol, the second part of this work focused on increasing carbon flux towards the EMCP to eventually siphon out intermediates like crotonyl-CoA. Multiple reports in literature demonstrated that deleting the competing PHB synthesis pathway was able to raise production titers of EMCP-derived products by increasing carbon flux towards the EMCP^{94,111,142}. While the knockout of *phaC* in *M. extorquens* significantly reduces PHB accumulation and increases flux into the EMCP, growth defects in $\Delta phaC$ strains reduces overall performance of this strain on methanol. As mentioned earlier, the reason for this was suspected to be an accumulation of reducing equivalents, which reduces the oxidative capacity of the strain. This is supported by another study, which introduced a *phaC* deletion in *Rhizobium etli*, where the observed growth defect was concomitant with a 3- to 17-fold increase in NAD(H) levels¹⁴³. I therefore suspected a pronounced redox imbalance to be the reason why the generation of $\Delta ccr\Delta phaC$ was not successful thus far. To minimize the potential lethality caused by this imbalance, I aimed to create the $\Delta ccr\Delta phaC$ phenotype through a genetic knockdown of *ccr* or *phaC* in the corresponding $\Delta phaC$ and Δccr knockout strains. For this, I designed different versions of a CRISPRi system to find a knockdown version which decreases *phaC* activity, but still produces a viable strain that is able to grow on methanol. Ideally, this could then be combined with the evolved *P45*. Testing different designs for the expression of CRISPRi showed that strain viability varies greatly depending on plasmid copy number and the promoter which controls the expression of dCas9 and gRNA.

5.2.1 Plasmid copy number strongly influences strain viability on methanol

The first variant was a two-plasmid system, with the expression of dCas9 from a single-copy plasmid, and the gRNA from a multi-copy plasmid, while both were under the control of strong constitutive promoters. When I tested constitutive expression of CRISPRi in the wildtype, cells showed a severe growth defect on methanol when *phaC* and *ccr* were targeted, while growth on succinate was not affected (Figure 15). I therefore suspected that expression levels of the CRISPRi machinery were toxic to the cells during growth on methanol. For this reason, I then used the single-copy plasmid, which contained both dCas9 and gRNA. Additionally, the constitutive promoter for dCas9 expression was exchanged by an IPTG-inducible promoter,

while the gRNAs were still constitutively expressed. When I introduced the CRISPRi system with the inducible dCas9 in Δccr and $\Delta phaC$ knockout strains, none of the strains were able to grow and I again suspected, that expression levels of both CRISPRi modules are too high, lowering gene repression levels, which was lethal to the cells (Supplementary Figure 7). Therefore, I put both dCas9 and gRNA under the control of the inducible promoter, in hopes to alleviate the toxicity of my knockdown system.

This improved viability of the wildtype, where I observed a growth deficit on methanol within the first 48 h of cultivation upon induction when targeting *ccr* (Figure 16). Interestingly, when *phaC* was targeted, growth of the wildtype was improved when the inducer was added. I suspected that a knockdown of *phaC* in the wildtype strain could increase flux towards the intact EMCP and may therefore result in a growth benefit. This hypothesis, however, contradicts studies, in which *phaC* mutants were constructed. Korotkova et al. described, that strains deleted in *phaC* showed a growth deficit on methanol. However, $\Delta phaC$ strains quickly regain wildtype-like growth on methanol through the emergence of suppressor mutants with high frequency, while the deletion of *phaC* remains stable and PHB accumulation is still decreased. To date, it is not known how the suppressor mutants restore the initial growth deficit¹²².

Introducing the same system in the Δccr and $\Delta phaC$ mutants yielded mixed results (Figure 16). While targeting *ccr* in $\Delta phaC$ with this knockdown system once again resulted in cell death, targeting *phaC* in Δccr did not affect growth. However, I was not able to reproduce these results. The knockdown of *phaC* in Δccr was lethal in some growth assays, and in others the addition of more inducer lead to improved growth. As targeting *ccr* in $\Delta phaC$ resulted in cell death every time, I suspected that the efficiency of downregulation of *phaC* varies, while the knockdown of *ccr* is strong in each growth assay. This is supported by qPCR data from my collaborators, who conducted growth experiments with a subsequent assessment of mRNA levels in a qPCR experiment. Here, no growth phenotype was observed during growth on methanol despite decreased levels of mRNA. However, it was shown that the knockdown of *phaC* did not decrease mRNA levels to the same degree as other knockdowns of the EMCP (Figure 21).

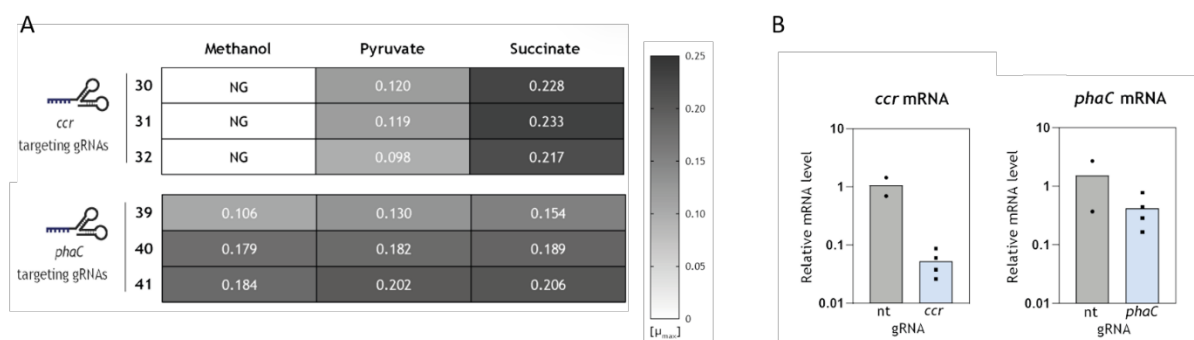


Figure 21: Tests of the inducible CRISPRi system. (A) Growth rates of the wildtype containing gRNAs targeting *ccr* or *phaC* during growth on methanol, pyruvate and succinate. (B) Validation of the CRISPRi mediated knockdown through qPCR. Results were taken and modified from the Master Thesis of Eric Ellenberger.

Based on these results, the lack of a reproducible growth phenotype of the *phaC* knockdown cannot be attributed to a definite cause. While the gRNA targeting *phaC* may not be strong enough to cause a growth phenotype, prolonged incubation of cells containing the gRNA for *phaC* could also lead to the emergence of suppressor mutants. Due to strong selection pressure, it is also plausible that cells might evade the CRISPRi system through mutation of the gRNA or the dCas9 enzyme. The loss of the CRISPRi plasmid is unlikely, as the pABC plasmids have shown to be highly stable, and constant antibiotic selection pressure necessitate the propagation of the vector¹⁰⁵. However, it could be that escapees mutate the gRNA or dCas9, either directly or in the promoter region. This effect has been observed multiple times in studies, where the expression level of plasmids or genes was toxic for the cells¹⁴⁴⁻¹⁴⁶.

Another possible explanation for the lack of a *phaC*- deficient growth phenotype is the inefficiency of the gRNA used for the *phaC* knockdown, which could explain the qPCR data. To solve this problem, it is crucial to determine whether the CRISPRi system used in my growth assays in Δccr leads to a decrease in mRNA and protein levels, PHB accumulation or if the CRISPRi machinery was evaded by mutations. If these factors were decreased, the lack of growth deficiency may be explained by suppressor mutations, which could potentially be identified via whole genome sequencing. It could be suspected that cells deficient in PhaC activity find a way to channel excess electrons into other pathways, therefore preventing the accumulation of NADP(H) and a potential redox imbalance, which would normally result in deficient growth. Elucidating the mechanism of suppression in these mutants could therefore lead to a discovery, which may enable the construction of $\Delta ccr\Delta phaC$ by reverse engineering the *phaC* mutant.

5.2.2 Mismatch gRNAs

In a last attempt to achieve viable strains with a $\Delta ccr\Delta phaC$ phenotype, I designed a mismatch gRNA library. By using gRNAs that have altered binding capacities, I hoped to alleviate potential selection pressure against the CRISPRi machinery in Δccr strain with a *phaC* knockdown, and to simultaneously find a variant for the *ccr* knockdown in $\Delta phaC$, which would not result in cell death. The first screen in the wildtype showed that the fully binding and non-truncated version of the *ccr* gRNA results in a strong growth defect upon induction. Here, I also observed that complementarity of position 5 of the gRNA is more important for efficient binding than position 10, whose relevance increased with a decrease in sequence length. This is in line with reports from literature, which state that mutations in close proximity to the PAM sequence have a stronger effect on binding than mutations that are further away^{124,125}.

The completely complementary gRNA targeting *phaC* on the other hand, led to the improved growth phenotype which I had observed in my previous growth assays. There were, however, gRNA versions that led to decreased growth in the wildtype, namely C5 gRNAs, whereby all truncated versions C5-C10 gRNAs resulted in growth reduction. The reason for this effect can not be explained, as I so far only tested gRNAs in growth assays. As I determined that there are no other targets predicted for this gRNA, off-target effects are rather unlikely. It could be that altered binding dynamics through less efficient but more frequent binding, such as a high K_m in enzyme kinetics. This way, the knockdown could be more effective, while the frequency of emergence of suppressor mutants might be reduced. Further experiments such as qPCR or proteomics are needed to find the cause for the growth deficiency with a C5-C10 gRNA. In an effort to combine the first and second part of this thesis, I introduced the C5-C10 gRNA in Δccr (P45). However, cells were unable to grow regardless of inducer presence. Going forward, prior determination of *phaC* knockdown efficiency would be important to ensure that 1. The knockdown is happening and 2. Cells may still be viable on methanol upon induction.

6 Concluding remarks

I successfully evolved an EMCP-deficient Δccr strain for sufficient utilization of the glyoxylate shunt, which led to improved growth on methanol. Analysis of the genome at different steps of the evolution showed few mutations in early passages, which are, however, likely the most namely relevant changes. This effect has previously been discussed in a review from Dragosits and Mattanovich¹⁴⁷, where it was described that the accumulation of beneficial mutations in *E. coli* and *S. cerevisiae* occurs within the first 100 to 500 generations, corresponding to an incubation time of roughly 2 months, with an expected fitness increase of 50-100%. The same review describes the relation between fitness increase and the number of generations, which is not linear. Hence, while prolonged incubation will lead to additional genomic mutations, they will not necessarily lead to an improved strain as the chance to gain a beneficial mutation decreases. Moreover, it has been described that single mutations that occur one after another may not lead to further growth improvement due to growing mutation network complexity, while on their own, they would actually lead to growth benefits¹⁴⁷.

For this reason, I stopped the evolution of Δccr pCM80-Glyox. after 45 serial transfers as growth rates approached levels comparable to other C1 assimilating organisms, and further increase in fitness would take considerably more time. While this part of the thesis was completed, the second part of my work would need further development. Throughout this project, I tested accumulation of crotonyl-CoA and crotonate, but could not find any condition, which allowed the production of either of these compounds to elevated levels or beyond micromolar concentrations on methanol so far. When crotonate production was attempted in *M. extorquens* AM1, maximum concentrations reached 25 μM upon acetate feeding, and PHB accumulation was stated as one of the major bottlenecks in for crotonate synthesis¹³⁶. The construction and testing of different CRISPRi systems showed varying knockdown strengths based on the expression system when *ccr* was targeted, whereas targeting *phaC* yielded mixed results. While there are many possible explanations for this observation, the utmost priority going forward is the confirmation of the *phaC* knockdown through evaluation of mRNA levels via qPCR. Once a sufficient CRISPRi system is constructed, ¹³C labelling experiments or PHB determination will be necessary to investigate the new carbon flux distribution. In case CRISPRi does not work for our purposes, there are several other strategies that could be explored. For example, one could try to knock out *phaR*, which is a transcriptional regulator involved in PHB metabolism, or phasins *gap11* and *gap20*, which stabilize PHB granules. It

has previously been demonstrated that the knockout of either of these genes resulted in decreased PHB accumulation and lower PHB granule stability¹²³. However, for the production of EMCP-derived acids, only a knockout of *phaC* increased production titers until suppressor mutants emerged, while the deletion of *phaR* did not result improve dicarboxylic acid production¹¹¹. Additionally, the overexpression of PHB depolymerases *depA/depB* could be attempted to repurpose intracellular PHB. Another promising strategy involves the introduction of a soluble transhydrogenase, which could stabilize the redox balance in Δccr strains, potentially enabling the generation of the $\Delta ccr\Delta phaC$ knockout strain. Furthermore, preventing reuptake of crotonic acid by deleting *DctA* or lowering sodium concentration of our minimal methanol medium could be a promising strategy to enhance crotonate production, as I was able to show that *M. extorquens* is able to consume crotonate during cultivation on methanol (Figure 9). The inactivation of dicarboxylic acid transporters was shown to downregulate *DctA* activity and increase production of mesaconic and (2S)-methylsuccinic acid by 2-fold, while growth rates were unaltered and concentrations of these acids remained constant in the cultivation medium at the end of exponential growth¹¹¹.

While the deletion of *DctA* may prevent uptake of crotonic acid, there are more enzymes that may contribute to its activation in *M. extorquens*. Through personal communication with Beau Dronsella, I found homologs to H16_B1148 and DmdB1 in *M. extorquens*, which were found among the most upregulated proteins involved in crotonic acid activation in *C. necator*. Therefore, while the deletion of some of these potential activators may enhance crotonate production, baseline level of crotonic acid activation through a variety of other enzymes likely unavoidable. A more promising idea may therefore be the employment of different thioesterases than *YciA*, as I could not observe the production of crotonate in any cultivation condition for *P45*. As mentioned previously, the activity of the promiscuous *YciA* could be insufficient to counter activities of crotonyl-CoA and crotonate activating enzymes, and while this thioesterases has been applicable for the production of mixed EMCP-derived acids, it may not be suitable for the specific production of crotonate. A more promising alternative would be the *Ydil* thioesterase from *E. coli*, which was shown to be more specific for crotonyl-CoA conversion to crotonate. Combined with a deletion of the PHB pathway, *C. necator* produced 148.0 ± 6.8 mg/L crotonate from formate¹⁴⁸. The employment of *Ydil* was also shown to lead to the production of 3.2 g/L crotonate during bioreactor cultivation of an *E. coli* strain devoid of any other known thioesterases¹⁴⁹.

In conclusion, this thesis has produced a promising strain for future production of EMCP-derived intermediates, while uncovering mutations that play a crucial role for efficient usage of the glyoxylate shunt. Here, I emphasize the importance of understanding the relevance of carbon flux distribution, as rewiring metabolism comes with several challenges. Further advancements in the metabolic engineering toolkit for *M. extorquens* could unlock the true potential of this methylotroph, and advance the progress towards a methanol-based bioindustry.

7 Acknowledgements

First and foremost, I would like to thank my first supervisor Tobias Erb. Thank you for allowing me to pursue my PhD in your lab, for supporting me through difficult times and for giving me the opportunity to attend so many exciting conferences and workshops, which helped me to grow as a scientist. I would also like to thank my Thesis Advisory Committee, namely Anke Becker, Katharina Höfer and Eckhard Boles for supervising my journey and all the feedback that contributed to the progress of this work. Thank you Eckhard for the experience to work in your lab as a Bachelor student, which introduced me to my all-time favorite organism *S. cerevisiae*, which holds a special place in my heart. Thank you Nina Odermatt for supervising me throughout my time as a Master student and for sharing my love for *S. cerevisiae*. Furthermore, I thank Doreen Meier and Eric Ellenberger for providing me with the vectors used in this work. Thank you Nicole Paczia for all the metabolomics measurements.

A big thank you goes out to all my amazing colleagues of the Erb lab. Thank you Markus for being the best bench-neighbor there is and for taking always care of my plants. Thank you Franzi for all the laughs and fun (at least for me) gym times. A special thanks goes out to my colleague Beau Dronsella, who helped me greatly in setting up the bioreactors, obtaining and interpreting sequencing results, his critical thinking and his everlasting optimism. I would also like to thank Scott, Elisabeth, Philipp, Alberto, Niels and Jan for their great help with various experiments and for their helpful scientific feedback and Johannes K. for his critical feedback to this work. Another thank you goes out to Elisabeth Petermann for your patience in trying to construct the *M. extorquens* knockouts with me, and for making tons of medium.

While this next section is dedicated to my friends and family, words cannot describe the gratitude I feel for having you in my life. Thank you Mama, for always being there for me, for helping me through difficult times and for giving me this wonderful life. Thank you Nicky, I am incredibly thankful for having you as my brother, we will always go through thick and thin together. I carry you both in my heart everywhere I go. I also want to thank Mario and Christiane, who have supported me from afar while writing this thesis. I am so thankful for all the amazing times we had together, may it be cooking evenings, vacations, or some other reason we find for celebrating.

Thank you Suzi, Jan, Yannick, Sarah, Freddy, Kiki and Josh for being the most amazing friends. Thank you Rebecca, for co-working with me as I was writing this thesis, for all the laughs and tears we shared throughout these years.

And of course, thank you Luca, my love, for being in my life. For all the constant support, for being there for me and for always lifting all weight off my shoulders. I treasure all the time I spend with you, may it be a night of gaming and snacking (yes, even all the times you beat me at Rise of the Necromancers), and all the fun times on vacations and night outs.

And last but not least, I thank Sammy, the best cat in the world. My little sunshine, who has been with me through my entire scientific journey. You never fail to make me smile and to light up my heart.

8 References

1. Intergovernmental Panel On Climate Change (Ippc). *Climate Change 2022 – Impacts, Adaptation and Vulnerability: Working Group II Contribution to the Sixth Assessment Report of the Intergovernmental Panel on Climate Change*. (Cambridge University Press, 2023). doi:10.1017/9781009325844.
2. Ippc. *Global Warming of 1.5°C: IPCC Special Report on Impacts of Global Warming of 1.5°C above Pre-Industrial Levels in Context of Strengthening Response to Climate Change, Sustainable Development, and Efforts to Eradicate Poverty*. (Cambridge University Press, 2022). doi:10.1017/9781009157940.
3. Emissions Trends and Drivers. in *Climate Change 2022 - Mitigation of Climate Change* (ed. Intergovernmental Panel On Climate Change (Ippc)) 215–294 (Cambridge University Press, 2023). doi:10.1017/9781009157926.004.
4. Main Greenhouse Gases. *Center for Climate and Energy Solutions*
<https://www.c2es.org/content/main-greenhouse-gases/>.
5. *GHG Emissions of All World Countries: 2025*. (Publications Office, Luxembourg, 2025). doi:10.2760/5917997.
6. Beer, C. *et al.* Terrestrial Gross Carbon Dioxide Uptake: Global Distribution and Covariation with Climate. *Science* **329**, 834–838 (2010).
7. Chang, J. *et al.* Climate warming from managed grasslands cancels the cooling effect of carbon sinks in sparsely grazed and natural grasslands. *Nat. Commun.* **12**, 118 (2021).
8. van der Woude, A. M. *et al.* Temperature extremes of 2022 reduced carbon uptake by forests in Europe.
9. Wolf, S. & Paul-Limoges, E. Drought and heat reduce forest carbon uptake. *Nat. Commun.* **14**, 6217 (2023).

10. Carbon dioxide levels increase by record amount to new highs in 2024. *World Meteorological Organization* <https://wmo.int/news/media-centre/carbon-dioxide-levels-increase-record-amount-new-highs-2024> (2025).
11. Ritchie, H. & Roser, M. CO₂ emissions. *Our World Data* <https://ourworldindata.org/co2-emissions> (2020).
12. Industry. in *Climate Change 2022 - Mitigation of Climate Change* (ed. Intergovernmental Panel On Climate Change (Ippc)) 1161–1244 (Cambridge University Press, 2023). doi:10.1017/9781009157926.013.
13. CO₂ Emissions – Global Energy Review 2025 – Analysis. *IEA* <https://www.iea.org/reports/global-energy-review-2025/co2-emissions>.
14. Friedlingstein, P. *et al.* Global Carbon Budget 2024. *Earth Syst. Sci. Data* **17**, 965–1039 (2025).
15. Hepburn, C. *et al.* The technological and economic prospects for CO₂ utilization and removal. *Nature* **575**, 87–97 (2019).
16. Total greenhouse gas emissions in the chemical industry (Indicator). <https://www.eea.europa.eu/en/european-zero-pollution-dashboards/indicators/total-greenhouse-gas-emissions-in-the-chemical-industry> (2024).
17. Gabrielli, P. *et al.* Net-zero emissions chemical industry in a world of limited resources. *One Earth* **6**, 682–704 (2023).
18. Waste generation in the chemical industry (Indicator). <https://www.eea.europa.eu/en/european-zero-pollution-dashboards/indicators/waste-generation-in-the-chemical-industry> (2024).
19. Akhundi, A., Habibi-Yangjeh, A., Abitorabi, M. & Rahim Pouran, S. Review on photocatalytic conversion of carbon dioxide to value-added compounds and renewable fuels by graphitic carbon nitride-based photocatalysts. *Catal. Rev.* **61**, 595–628 (2019).

20. de Jong, E. *et al.* Bio-based Chemicals Value Added Products from Biorefineries.
21. Arevalo-Gallegos, A., Ahmad, Z., Asgher, M., Parra-Saldivar, R. & Iqbal, H. M. N. Lignocellulose: A sustainable material to produce value-added products with a zero waste approach—A review. *Int. J. Biol. Macromol.* **99**, 308–318 (2017).
22. Keasling, J. *et al.* Microbial production of advanced biofuels. *Nat. Rev. Microbiol.* **19**, 701–715 (2021).
23. Rodríguez Couto, S. Exploitation of biological wastes for the production of value-added products under solid-state fermentation conditions. *Biotechnol. J.* **3**, 859–870 (2008).
24. Du, J., Shao, Z. & Zhao, H. Engineering microbial factories for synthesis of value-added products. *J. Ind. Microbiol. Biotechnol.* **38**, 873–890 (2011).
25. Ramos, J. L., Pakuts, B., Godoy, P., García-Franco, A. & Duque, E. Addressing the energy crisis: using microbes to make biofuels. *Microb. Biotechnol.* **15**, 1026–1030 (2022).
26. Verlinden, R. A. *et al.* Production of polyhydroxyalkanoates from waste frying oil by *Cupriavidus necator*. *AMB Express* **1**, 11 (2011).
27. Steele, T. S. *et al.* Biosynthesis of Haloterpenoids in Red Algae via Microbial-like Type I Terpene Synthases. *ACS Chem. Biol.* **19**, 185–192 (2024).
28. Dai, Z. *et al.* Metabolic engineering of *Saccharomyces cerevisiae* for production of ginsenosides. *Metab. Eng.* **20**, 146–156 (2013).
29. Ahmed, B. *et al.* Enhanced production of select phytocannabinoids in medical Cannabis cultivars using microbial consortia. *Front. Plant Sci.* **14**, 1219836 (2023).
30. Nakagawa, A. *et al.* A bacterial platform for fermentative production of plant alkaloids. *Nat. Commun.* **2**, 326 (2011).

31. Yang, P. *et al.* Ethanol yield improvement in *Saccharomyces cerevisiae* GPD2 Delta FPS1 Delta ADH2 Delta DLD3 Delta mutant and molecular mechanism exploration based on the metabolic flux and transcriptomics approaches. *Microb. Cell Factories* **21**, 160 (2022).
32. Hülber-Beyer, É., Bélafi-Bakó, K., Rózsenszki, T., Komáromy, P. & Nemestóthy, N. Evaluating the potential of semi-continuous itaconic acid fermentation by *Aspergillus terreus*: operational profile and experiences. *World J. Microbiol. Biotechnol.* **39**, 346 (2023).
33. Novy, V., Brunner, B. & Nidetzky, B. l-Lactic acid production from glucose and xylose with engineered strains of *Saccharomyces cerevisiae*: aeration and carbon source influence yields and productivities. *Microb. Cell Factories* **17**, 59 (2018).
34. Wernig, F., Baumann, L., Boles, E. & Oreb, M. Production of octanoic acid in *Saccharomyces cerevisiae* : Investigation of new precursor supply engineering strategies and intrinsic limitations. *Biotechnol. Bioeng.* **118**, 3046–3057 (2021).
35. Annamalai, N. & Sivakumar, N. Production of polyhydroxybutyrate from wheat bran hydrolysate using *Ralstonia eutropha* through microbial fermentation. *J. Biotechnol.* **237**, 13–17 (2016).
36. García, A. *et al.* High production of poly- β -hydroxybutyrate (PHB) by an *Azotobacter vinelandii* mutant altered in PHB regulation using a fed-batch fermentation process. *Biochem. Eng. J.* **82**, 117–123 (2014).
37. Niehus, X., Crutz-Le Coq, A.-M., Sandoval, G., Nicaud, J.-M. & Ledesma-Amaro, R. Engineering *Yarrowia lipolytica* to enhance lipid production from lignocellulosic materials. *Biotechnol. Biofuels* **11**, 11 (2018).

38. Lee, Y.-G. & Seo, J.-H. Production of 2,3-butanediol from glucose and cassava hydrolysates by metabolically engineered industrial polyploid *Saccharomyces cerevisiae*. *Biotechnol. Biofuels* **12**, 204 (2019).
39. Kuyper, M. *et al.* Evolutionary engineering of mixed-sugar utilization by a xylose-fermenting strain. *FEMS Yeast Res.* **5**, 925–934 (2005).
40. Sutor, J. T., Varzandeh, S. & Wallace, S. One-Pot Synthesis of Adipic Acid from Guaiacol in *Escherichia coli*. *ACS Synth. Biol.* **9**, 2472–2476 (2020).
41. Noda, S. *et al.* Reconstruction of metabolic pathway for isobutanol production in *Escherichia coli*. *Microb. Cell Factories* **18**, 124 (2019).
42. Brink, H. G. & Nicol, W. Succinic acid production with *Actinobacillus succinogenes*: rate and yield analysis of chemostat and biofilm cultures. *Microb. Cell Factories* **13**, 111 (2014).
43. Hawkins, K. M. & Smolke, C. D. Production of benzyloquinoline alkaloids in *Saccharomyces cerevisiae*. *Nat. Chem. Biol.* **4**, 564–573 (2008).
44. Renewables - Energy System. *IEA* <https://www.iea.org/energy-system/renewables>.
45. Sikarwar, V. S. *et al.* An overview of advances in biomass gasification. *Energy Environ. Sci.* **9**, 2939–2977 (2016).
46. Yasin, M. *et al.* Syngas Fermentation Into Biofuels and Biochemicals. in *Biofuels: Alternative Feedstocks and Conversion Processes for the Production of Liquid and Gaseous Biofuels* 301–327 (Elsevier, 2019). doi:10.1016/B978-0-12-816856-1.00013-0.
47. Gao, Y. *et al.* Syngas Production from Biomass Gasification: Influences of Feedstock Properties, Reactor Type, and Reaction Parameters. *ACS Omega* **8**, 31620–31631 (2023).
48. Al-Breiki, M. & Bicer, Y. Methanol. in *Sustainable Energy Carriers for Energy Storage and Transport* 83–104 (Springer Nature Switzerland, Cham, 2025). doi:10.1007/978-3-031-91615-1_5.

49. Wissner, N., Cames, M., Healy, S. & Sutter, J. Methanol as a marine fuel.
50. Khalafalla, S. *et al.* Conceptual Design Development of Coal-to-Methanol Process with Carbon Capture and Utilization. *Energies* **13**, 6421 (2020).
51. Frazão, C. J. R. & Walther, T. Syngas and Methanol-Based Biorefinery Concepts. *Chem. Ing. Tech.* **92**, 1680–1699 (2020).
52. Dang, S. *et al.* A review of research progress on heterogeneous catalysts for methanol synthesis from carbon dioxide hydrogenation. *Catal. Today* **330**, 61–75 (2019).
53. Hogendoorn, C., Pol, A., Nuijten, G. H. L. & Op Den Camp, H. J. M. Methanol Production by “*Methylacidiphilum fumariolicum*” SolV under Different Growth Conditions. *Appl. Environ. Microbiol.* **86**, e01188-20 (2020).
54. Kaiser, D., Beckmann, L., Walter, J. & Bertau, M. Conversion of Green Methanol to Methyl Formate. *Catalysts* **11**, 869 (2021).
55. Bar-Even, A. Formate Assimilation: The Metabolic Architecture of Natural and Synthetic Pathways. *Biochemistry* **55**, 3851–3863 (2016).
56. Hank, C. *et al.* Economics & carbon dioxide avoidance cost of methanol production based on renewable hydrogen and recycled carbon dioxide – power-to-methanol. *Sustain. Energy Fuels* **2**, 1244–1261 (2018).
57. Savakis, P. & Hellingwerf, K. J. Engineering cyanobacteria for direct biofuel production from CO₂. *Curr. Opin. Biotechnol.* **33**, 8–14 (2015).
58. Oliver, J. W. K., Machado, I. M. P., Yoneda, H. & Atsumi, S. Cyanobacterial conversion of carbon dioxide to 2,3-butanediol. *Proc. Natl. Acad. Sci.* **110**, 1249–1254 (2013).
59. Kong, W. *et al.* *Chlorella vulgaris* cultivation in simulated wastewater for the biomass production, nutrients removal and CO₂ fixation simultaneously. *J. Environ. Manage.* **284**, 112070 (2021).

60. Politaeva, N., Ilin, I., Velmozhina, K. & Shinkevich, P. Carbon Dioxide Utilization Using *Chlorella* Microalgae. *Environments* **10**, 109 (2023).
61. Jo, Y. Y. *et al.* Enhanced production of poly(3-hydroxybutyrate-co-3-hydroxyvalerate) with modulated 3-hydroxyvalerate fraction by overexpressing acetolactate synthase in *Cupriavidus necator* H16. *Int. J. Biol. Macromol.* **242**, 125166 (2023).
62. Li, Z. *et al.* Development of an autotrophic fermentation technique for the production of fatty acids using an engineered *Ralstonia eutropha* cell factory. *J. Ind. Microbiol. Biotechnol.* **46**, 783–790 (2019).
63. Gascoyne, J. L., Bommareddy, R. R., Heeb, S. & Malys, N. Engineering *Cupriavidus necator* H16 for the autotrophic production of (R)-1,3-butanediol. *Metab. Eng.* **67**, 262–276 (2021).
64. Donati, S. & Johnson, C. W. Optimizing *Cupriavidus necator* H16 as a host for aerobic C1 conversion. *Curr. Opin. Biotechnol.* **93**, 103306 (2025).
65. Langsdorf, A., Schütz, J. P., Ulber, R., Stöckl, M. & Holtmann, D. Production of polyhydroxybutyrate from industrial flue gas by microbial electrosynthesis. *J. CO2 Util.* **83**, 102800 (2024).
66. Liu, X. *et al.* Characterization and directed evolution of propionyl-CoA carboxylase and its application in succinate biosynthetic pathway with two CO₂ fixation reactions. *Metab. Eng.* **62**, 42–50 (2020).
67. Li, L., Zhou, X., Gao, Z., Xiong, P. & Liu, X. Production of succinate with two CO₂ fixation reactions from fatty acids in *Cupriavidus necator* H16. *Microb. Cell Factories* **23**, 194 (2024).
68. Liew, F. E. *et al.* Carbon-negative production of acetone and isopropanol by gas fermentation at industrial pilot scale. *Nat. Biotechnol.* **40**, 335–344 (2022).

69. Richter, H., Martin, M. & Angenent, L. A Two-Stage Continuous Fermentation System for Conversion of Syngas into Ethanol. *Energies* **6**, 3987–4000 (2013).
70. Arora, D. K., Ko, C.-W. & Randall, J. (76) Inventors: James L. Gaddy, Fayetteville, AR. (2003).
71. Liu, K. *et al.* Continuous syngas fermentation for the production of ethanol, n-propanol and n-butanol. *Bioresour. Technol.* **151**, 69–77 (2014).
72. Tarraran, L. *et al.* High-pressure fermentation of CO₂ and H₂ by a modified *Acetobacterium woodii*. *J. CO₂ Util.* **76**, 102583 (2023).
73. Krüsemann, J. L., Rainaldi, V., Cotton, C. A., Claassens, N. J. & Lindner, S. N. The cofactor challenge in synthetic methylotrophy: bioengineering and industrial applications. *Curr. Opin. Biotechnol.* **82**, 102953 (2023).
74. Ward, N. *et al.* Genomic Insights into Methanotrophy: The Complete Genome Sequence of *Methylococcus capsulatus* (Bath). *PLoS Biol.* **2**, e303 (2004).
75. Arfman, N. *et al.* Methanol metabolism in thermotolerant methylotrophic *Bacillus* strains involving a novel catabolic NAD-dependent methanol dehydrogenase as a key enzyme. *Arch. Microbiol.* **152**, 280–288 (1989).
76. Sarwar, A. & Lee, E. Y. Methanol-based biomanufacturing of fuels and chemicals using native and synthetic methylotrophs. *Synth. Syst. Biotechnol.* **8**, 396–415 (2023).
77. Crowther, G. J., Kosály, G. & Lidstrom, M. E. Formate as the Main Branch Point for Methylotrophic Metabolism in *Methylobacterium extorquens* AM1. *J. Bacteriol.* **190**, 5057–5062 (2008).
78. Schulz-Mirbach, H., Dronsella, B., He, H. & Erb, T. J. Creating new-to-nature carbon fixation: A guide. *Metab. Eng.* **82**, 12–28 (2024).

79. He, H., Edlich-Muth, C., Lindner, S. N. & Bar-Even, A. Ribulose Monophosphate Shunt Provides Nearly All Biomass and Energy Required for Growth of *E. coli*. *ACS Synth. Biol.* **7**, 1601–1611 (2018).
80. Chen, C.-T. *et al.* Synthetic methanol auxotrophy of Escherichia coli for methanol-dependent growth and production. *Metab. Eng.* **49**, 257–266 (2018).
81. Keller, P. *et al.* Methanol-dependent Escherichia coli strains with a complete ribulose monophosphate cycle. *Nat. Commun.* **11**, 5403 (2020).
82. Chen, F. Y.-H., Jung, H.-W., Tsuei, C.-Y. & Liao, J. C. Converting Escherichia coli to a Synthetic Methylophile Growing Solely on Methanol. *Cell* **182**, 933-946.e14 (2020).
83. Espinosa, M. I. *et al.* Adaptive laboratory evolution of native methanol assimilation in *Saccharomyces cerevisiae*. *Nat. Commun.* **11**, 5564 (2020).
84. Dronsella, B. *et al.* One-carbon fixation via the synthetic reductive glycine pathway exceeds yield of the Calvin cycle. *Nat. Microbiol.* **10**, 646–653 (2025).
85. He, H., Höper, R., Dodenhöft, M., Marlière, P. & Bar-Even, A. An optimized methanol assimilation pathway relying on promiscuous formaldehyde-condensing aldolases in *E. coli*. *Metab. Eng.* **60**, 1–13 (2020).
86. Keller, P. *et al.* Methanol-dependent Escherichia coli strains with a complete ribulose monophosphate cycle. *Nat. Commun.* **11**, 5403 (2020).
87. Keller, P. *et al.* Generation of an Escherichia coli strain growing on methanol via the ribulose monophosphate cycle. *Nat. Commun.* **13**, 5243 (2022).
88. Chen, F. Y.-H., Jung, H.-W., Tsuei, C.-Y. & Liao, J. C. Converting Escherichia coli to a Synthetic Methylophile Growing Solely on Methanol. *Cell* **182**, 933-946.e14 (2020).
89. Reiter, M. A. *et al.* A synthetic methylophilic Escherichia coli as a chassis for bioproduction from methanol. *Nat. Catal.* **7**, 560–573 (2024).

90. Witthoff, S. *et al.* Metabolic Engineering of *Corynebacterium glutamicum* for Methanol Metabolism. *Appl. Environ. Microbiol.* **81**, 2215–2225 (2015).
91. Wang, J. *et al.* Engineering the native methylotrophs for the bioconversion of methanol to value-added chemicals: current status and future perspectives. *Green Chem. Eng.* **4**, 199–211 (2023).
92. Hu, B. & Lidstrom, M. E. Metabolic engineering of *Methylobacterium extorquens* AM1 for 1-butanol production. *Biotechnol. Biofuels* **7**, 156 (2014).
93. Ma, Z. *et al.* Metabolomic analysis improves bioconversion of methanol to isobutanol in *Methylobacterium extorquens* AM1. *Biotechnol. J.* **16**, 2000413 (2021).
94. Lim, C. K. *et al.* Designing and Engineering *Methylobacterium extorquens* AM1 for Itaconic Acid Production. *Front. Microbiol.* **10**, 1027 (2019).
95. Chang, W., Yoon, J. & Oh, M.-K. Production of Polyhydroxyalkanoates with the Fermentation of *Methylobacterium extorquens* Using Formate as a Carbon Substrate. *Biotechnol. Bioprocess Eng.* **27**, 268–275 (2022).
96. Bourque, D., Pomerleau, Y. & Groleau, D. High-cell-density production of poly- β -hydroxybutyrate (PHB) from methanol by *Methylobacterium extorquens*: production of high-molecular-mass PHB.
97. Sonntag, F. *et al.* Engineering *Methylobacterium extorquens* for de novo synthesis of the sesquiterpenoid α -humulene from methanol. *Metab. Eng.* **32**, 82–94 (2015).
98. Zhu, W.-L. *et al.* Bioconversion of methanol to value-added mevalonate by engineered *Methylobacterium extorquens* AM1 containing an optimized mevalonate pathway. *Appl. Microbiol. Biotechnol.* **100**, 2171–2182 (2016).
99. Marx, C. J. & Lidstrom, M. E. Broad-Host-Range *cre-lox* System for Antibiotic Marker Recycling in Gram-Negative Bacteria. *BioTechniques* **33**, 1062–1067 (2002).

100. Marx, C. J. Development of a broad-host-range *sacB*-based vector for unmarked allelic exchange. *BMC Res. Notes* **1**, 1 (2008).
101. Volke, D. C., Orsi, E. & Nickel, P. I. Emergent CRISPR–Cas-based technologies for engineering non-model bacteria. *Curr. Opin. Microbiol.* **75**, 102353 (2023).
102. Qi, L. S. *et al.* Repurposing CRISPR as an RNA-Guided Platform for Sequence-Specific Control of Gene Expression. *Cell* **152**, 1173–1183 (2013).
103. Larson, M. H. *et al.* CRISPR interference (CRISPRi) for sequence-specific control of gene expression. *Nat. Protoc.* **8**, 2180–2196 (2013).
104. Mo, X.-H. *et al.* Establishment of CRISPR interference in *Methylobacterium extorquens* and application of rapidly mining a new phytoene desaturase involved in carotenoid biosynthesis. *Appl. Microbiol. Biotechnol.* **104**, 4515–4532 (2020).
105. Carrillo, M. *et al.* Design and Control of Extrachromosomal Elements in *Methylobacterium extorquens* AM1. *ACS Synth. Biol.* **8**, 2451–2456 (2019).
106. Marx, C. J. & Lidstrom, M. E. Development of improved versatile broad-host-range vectors for use in methylotrophs and other Gram-negative bacteria.
107. Pöschel, L., Gehr, E. & Buchhaupt, M. A pBBR1-based vector with IncP group plasmid compatibility for *Methylobacterium extorquens*. *MicrobiologyOpen* **11**, e1325 (2022).
108. Erb, T. J. *et al.* Synthesis of C₅-dicarboxylic acids from C₂-units involving crotonyl-CoA carboxylase/reductase: The ethylmalonyl-CoA pathway. *Proc. Natl. Acad. Sci.* **104**, 10631–10636 (2007).
109. Schneider, K. *et al.* The Ethylmalonyl-CoA Pathway Is Used in Place of the Glyoxylate Cycle by *Methylobacterium extorquens* AM1 during Growth on Acetate. *J. Biol. Chem.* **287**, 757–766 (2012).

110. Kornberg, H. L. & Krebs, H. A. Synthesis of Cell Constituents from C2-Units by a Modified Tricarboxylic Acid Cycle. *Nature* **179**, 988–991 (1957).
111. Sonntag, F. *et al.* High-level production of ethylmalonyl-CoA pathway-derived dicarboxylic acids by *Methylobacterium extorquens* under cobalt-deficient conditions and by polyhydroxybutyrate negative strains. *Appl. Microbiol. Biotechnol.* **99**, 3407–3419 (2015).
112. Schada von Borzyskowski, L. *et al.* Replacing the Ethylmalonyl-CoA Pathway with the Glyoxylate Shunt Provides Metabolic Flexibility in the Central Carbon Metabolism of *Methylobacterium extorquens* AM1. *ACS Synth. Biol.* **7**, 86–97 (2018).
113. Peyraud, R. *et al.* Genome-scale reconstruction and system level investigation of the metabolic network of *Methylobacterium extorquens* AM1. *BMC Syst. Biol.* **5**, 189 (2011).
114. LaCroix, R. A. *et al.* Use of Adaptive Laboratory Evolution To Discover Key Mutations Enabling Rapid Growth of *Escherichia coli* K-12 MG1655 on Glucose Minimal Medium. *Appl. Environ. Microbiol.* **81**, 17–30 (2015).
115. Šmejkalová, H., Erb, T. J. & Fuchs, G. Methanol Assimilation in *Methylobacterium extorquens* AM1: Demonstration of All Enzymes and Their Regulation. *PLoS ONE* **5**, e13001 (2010).
116. Zhang, W., Bevins, M. A., Plantz, B. A., Smith, L. A. & Meagher, M. M. Modeling *Pichia pastoris* growth on methanol and optimizing the production of a recombinant protein, the heavy-chain fragment C of botulinum neurotoxin, serotype A. *Biotechnol. Bioeng.* **70**, 1–8 (2000).
117. Cotton, C. A., Claassens, N. J., Benito-Vaquerizo, S. & Bar-Even, A. Renewable methanol and formate as microbial feedstocks. *Curr. Opin. Biotechnol.* **62**, 168–180 (2020).

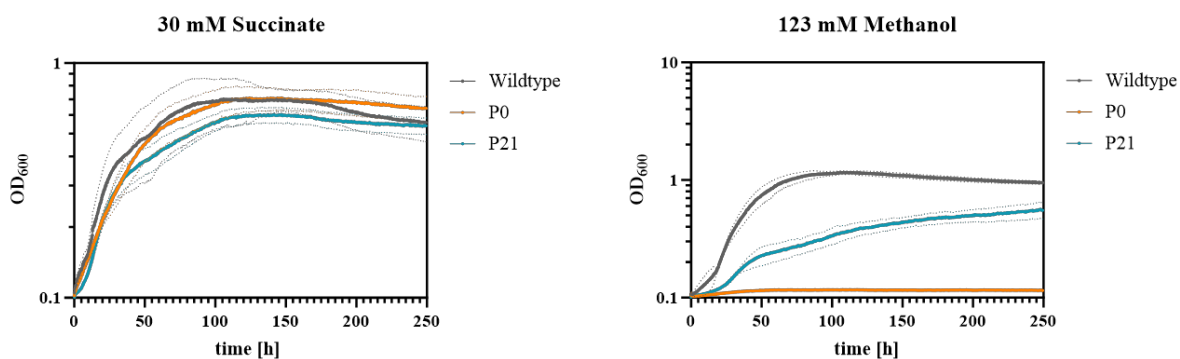
118. Ochsner, A. M. *et al.* Transposon Sequencing Uncovers an Essential Regulatory Function of Phosphoribulokinase for Methylophony. *Curr. Biol.* **27**, 2579-2588.e6 (2017).
119. Kalyuzhnaya, M. G. & Lidstrom, M. E. QscR, a LysR-Type Transcriptional Regulator and CbbR Homolog, Is Involved in Regulation of the Serine Cycle Genes in *Methylobacterium extorquens* AM1. *J. Bacteriol.* **185**, 1229–1235 (2003).
120. Bazaruto, J. V., Bruger, E. L., Lee, J. A., Lambert, L. B. & Marx, C. J. Formaldehyde-Responsive Proteins TtmR and EfgA Reveal a Trade-off between Formaldehyde Resistance and Efficient Transition to Methylophony in *Methylobacterium extorquens*. *J. Bacteriol.* **203**, (2021).
121. Wang, B., Pugh, S., Nielsen, D. R., Zhang, W. & Meldrum, D. R. Engineering cyanobacteria for photosynthetic production of 3-hydroxybutyrate directly from CO₂. *Metab. Eng.* **16**, 68–77 (2013).
122. Korotkova, N. & Lidstrom, M. E. Connection between Poly-^N-Hydroxybutyrate Biosynthesis and Growth on C1 and C2 Compounds in the Methylophony *Methylobacterium extorquens* AM. *J BACTERIOL* **183**, (2001).
123. Korotkova, N., Chistoserdova, L. & Lidstrom, M. E. Poly-^N-Hydroxybutyrate Biosynthesis in the Facultative Methylophony *Methylobacterium extorquens* AM1: Identification and Mutation of gap11, gap20, and phaR. *J BACTERIOL* **184**, (2002).
124. Stukenberg, D., Faber, A. & Becker, A. Graded-CRISPRi, a Tool for Tuning the Strengths of CRISPRi-Mediated Knockdowns in *Vibrio natriegens* Using gRNA Libraries. *ACS Synth. Biol.* **13**, 2091–2104 (2024).
125. Feng, H., Guo, J., Wang, T., Zhang, C. & Xing, X. Guide-target mismatch effects on dCas9–sgRNA binding activity in living bacterial cells. *Nucleic Acids Res.* **49**, 1263–1277 (2021).

126. Godoy, C. A. *et al.* Disulfide Engineered Lipase to Enhance the Catalytic Activity: A Structure-Based Approach on BTL2. *Int. J. Mol. Sci.* **20**, 5245 (2019).
127. Han, Z., Han, S., Zheng, S. & Lin, Y. Enhancing thermostability of a *Rhizomucor miehei* lipase by engineering a disulfide bond and displaying on the yeast cell surface. *Appl. Microbiol. Biotechnol.* **85**, 117–126 (2009).
128. Li, L. *et al.* Enhancing thermostability of *Yarrowia lipolytica* lipase 2 through engineering multiple disulfide bonds and mitigating reduced lipase production associated with disulfide bonds. *Enzyme Microb. Technol.* **126**, 41–49 (2019).
129. Springer, A. L., Morris, C. J. & Lidstrom, M. E. Molecular analysis of mxbD and mxbM, a putative sensor-regulator pair required for oxidation of methanol in *Methylobacterium extorquens* AM1. *Microbiology* **143**, 1737–1744 (1997).
130. Skovran, E., Palmer, A. D., Rountree, A. M., Good, N. M. & Lidstrom, M. E. XoxF Is Required for Expression of Methanol Dehydrogenase in *Methylobacterium extorquens* AM1. *J. Bacteriol.* **193**, 6032–6038 (2011).
131. Nakagawa, T. *et al.* A Catalytic Role of XoxF1 as La³⁺-Dependent Methanol Dehydrogenase in *Methylobacterium extorquens* Strain AM1. *PLoS ONE* **7**, e50480 (2012).
132. Vu, H. N. *et al.* Lanthanide-Dependent Regulation of Methanol Oxidation Systems in *Methylobacterium extorquens* AM1 and Their Contribution to Methanol Growth. *J. Bacteriol.* **198**, 1250–1259 (2016).
133. Good, N. M., Moore, R. S., Suriano, C. J. & Martinez-Gomez, N. C. Contrasting in vitro and in vivo methanol oxidation activities of lanthanide-dependent alcohol dehydrogenases XoxF1 and ExaF from *Methylobacterium extorquens* AM1. *Sci. Rep.* **9**, 4248 (2019).

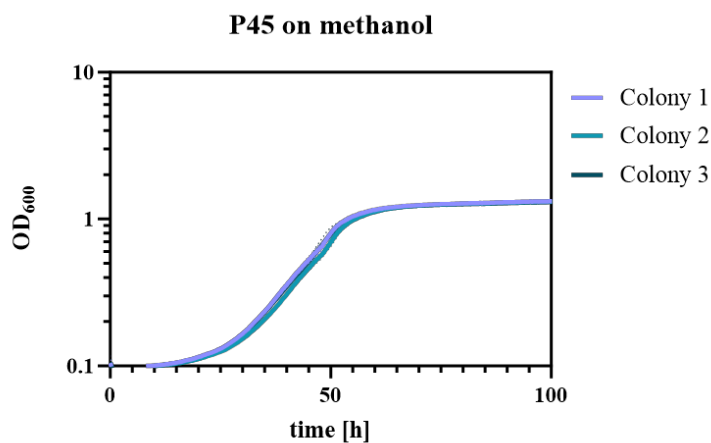
134. Tayri-Wilk, T. *et al.* Mass spectrometry reveals the chemistry of formaldehyde cross-linking in structured proteins. *Nat. Commun.* **11**, 3128 (2020).
135. Davis López, S. A., Griffith, D. A., Choi, B., Cate, J. H. D. & Tullman-Ercek, D. Evolutionary engineering improves tolerance for medium-chain alcohols in *Saccharomyces cerevisiae*. *Biotechnol. Biofuels* **11**, 90 (2018).
136. Severi, F. New central carbon metabolic pathways in Alphaproteobacteria: from natural to synthetic metabolism. (Philipps-Universität Marburg Marburg, 2022).
doi:10.17192/z2022.0099.
137. Schada Von Borzyskowski, L. *et al.* Replacing the Ethylmalonyl-CoA Pathway with the Glyoxylate Shunt Provides Metabolic Flexibility in the Central Carbon Metabolism of *Methylobacterium extorquens* AM1. *ACS Synth. Biol.* **7**, 86–97 (2018).
138. Carroll, S. M. & Marx, C. J. Evolution after Introduction of a Novel Metabolic Pathway Consistently Leads to Restoration of Wild-Type Physiology. *PLoS Genet.* **9**, e1003427 (2013).
139. Kämäräinen, J. *et al.* Pyridine nucleotide transhydrogenase Pnt AB is essential for optimal growth and photosynthetic integrity under low-light mixotrophic conditions in *Synechocystis* sp. PCC 6803. *New Phytol.* **214**, 194–204 (2017).
140. Park, S. Y., Eun, H., Lee, M. H. & Lee, S. Y. Metabolic engineering of *Escherichia coli* with electron channelling for the production of natural products. *Nat. Catal.* **5**, 726–737 (2022).
141. Zhang, Y.-H. P. Substrate channeling and enzyme complexes for biotechnological applications. *Biotechnol. Adv.* **29**, 715–725 (2011).
142. Collas, F. *et al.* Engineering the biological conversion of formate into crotonate in *Cupriavidus necator*. *Metab. Eng.* **79**, 49–65 (2023).

143. Cevallos, M. A., On, S. E., Leija, A., Mora, Y. & Mora, J. Genetic and Physiological Characterization of a *Rhizobium etli* Mutant Strain Unable To Synthesize Poly- β -Hydroxybutyrate.
144. Stirling, F. *et al.* Rational Design of Evolutionarily Stable Microbial Kill Switches. *Mol. Cell* **68**, 686-697.e3 (2017).
145. James, J. *et al.* Protein over-expression in *Escherichia coli* triggers adaptation analogous to antimicrobial resistance. *Microb. Cell Factories* **20**, 13 (2021).
146. Halvorsen, T. M., Ricci, D. P., Park, D. M., Jiao, Y. & Yung, M. C. Comprehensive analysis of the kill switch effector landscape reveals drivers of lethality, stability, and escape in *Pseudomonas fluorescens*.
147. Chou, H.-H., Chiu, H.-C., Delaney, N. F., Segrè, D. & Marx, C. J. Diminishing Returns Epistasis Among Beneficial Mutations Decelerates Adaptation. *Science* **332**, 1190–1192 (2011).
148. Collas, F. *et al.* Engineering the biological conversion of formate into crotonate in *Cupriavidus necator*. *Metab. Eng.* **79**, 49–65 (2023).
149. Kim, S., Cheong, S. & Gonzalez, R. Engineering *Escherichia coli* for the synthesis of short- and medium-chain α,β -unsaturated carboxylic acids. *Metab. Eng.* **36**, 90–98 (2016).

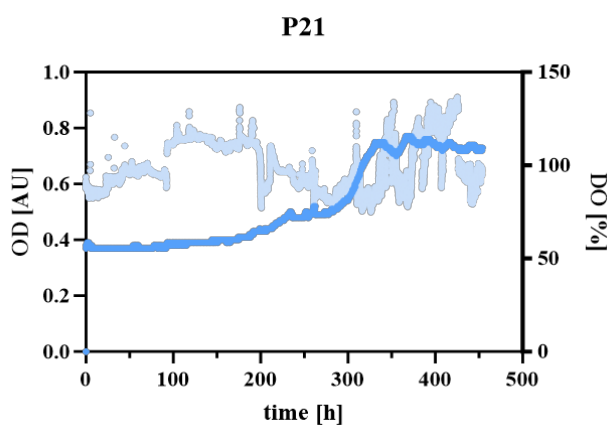
9 Supplementary information



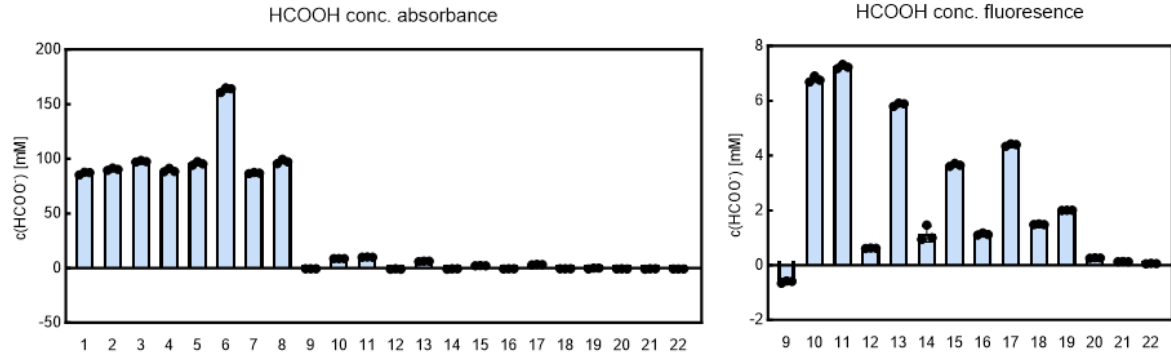
Supplementary Figure 1: Growth of Δccr *P0*, *P21* and the Wt on 30 mM succinate and 123 mM methanol. Growth assays were conducted in five biological replicates.



Supplementary Figure 2 Growth of single colonies of *P45* on 123 mM methanol minimal medium. Growth assays were done in three biological replicates.

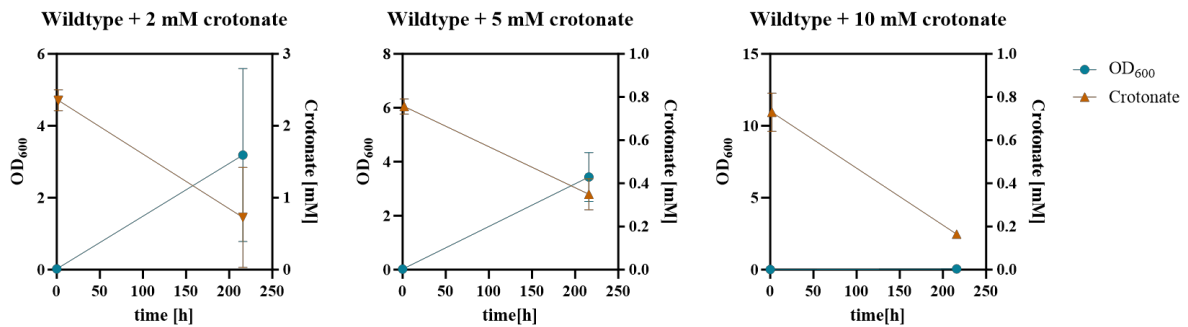


Supplementary Figure 3: Bioreactor chemostat cultivation of *P21* on formate as sole carbon source. The pH was controlled by titration of formic acid throughout cultivation.



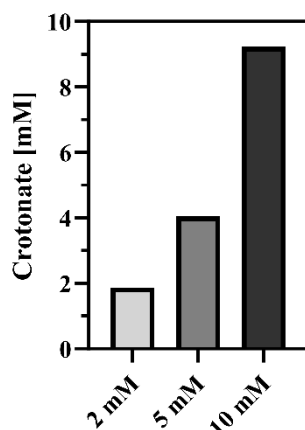
Sample	Strain	Set Flow rate	Actual Flow rate	Description
1	cel	10	12	Medium
2	cel	20	14	Medium
3	cel	30	24	Medium
4	cel	50	40	Medium
5	cel	50	40	Medium
6	P45	10	12	Medium
7	P45	20	14	Medium
8	P45	30	24	Medium
9	P21	50	40	Supernatant
10	cel	10	12	Supernatant
11	P45	10	12	Supernatant
12	cel	20	14	Supernatant
13	P45	20	14	Supernatant
14	cel	20	14	Supernatant
15	P45	20	14	Supernatant
16	cel	30	24	Supernatant
17	P45	30	24	Supernatant
18	cel	50	40	Supernatant
19	cel	50	40	Supernatant
20	P21	50	40	Supernatant
21	P21	50	40	Supernatant
22	P21	50	40	Supernatant

Supplementary Figure 4: Formate consumption tests including a sample list. Each sample was taken during bioreactor cultivation in chemostat mode at a set flow rate in 1L culture medium.

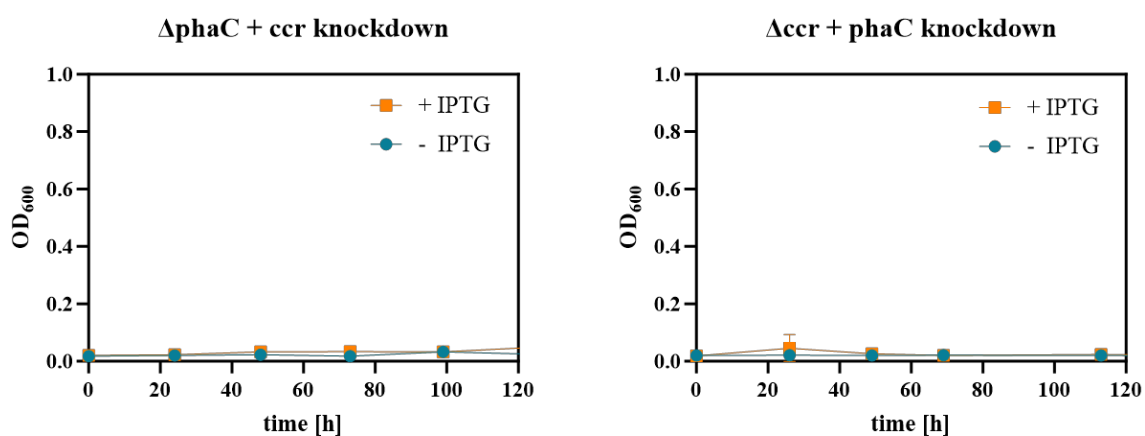


Supplementary Figure 5: Crotonate consumption growth assay of the wildtype during flask cultivation on 123 mM methanol as sole carbon source, with the addition of 2, 5 and 10 mM crotonate. OD_{600} (teal) was measured at the start of the growth assay and after 216 hours. Samples for exometabolomic analysis of crotonate (orange) were taken at the same timepoints. Each sample point represents three biological replicates.

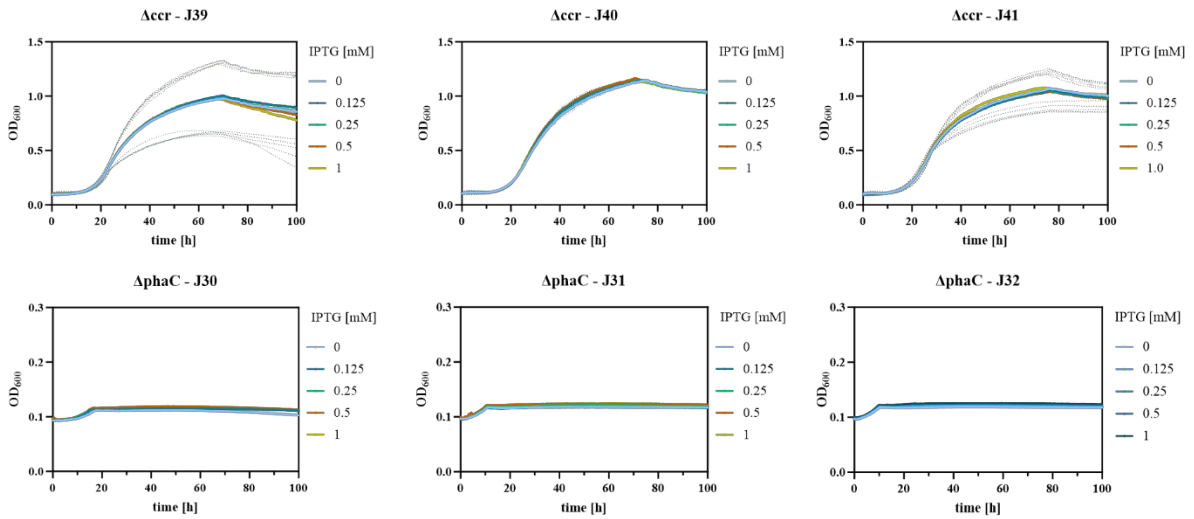
Media controls for crotonate degradation



Supplementary Figure 6: Methanol medium containing 2, 5, and 10 mM crotonate without cells to determine crotonate degradation at cultivation conditions after 216 h.

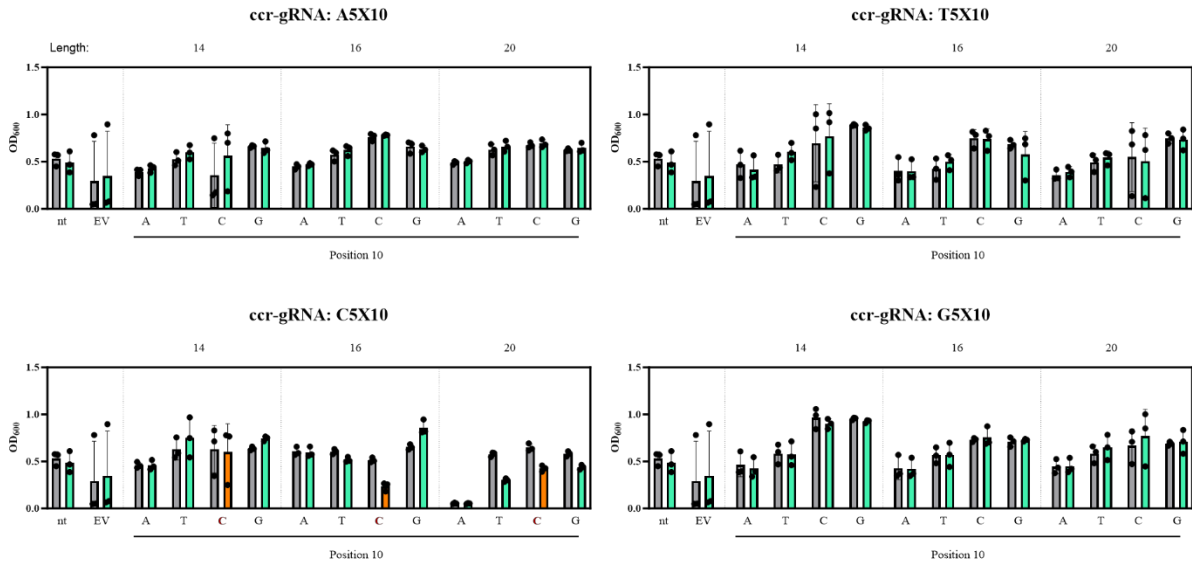


Supplementary Figure 7: Test of single plasmid system with inducible expression of dCas9 and constitutive expression of gRNA in *ΔphaC* and *Δaccr* containing the corresponding gRNAs for the targeted knockdown of *ccr* and *phaC*. Cultures were grown in liquid minimal medium, and growth was monitored in presence of the inducer (1 mM IPTG; orange) and absence of the inducer (teal). Each sampling point represents three biological replicates.

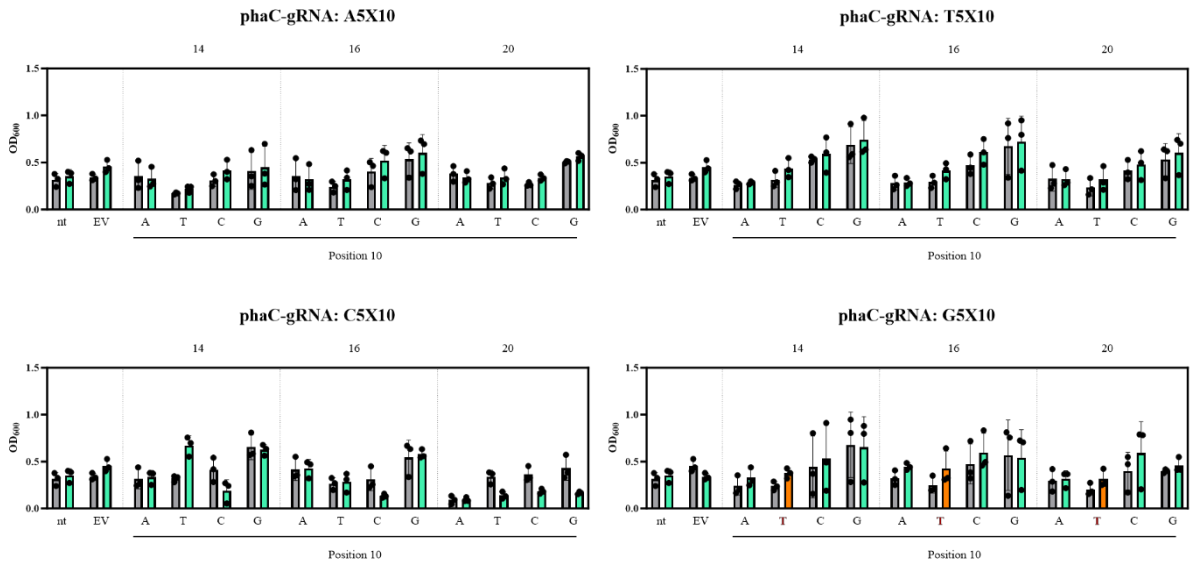


Supplementary Figure 8: Test of the double-inducible CRISPRi system expressed from pABCjx and controlled by the inducible P_{A10403} promoter during a growth assay on methanol. The knockdown system was tested in Δccr and $\Delta phaC$, containing three different gRNAs for the targeted knockdown of *phaC* (J39, J40, J41) and of *ccr* (J30, J31, J32).

A



B



Supplementary Figure 9: Growth assays of the wildtype containing mismatched gRNAs during growth on methanol. Cultures were grown in 3 ml cultures in tubes and induced with 1 mM IPTG. Final OD₆₀₀ was measured after 56 h in non-induced (grey bars) and induced (green bars) cultures. A: Mismatch gRNAs targeting *ccr* (fully binding: C5C10). B: Mismatch gRNAs targeting *phaC* (fully binding: G5T10). Each bar represents three biological replicates.

Supplementary Table 1: Oligos used for the construction of the mismatch gRNA library through Golden Gate cloning. Each oligo was ordered in forward and reverse direction for subsequent annealing. They contained cutting sites for BsaI for the construction of the final pABCjx-gRNA plasmid for targeting *ccr* via Golden Gate cloning. The gRNA name describes truncation level (20, 16, 14 bp) and the order of introduced mismatches (position 5, position 10).

gRNA name	Sequence (5`-3`)
20_A_A- <i>ccr</i>	TACTgccgtctgccaggtaagc
20_A_T- <i>ccr</i>	TACTgccgtctgcctggtaagc
20_A_C- <i>ccr</i>	TACTgccgtctgcccggtaagc
20_A_G- <i>ccr</i>	TACTgccgtctgccgggtaagc
16_A_A- <i>ccr</i>	TACTtctgccaggtaagc
16_A_T- <i>ccr</i>	TACTtctgcctggtaagc
16_A_C- <i>ccr</i>	TACTtctgcccggtaagc
16_A_G- <i>ccr</i>	TACTtctgccgggtaagc
14_A_A- <i>ccr</i>	TACTtgccaggtaagc
14_A_T- <i>ccr</i>	TACTtgccctggtaagc
14_A_C- <i>ccr</i>	TACTtgcccggtaagc
14_A_G- <i>ccr</i>	TACTtgccgggtaagc
20_T_A- <i>ccr</i>	TACTgccgtctgccaggctagc
20_T_T- <i>ccr</i>	TACTgccgtctgcctggctagc
20_T_C- <i>ccr</i>	TACTgccgtctgcccggctagc
20_T_G- <i>ccr</i>	TACTgccgtctgccgggctagc
16_T_A- <i>ccr</i>	TACTtctgccaggctagc
16_T_T- <i>ccr</i>	TACTtctgcctggctagc
16_T_C- <i>ccr</i>	TACTtctgcccggctagc
16_T_G- <i>ccr</i>	TACTtctgccgggctagc
14_T_A- <i>ccr</i>	TACTtgccaggctagc
14_T_T- <i>ccr</i>	TACTtgccctggctagc
14_T_C- <i>ccr</i>	TACTtgcccggctagc
14_T_G- <i>ccr</i>	TACTtgccgggctagc
20_C_A- <i>ccr</i>	TACTgccgtctgccaggccagc
20_C_T- <i>ccr</i>	TACTgccgtctgcctggccagc
20_C_C- <i>ccr</i>	TACTgccgtctgcccggccagc
20_C_G- <i>ccr</i>	TACTgccgtctgccgggccagc
16_C_A- <i>ccr</i>	TACTtctgccaggccagc
16_C_T- <i>ccr</i>	TACTtctgcctggccagc
16_C_C- <i>ccr</i>	TACTtctgcccggccagc
16_C_G- <i>ccr</i>	TACTtctgccgggccagc
14_C_A- <i>ccr</i>	TACTtgccaggccagc
14_C_T- <i>ccr</i>	TACTtgccctggccagc
14_C_C- <i>ccr</i>	TACTtgcccggccagc
14_C_G- <i>ccr</i>	TACTtgccgggccagc
20_G_A- <i>ccr</i>	TACTgccgtctgccaggtcgagc
20_G_T- <i>ccr</i>	TACTgccgtctgcctggtcgagc
20_G_C- <i>ccr</i>	TACTgccgtctgcccggtcgagc
20_G_G- <i>ccr</i>	TACTgccgtctgccgggtcgagc
16_G_A- <i>ccr</i>	TACTtctgccaggtcgagc
16_G_T- <i>ccr</i>	TACTtctgcctggtcgagc
16_G_C- <i>ccr</i>	TACTtctgcccggtcgagc
16_G_G- <i>ccr</i>	TACTtctgccgggtcgagc
14_G_A- <i>ccr</i>	TACTtgccaggtcgagc
14_G_T- <i>ccr</i>	TACTtgccctggtcgagc
14_G_C- <i>ccr</i>	TACTtgcccggtcgagc

Supplementary Table 2: Oligos used for the construction of the mismatch gRNA library through Golden Gate cloning. Each oligo was ordered in forward and reverse direction for subsequent annealing. They contained cutting sites for BsaI for the construction of the final pABCjx-gRNA plasmid for targeting *phaC* via Golden Gate cloning. The gRNA name describes truncation level (20, 16, 14 bp) and the order of introduced mismatches (position 5, position 10).

20_A_A-phaC	TACTcggggcgggaagcggacgga
20_A_T-phaC	TACTcggggcgggatgcggacgga
20_A_C-phaC	TACTcggggcgggacgcggacgga
20_A_G-phaC	TACTcggggcgggaggcggacgga
16_A_A-phaC	TACTgcggaagcggacgga
16_A_T-phaC	TACTgcgggatgcggacgga
16_A_C-phaC	TACTgcgggacgcggacgga
16_A_G-phaC	TACTgcgggaggcggacgga
14_A_A-phaC	TACTgggaagcggacgga
14_A_T-phaC	TACTgggatgcggacgga
14_A_C-phaC	TACTgggacgcggacgga
14_A_G-phaC	TACTgggaggcggacgga
20_T_A-phaC	TACTcggggcgggaagcggtcgga
20_T_T-phaC	TACTcggggcgggatgcggtcgga
20_T_C-phaC	TACTcggggcgggacgcggtcgga
20_T_G-phaC	TACTcggggcgggaggcggtcgga
16_T_A-phaC	TACTgcggaagcggtcgga
16_T_T-phaC	TACTgcgggatgcggtcgga
16_T_C-phaC	TACTgcgggacgcggtcgga
16_T_G-phaC	TACTgcgggaggcggtcgga
14_T_A-phaC	TACTgggaagcggtcgga
14_T_T-phaC	TACTgggatgcggtcgga
14_T_C-phaC	TACTgggacgcggtcgga
14_T_G-phaC	TACTgggaggcggtcgga
20_C_A-phaC	TACTcggggcgggaagcggccgga
20_C_T-phaC	TACTcggggcgggatgcggccgga
20_C_C-phaC	TACTcggggcgggacgcggccgga
20_C_G-phaC	TACTcggggcgggaggcggccgga
16_C_A-phaC	TACTgcggaagcggccgga
16_C_T-phaC	TACTgcgggatgcggccgga
16_C_C-phaC	TACTgcgggacgcggccgga
16_C_G-phaC	TACTgcgggaggcggccgga
14_C_A-phaC	TACTgggaagcggccgga
14_C_T-phaC	TACTgggatgcggccgga
14_C_C-phaC	TACTgggacgcggccgga
14_C_G-phaC	TACTgggaggcggccgga
20_G_A-phaC	TACTcggggcgggaagcgggcgga
20_G_T-phaC	TACTcggggcgggatgcgggcgga
20_G_C-phaC	TACTcggggcgggacgcgggcgga
20_G_G-phaC	TACTcggggcgggaggcgggcgga
16_G_A-phaC	TACTgcggaagcgggcgga
16_G_T-phaC	TACTgcgggatgcgggcgga
16_G_C-phaC	TACTgcgggacgcgggcgga
16_G_G-phaC	TACTgcgggaggcgggcgga
14_G_A-phaC	TACTgggaagcgggcgga
14_G_T-phaC	TACTgggatgcgggcgga
14_G_C-phaC	TACTgggacgcgggcgga
14_G_G-phaC	TACTgggaggcgggcgga